MANUFACTURING PROCESS MODELLING OF THERMOPLASTIC COMPOSITE RESISTANCE WELDING

By

Edith Talbot

Mechanical Engineering Department

McGill University, Montreal

June 2005

A thesis submitted to McGill University in partial fulfillment of the requirements of the degree of Edith Talbot

Your file Votre référence
ISBN: 978-0-494-22673-5
Our file Notre référence
ISBN: 978-0-494-22673-5

Abstract

One-, two- and three-dimensional transient heat transfer finite element models are developed to simulate the resistance welding process of pre-consolidated unidirectional AS4 carbon fibre reinforced Poly-ether-ether-ketone (APC-2/AS4) laminates with a metal mesh heating element, in a lap-shear configuration. The finite element models are used to investigate the effect of process and material parameters on the thermal behaviour of the coupon size welds, yielding to a better understanding of the process. The 1-D model determines: a) the importance of including the latent heat of PEEK, and b) the through-thickness temperature gradient away from the edges, for different tooling plate materials. The 2-D model simulates the cross-section of the process, considering the convective and irradiative heat losses from the areas of the heating element exposed to air. The 3-D model includes the heat conduction along the length of the laminates, to fully depict the thermal behaviour of the welds. Finally, the models are compared with experimental data.

Résumé

Le procédé de soudage par résistance de laminés unidirectionnels de poly-éther-éther-cétone renforcés de fibres de carbone AS4 continues (APC-2/AS4), avec un élément chauffant en treillis métallique, a été modélisé en 1-D, 2-D et 3-D. Les modèles par éléments finis ont été utilisés pour déterminer l'effet de différents paramètres sur le comportement thermique des soudures, de façon à mieux comprendre le procédé. Le modèle 1-D détermine l'importance d'inclure la chaleur massique de fusion du polymère dans l'analyse, ainsi que le gradient de température à travers l'épaisseur des laminés, loin des côtés, pour différents isolants. Le modèle 2-D simule une vue en coupe du procédé, pour considérer l'influence des pertes par convection et radiation provenant des parties de l'élément chauffant exposées à l'air. Le modèle 3-D inclut le transfert de chaleur dans les laminés, de façon à mieux représenter le comportement thermique du procédé. Finalement, les modèles sont comparés avec des données expérimentales.

Acknowledgements

I am extremely grateful to the following people and organisations for their help regarding my work.

- Professor Pascal Hubert, McGill University, for supervision, advice and financial assistance.
- Dr. Ali Yousefpour, Research Officer at Aerospace Manufacturing Technology Center and Adjunct Professor at McGill University, for supervision, advice and technical support for the experimental setup.
- Aerospace Manufacturing Technology Center, Dr. Mehdi Hojjati, Composite Group Leader, for providing support to the project.
- Mario Simard, ETS student, for his help with the experimental setup.
- Alexandra Camargo-Salinas, McGill University student, for her Taguchi Analysis of the 1-D model.
- Eric St-Amant, Research Assistant at McGill University, for computer technical support and DSC experiments.
- Martine Dubé, Ph. D. candidate, McGill University, for her help to debug the experimental setup.

Table of Contents

List of Figures

List of Tables

1 Introduction

In the aerospace industry, strength- and stiffness-to-weight ratios of materials play great roles in the design and manufacture of aerospace components. In that sense, organic matrix (elastomer, thermoset and thermoplastic) composite materials are advantageous; they can reduce the weight, increase payload capacity, increase operational range and enhance the mechanical performance of structures [1]. These advantages clearly justify the need for the development of composite manufacturing and joining methods.

Many joining methods are currently available for composite materials, such as adhesive bonding and mechanical fastening. In the case of thermoplastic composite materials, welding can be another viable joining method, due to the re-processing properties of thermoplastic polymers [2]. Welding or fusion bonding consists of heating the polymer matrix at the interface of the laminates to be joined, physically causing polymer chain inter-diffusion, and then cooling the polymer to consolidate the joint. The heat at the interface can be generated by several methods, such as direct input of heat and generation of heat through frictional work or electromagnetic field [2].

Resistance welding has been identified to be a promising technique among various fusion-bonding methods [2]. It is a fast process with short welding times, ranging from 1 to 5 minutes, it requires little to no surface preparation and it is applicable to all thermoplastic polymers. In addition, the welding equipment is generally simple and inexpensive and can be designed to be portable for repair purposes [3]. In this method, the weld interface is heated by passing an electrical current through a resistive implant, a

so-called heating element, which is placed between the surfaces of the parts to be joined. The polymer at the interface melts by Joule heating of the heating element, and then diffuses and consolidates under the application of pressure, resulting in a weld. This technique also offers the possibility for reprocessing, if defects are detected at the weld interface, by re-heating the resistive implant.

The resistance welding process has been studied numerically and experimentally [2-4, 6]. Several issues such as overheating of the edges of the weld, non-uniform temperature distribution at the weld interface, and inconsistent weld strength have been reported [5-6].

1.1 General Goal

The main goal of this work is to extensively study the manufacturing process modelling of thermoplastic composites resistance welding, in order to investigate the issue of non-uniform temperature distribution at the weld interface and to propose possible solutions to overcome this issue.

1.2 Organisation of this Work

This thesis will present the thermal modelling of the resistance welding process and is organised as follows:

- Section 2 will provide a general overview of the joining of thermoplastic composites.

- Section 3 will present the history of the resistance welding process, focusing on thermal modelling and current issues with resis#tance welding, as well as the precise objectives of this thesis.
- Section 4 will introduce the finite element models developed in this study, along with the material properties and assumptions made in these models.
- Section 5 will use the models developed in section 4, in order to investigate the influence of different processing parameters on the thermal behaviour of the weld interface.
- Section 6 will compare numerical results with experimental data, and propose a modified 3-D model, more adapted to the setup used.
- Section 7 will resume the main outcomes of this work and propose future work.

2 Thermoplastic Composites

Unlike metals, the mechanical properties of polymer composites depend mostly upon ambient temperature and loading rate [7]. The behaviour of a composite material highly depends upon the glass transition temperature of its polymer matrix. Near this defined glass transition temperature (T_g), the polymers change from a hard, glasslike, sometimes brittle, solid state, to a softer, rubberlike, but tougher solid. Below T_g, the composites behave as elastic materials such as metals. Around T_g, the material becomes highly viscoelastic. When increasing the temperature, the material changes into a rubberlike solid, capable of undergoing large elastic deformations. As the temperature is increased further, amorphous and semi-crystalline thermoplastics achieve highly viscous states. Semi-crystalline thermoplastics also show a sharp transition in the mechanical properties at the crystalline melting point (T_m), where all the crystals melt and the polymer becomes fully amorphous and viscous, as opposed to a thermoset polymer, where the rubberlike state directly burns, as the temperature gets too high.

Thermoplastic polymers are defined as polymers having a linear chemical structure, with no cross-linking between them [7]. These polymers are held in place by weak chemical bonds. Therefore, under the application of heat and pressure, these bonds can be temporarily broken and the molecules can move relative to each other. Upon cooling, these molecules freeze in their new position, and weak chemical bonds are re-established. Hence, a thermoplastic polymer can be heated, softened and reshaped. This is what makes welding possible.

Finally, the main advantages of thermoplastic polymers over thermoset polymers are: higher strain-to-failure, higher impact strength and fracture toughness, and better damage tolerance and fatigue resistance. Thermoplastic polymers also offer an infinite shelf life, shorter fabrication times, excellent corrosion and solvent resistance, ease of handling and possibility of post-forming, such as thermoforming, welding and recycling [1-2, 7]. However, thermoplastic polymers have some drawbacks in comparison with thermoset polymers, such as higher melt viscosities, lower creep resistance and higher processing temperatures.

2.1 Poly-ether-ether-ketone

In this study, poly-ether-ether-ketone (PEEK) has been chosen as the matrix for the carbon fibre composite. PEEK is a thermoplastic matrix that may replace epoxies in many aerospace applications, due to its outstanding fracture toughness, being 50 – 100 times higher than epoxies. Other important characteristics of PEEK include its low water absorption and high chemical resistance. The molecular structure of poly-ether-ether-ketone is shown in Figure 1.

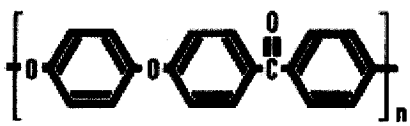

Figure 1: Representation of a poly-ether-ether-ketone molecule [7]

PEEK is a semi-crystalline polymer that can achieve a crystallinity level of up to 48% under slow cooling rate conditions such as 0.5°C/min. However, under normal cooling conditions, i.e. 5 – 50°C/min, a crystallinity level of about 30 – 35% is achieved. Increasing PEEK crystallinity increases its modulus and yield strength, but decreases its strain-to-failure. PEEK has a glass-transition temperature (T_g) of 143°C and a crystalline melting range between 330°C and 343°C. The typical processing temperatures of PEEK are at 370 – 390°C [7].

2.2 Joining of Thermoplastic Composites

Advanced thermoplastic composite materials have many advantages that clearly justify knowledge development in the areas of manufacturing and joining of thermoplastic composites. Figure 2 shows the different methods that can be used for joining thermoplastic matrix composites. The three main classes are adhesive bonding, mechanical fastening and welding or fusion bonding.

Many studies have showed that fusion bonding is a good alternative way to assemble thermoplastic composite parts over mechanical fastening and adhesive bonding [8-10]. Fusion bonding, in principle, consists of surface preparation (if necessary), heating the polymer at the interface to a viscous state, physically causing polymer chains to inter-diffuse, and cooling the polymer for joint consolidation. In fusion bonding, the heat at the welding interface can be applied in different ways, which classify the different types of fusion bonding.

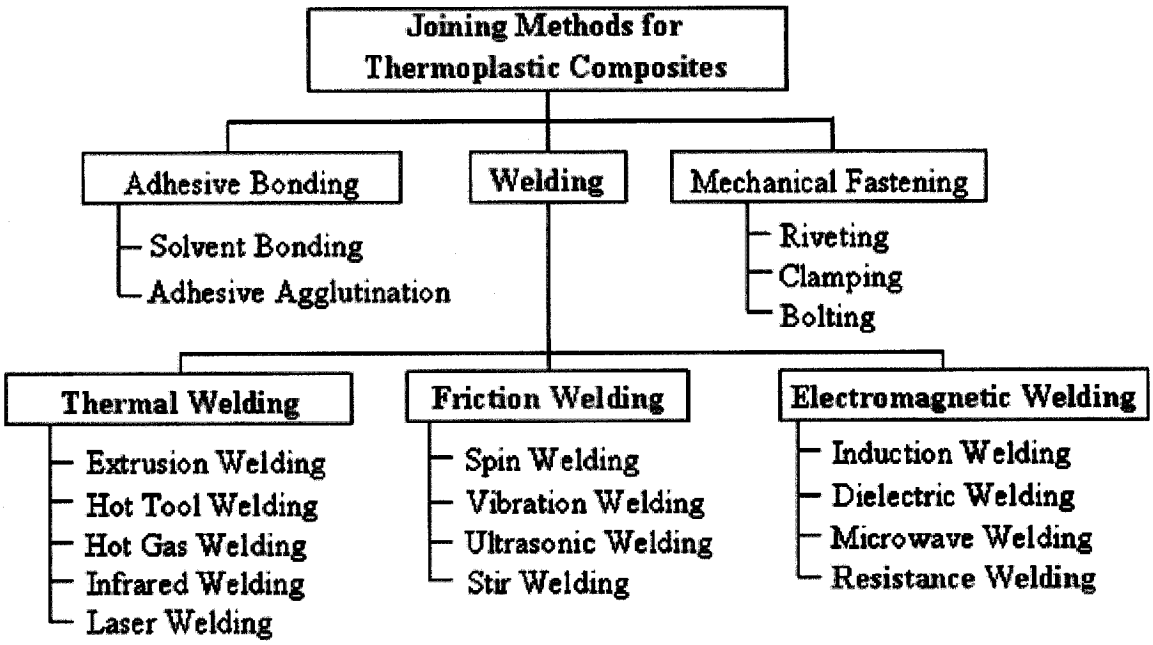

Figure 2: Methods for joining thermoplastic composites [2]

2.2.1 Thermal Welding

Thermal welding consists of using an external heat source, e.g., hot-tool, infrared, hot-gas, laser, etc., to apply heat directly to the individual bonding surfaces, to melt the matrix. Then, the parts are brought together under the forging pressure. However, thermal welding has limitations, in terms of size of components to be welded, since the entire welding surfaces must be heated in a single step. This technique also requires a long heating period, as well as a high welding pressure to consolidate the polymer [2]. Figure 3 shows schematics of different thermal welding methods.

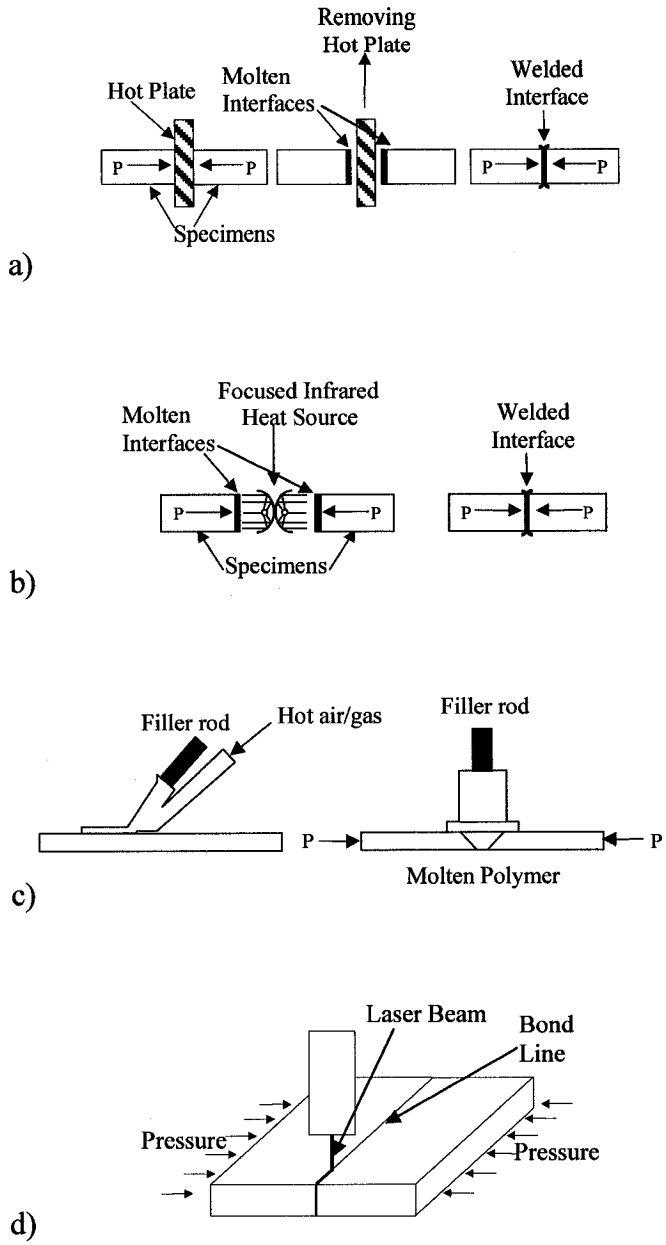

Figure 3: Schematic of different thermal welding methods a) Hot-tool welding, b) Infrared welding, c) Hot-gas welding, d) Laser welding [2]

Hot-tool or hot-plate welding (Figure 3a) consists of placing a hot tool/plate between the parts to be joined, in order to melt the interfaces. Then, the hot-tool is removed and the parts are brought together under an applied pressure, until the polymer solidifies [11].

There are several advantages with this technique. Dissimilar thermoplastics can be welded, the temperature of the molten interfaces can be accurately controlled, surface inaccuracies can be taken into account during the process, and it can handle complex geometries. However, its use is limited since the melted polymer has a tendency to stick to the hot-tool. Hot-tool welding has applications in the automotive industry. It has been used to join plastic battery cases, fuel tanks, and fuel pipes. Infrastructure applications, such as gas and water distribution, sewage and effluent disposal pipes, have also used hot plate welding [12].

In contrast to hot-tool welding, infrared welding (Figure 3b) is a non-contact welding technique. In this technique, the interfaces to be bonded are heated through exposure to intense infrared radiations, produced by high-intensity quartz lamps. Then, the infrared heater is removed and the parts are pressed together until the polymer solidifies [13].

Hot gas welding of thermoplastics (Figure 3c) is somewhat similar to gas welding of metals, except that the open flame is replaced by a stream of hot gas [14]. In this technique, the bond surfaces are melted with the hot air/gas stream, then, the thermoplastic filler rod is pushed into a groove cut between two sheets, as in a butt weld, and is heated until it softens enough to fuse the surfaces under pressure. However, this technique may not be suitable for lap shear joints.

Extrusion welding (Figure 3d) is similar to the hot gas welding except that the molten filler material is extruded into the joint [15]. Hot gas is still needed to heat the interfaces. Hot gas and extrusion welding are flexible techniques that each require simple and portable equipment, and can be used for fabricating large, complex parts. However, these

techniques are slow processes, difficult to control, and not suitable for high production rates. Hot gas and extrusion welding are used for welding polyolefin tanks and repair of thermoplastic containers. Hot gas and extrusion welding are mostly applied to thermoplastic parts and have the potential to weld particle filled thermoplastic or short fibre reinforced thermoplastic composites.

Most laser welding applications are limited to metals. However, laser beams can also be used to weld thermoplastic polymer and even thermoplastic composite parts. The two parts are pressed together as the laser beam passes along the bondline. The laser beam decomposes (burns) some of the polymer along its path but leaves behind a thin layer of molten polymer at the bond line, which under pressure are brought together to solidify, thereby resulting in a weld [16].

2.2.2 Friction Welding

Friction welding consists of heating the surfaces of the parts to be joined by frictional work under pressure, followed by cooling and consolidation of the polymer. Several methods are available to generate heat at the joint interface from frictional work, such as linear vibration welding, spin welding, ultrasonic welding, and friction stir welding. Figure 4 shows these friction welding methods.

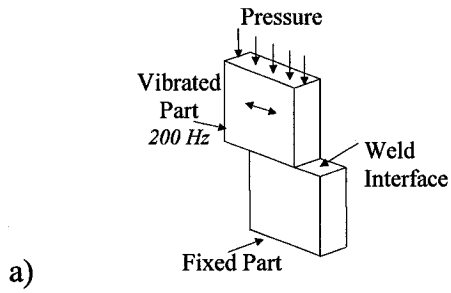

a)

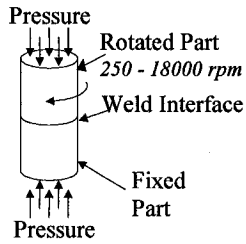

b)

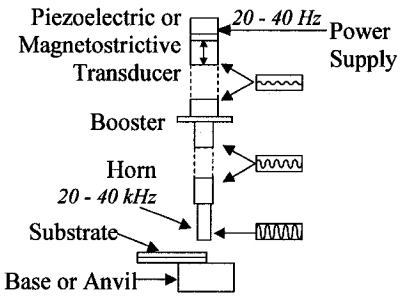

c)

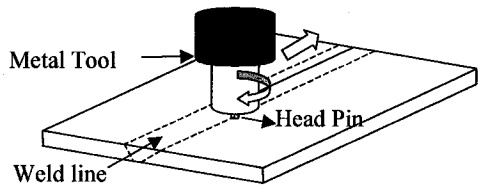

d)

Figure 4: Schematic of various friction welding methods a) Linear vibration welding, b) Spin welding, c) Ultrasonic welding, d) Friction-stir welding [2]

In linear vibration welding (Figure 4a), the two parts to be joined are brought into contact under pressure. One part is fixed and the other is vibrated parallel to the interface at a suitable frequency, until enough heat is generated by mechanical friction and shear stresses at the interface to melt and mix the thermoplastic polymer. Afterwards, the linear vibratory motion is stopped, the parts are aligned and the molten polymer consolidates under applied pressure, resulting in a weld [17]. The main advantages of vibration welding are high production rates, relatively short cycle times, ability to weld a number of components simultaneously, suitability for welding small-to-medium sized parts, ability to weld almost all thermoplastic materials including amorphous, semi-crystalline, and crystalline polymers, ease of process control, and insensitivity to surface preparation. However, this technique is not suitable for welding non-flat–seamed parts and causes fibre distortion/displacement at the interface. Finally, machines that can provide a wide range of welding frequencies, amplitudes, and pressures with good control are expensive. Vibration welding has found its main applications in the automotive and domestic appliance industries. Automotive applications include front and rear light assemblies, fuel filler doors, spoilers, instrument panels, ductwork and reservoirs for brakes, power steering, and vacuum systems [14].

Spin welding (Figure 4b) is one of the most common friction welding techniques used to weld thermoplastics and filler-reinforced thermoplastic composite components along circular mating surfaces. In this process, one of the parts is fixed while the other is rotationally rubbed against the fixed part under a specific angular velocity and axial pressure until melting occurs, followed by the cooling and solidification of the polymer. The advantages of spin welding are high weld quality, simplicity, speed, and

reproducibility [19]. In most cases, little surface preparation is necessary. This method is mostly suitable for circular components and hollow sections with thin walls. Orbital welding can be used in the case of non-circular components, however the process is much more complex than spin welding although the principle is the same. Spin welding is mainly used to join thermoplastic polymer parts such as sealing water-filled compasses by spinning the cover onto the base while the base is immersed in a fluid, manufacturing of floats and aerosol bottles, and attaching studs to plastic parts [12]. Spin welding has the potential to weld thermoplastic composite parts and it is believed that this is a suitable technique to weld together thermoplastic composite tubes or tubes to flat plates.

Ultrasonic welding (Figure 4c) is a process that uses a high frequency, i.e., ultrasonic, mechanical vibration to weld parts. The parts to be welded are held together under pressure and then subjected to a high frequency vertical or parallel oscillation, depending on joint geometry, to transmit vibrations through the material. The heat is generated by a combination of surface and intermolecular friction in the material. Ultrasonic welding is a fast and clean process, and usually produces welds that are relatively free of flash. The main disadvantages of this technique are the difficulty of providing ultrasonic energy directors on sheet components and the consequent risk of fibre disruption at interfaces under the high deformation necessary to obtain a satisfactory bond. Another difficulty in ultrasonically welding thermoplastic composites is heat conduction by graphite fibres away from the bonding surface, which leads to a long welding time [20]. The size and power of a welding machine also limits the area that can be bonded in one operation. Ultrasonic welding is mainly used in automotive parts, floppy disks, medical devises, and

battery housings. This process has great potential for spot welding of thermoplastic composite parts, particularly in aerospace applications.

In friction stir welding (Figure 4d), the parts to be welded are placed firmly together and a rotating metal tool or head-pin (HP) drives along the joint line. The frictional work generated by rotation of the tool shoulder and the HP converts to heat and causes softening or melting of the material at the bond line. As the tool translates along the joint line, softened polymer is stirred and forged [21]. Friction stir welding has great potential for welding particle-filled thermoplastics or short-fibre reinforced thermoplastic composites, but its potential to weld continuous fibre reinforcement thermoplastic composites still requires further investigation [2].

2.2.3 Electromagnetic Welding

The last class of fusion bonding techniques is electromagnetic welding. Electromagnetic welding consists of applying a high-frequency magnetic field to a magnetic material, such as opaque powders or iron oxide, stainless steel, ceramic, ferrite, or graphite inserts, usually placed between the parts to be joined, causing joule heating and melting the polymer at the joint interface [22]. Electromagnetic welding techniques include induction welding, dielectric welding, microwave welding, and resistance welding. Figure 5 shows these electromagnetic welding methods.

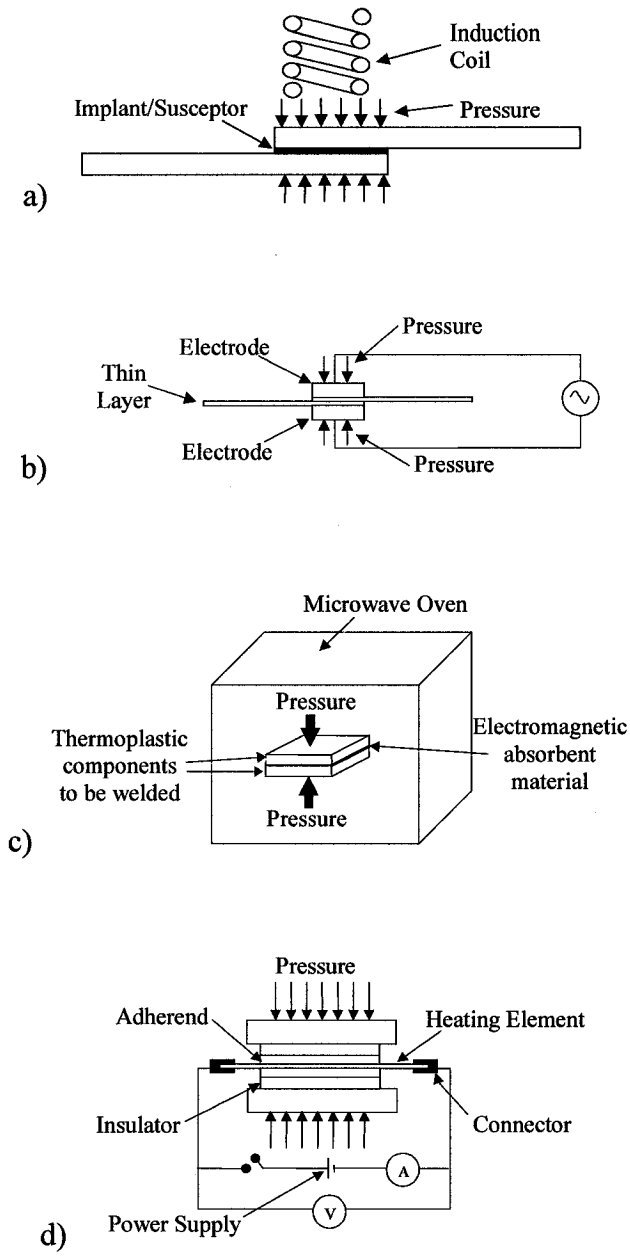

Figure 5: Schematic of various electromagnetic welding methods a) Induction welding, b) Dielectric welding, c) Microwave welding, d) Resistance welding [2]

In induction welding (Figure 5a), heat is supplied to the thermoplastic polymer by an implant or susceptor positioned in a high- (radio-) frequency electromagnetic field in the range of 200 to 500 kHz. The implant is made of ferromagnetic materials and conforms

to the shape of the bond area. The implant can be in the form of foil-like tape, or micron sized particles molded in the polymer. An electromagnetic coil generates a magnetic field and induces eddy currents within the implant, where the heating occurs by resistance heating. The increasing temperature of the implant brings the surrounding polymer to the melting temperature. The joint is pressurized until the thermoplastic polymer solidifies, resulting in a weld [23]. Induction welding is a fast and clean process. It can be applied to complex geometries with irregular contoured surfaces. In this process, the weld can be re-opened by induction re-heating which makes it possible to open an assembly for internal repair, part replacement, and repair defective welds [24]. The main drawbacks of this process are high cost of the insert materials, non-uniform heat distribution at the bondline, and difficulty of welding large parts [14].

In dielectric welding (Figure 5b), also called radio-frequency welding, an intensive electromagnetic field, in the MHz frequency region, is applied to heat the polymer [14]. Polymers with high dielectric loss factor convert some of the field energy to heat during changing of the field polarity. The intense field is applied to the polymer by two electrodes that are pressed against both sides of the parts to be joined. This technique is more suitable for thin thermoplastic composite structures. Dielectric fields are commonly applied for heating and melting thermoplastic and thermoset curing as well as for adhesive curing of bonded joints. The main application for this process is medical equipment such as sealed bags. The ports for entry into the sealed bags can be made in one to several seconds depending on the material, film thickness, and weld area [12].

In microwave welding (Figure 5c), a thin layer of electromagnetic absorbent material is placed between the joint elements in the presence of welding pressure and then intense

microwave energy in the GHz region is applied. The microwave energy induces a temperature increase in the electromagnetic absorbent material and consequently the electromagnetic absorbent material conducts heat to the joint elements and bondline, creating a molten layer of polymer at the interface. The electromagnetic absorbent material can be heated with different mechanisms including eddy current, hysteresis, or dielectric loss [25]. Microwave welding is a clean and fast process. In the presence of sufficient electromagnetic absorbent material at the interface, the part can be repaired or disassembled by microwave re-heating [25-26]. The temperature distribution at the joint depends on the electromagnetic absorbent material and the oven configuration. This limits the size of the parts that can be welded [18]. The main concern in welding composite structures using this method, especially for graphite-reinforced composites, is the shielding effect of fibres to the electromagnetic field at microwave frequencies (i.e., 1 to 100 GHz), causing bulk heating of joint elements. [27]. The shielding effects are due to reflection and absorption of the radiation within the top layers of multidirectional composites.

In resistance welding (Figure 5d), an electrical current is applied to a resistive implant to increase its temperature, due to resistance heating. The increased temperature of the implant, melts the polymer at the weld interface, and creates a weld under the application of pressure [2]. Resistance welding has found applications in the automotive industry [12] , i.e. vehicle bumpers and other parts. It is also used to weld plastic pipes, containers and medical devices. Moreover, it has shown great potential for welding thermoplastic composite parts. Resistance welding will be discussed in detail, in Section 3.

3 Resistance Welding Process Review

Among the different methods of fusion bonding, resistance welding is one of the most promising [28]. Resistance welding is a fast, simple and inexpensive process that can be made portable for repair purposes. Resistance welding is a special type of electromagnetic welding, where an electrical current is applied to a heating element placed at the bond-surface (or weld interface) of the thermoplastic composite parts to be welded. This element heats up, due to Joule heating, thereby softening and melting of the polymer at the weld interface. When the temperature of the polymer reaches the processing temperature, the electrical current is stopped. Under the application of pressure, molecular diffusion, entanglement, consolidation and solidification of the matrix occur [29-30], resulting in a weld. Resistance welding can be used to weld most thermoplastic-based materials. Moreover, this process can be applied to large structures [31]. Since the implant remains in the bond, material compatibility between the elements to be joined is important.

3.1 Set-up Components

Figure 6 shows the schematic of a typical resistance welding set-up [30-32]. The main components of the set-up consist of the parts to be welded or adherends, a heating element, an electrical power supply, tooling-plates, and a pressure system. Process parameters, such as melting temperature, input power, welding time, and applied pressure, depend on the material of the parts to be welded. As an example, an input power of 100W and a welding time of 50s were reported for a coupon size weld, i.e. 12.7

mm by 25.4 mm lap-shear overlap of two APC-2/CF laminates having a typical melting temperature of 343°C [33-34].

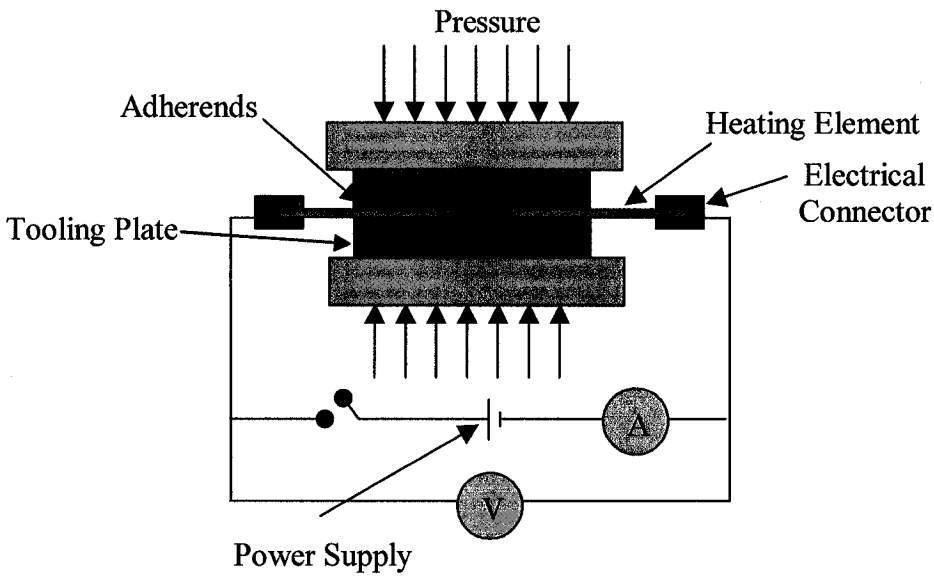

Figure 6: Schematic of a typical resistance welding set-up

3.1.1 Power and Pressure Systems

A controllable DC power supply inputs the proper power to the heating element during the heating step of the process [35-36]. The pressure system provides adequate pressure through the tooling-plates on the weld to prevent any undesirable movement of the adherends and to ensure polymer diffusion, consolidation, and solidification at the weld.

3.1.2 Adherends

The adherends are made of a thermoplastic composite material. In the past 20 years, researchers focussed on poly-ether-ether-ketone (PEEK) matrix composites, reinforced with carbon fibres [3, 30, 36-37-38]. However, recently, poly-ether-imide (PEI) reinforced with carbon or glass fibres has gained interest [32-35, 39- 40- 41]. Some studies were also conducted on polypropylene reinforced with glass fibres [42] or carbon fibres [43]. Various reinforcement orientation have been studied, such as 0° laminates [3, 28, 36, 47-48, 53, 56], 90° laminates [3, 36], quasi-isotropic laminates $(0/\pm45/90)_{2S}$, [31, 44], and satin woven fabric (0/90) laminates [5, 39-40, 66].

3.1.3 Heating Element

The heating element is the component that generates the necessary energy at the interface of the two adherends to be joined. The heating element can be made of a layer of any conductive material, but a layer of metal mesh, carbon strip or conductive prepreg thermoplastic composite are commonly used [43]. After the welding, the heating element remains trapped in the joint.

The heating element is usually sandwiched between two layers of neat thermoplastic polymer film. These neat polymer films act as insulators, facilitate melt flow at the bond surface, stop current leakage, prevent preferential heating, and consequently provide better weld quality [36-38, 45-].

Metal mesh heating elements offer a number of advantages compared to carbon fibre heating elements, producing welds with better consistency and higher average strength

[43, 47]. Stainless steel heating elements show a very good bonding between the mesh and polymer matrix, allowing for a larger processing window [39-40]. Also, a stainless steel mesh yields welds with negligible fibre disturbance and consistently high failure strength as compared to prepreg heating elements [48]. However, the main disadvantage of using a metal mesh is the potential corrosion of the implant [49-50].

The ends of the heating element are connected to a DC or AC electrical power supply through electrical connectors (see Figure 6). These electrical connectors are usually made of brass or copper. The metal mesh heating elements are also much less sensitive to the clamping pressure achieving the connection than the carbon fibre heating element [32]. A minimum pressure of 4 MPa must be applied [32], in order to have a constant electrical connection, but an excessive clamping pressure over 20 MPa [32] may damage the heating element and decrease its efficiency.

3.2 Welding Parameters

Resistance welding is a delicate process [6]. In order to obtain the optimal joint, the welding parameters, such as welding pressure, power and total energy input in the weld, must be carefully optimized, for each welding set-up configuration.

3.2.1 Welding Pressure

The welding process pressure can be applied under constant load or displacement control [40, 45]. The constant load must be used when more polymer is squeezed out of the weld, in order to assure an adequate pressure during the whole process, whereas a displacement

control can be used when only a small region of polymer is affected, so a sufficient pressure can be maintained.

3.2.2 Power Input

The resistance of the heating element determines the power level input during the process, since the power generated inside the weld is calculated from $P = RI^2$ [51]. The power input in the weld influences the weld quality [45-46, 52]. Also, controlling the heating/cooling rates improves the weld quality and mechanical performance of the weld. Thermal insulation, adherend fibre orientation, and type of heating element also influence the welding time, the quality and the performance of the resistance welded parts [52]. Ageorges *et al.* [32] also monitored the variation of the resistance of the heating element, during heating, indicating that the power generated at the weld interface may vary with time.

3.3 Temperature Distribution

Due to heat losses in the laminates, tooling and environment and to the fact that the temperature distribution is time dependant, an ideal uniform temperature distribution at the weld interface cannot be achieved. This non-uniform temperature distribution leads to substantial problems such as preferential heating and melt front propagation, the melted region expanding through the thickness of the weld. It can also be a problem during the scale-up of the process.

3.3.1 Preferential Heating

Eveno *et al.* [36] observed local heating within the heating element and at the edges of the weld, resulting in incomplete welds and current leakage into the adherends. Various experimental solutions to this problem have been proposed, such as active cooling of the edges of the weld [31, 53] and insulation of the heating element [41]. Moving the clamps closer to the edges of the welded part was also reported to have a significant influence on the temperature distribution along the direction of the heating element [5-6].

3.3.2 Melt Front Propagation

Eveno *et al.* [36] experimentally observed that the temperature at the edges of the weld was substantially higher compared to the interior regions. They explained the phenomenon by the transition of the heat transfer mechanism from convection to air into conduction to the laminate at the edges of the weld. This non-uniform temperature distribution at the weld interface creates a melt front propagation as the welding takes place. They also [36] observed that this phenomenon is in fact three-dimensional, meaning that the penetration depth of the melt front varies along the length of the laminates and across the width of the weld.

Hou *et al.* [49] studied the melt front propagation by looking at the temperature distribution at the weld interface. They showed that the melting first initiates at the edges of the weld. Then, the two melted regions at the edges of the weld extend towards the center of the weld interface, in the direction of the electrical current. Finally, when the two initially melted regions meet, the melt front widens, until the welding interface is completely melted, as shown in Figure 7.

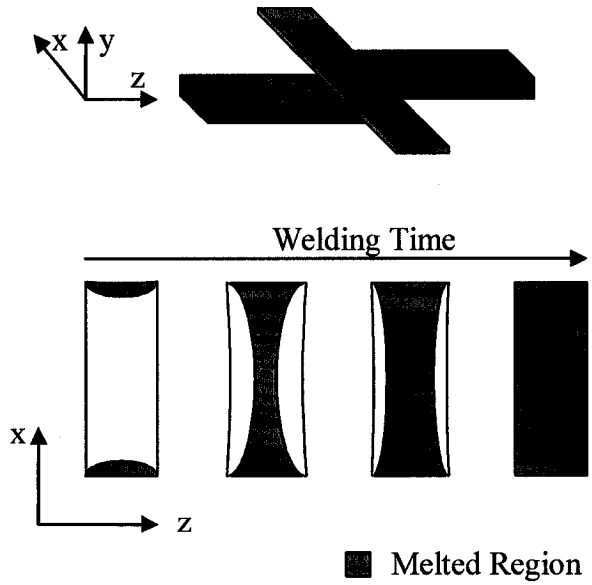

Figure 7: Schematic illustration of the melting process [49]

3.4 Alternative Methods

As a result of its numerous advantages for joining thermoplastic composites, many techniques emerged using the resistance welding principle.

3.4.1 Sequential Welding

Most studies undertaken on resistance welding were performed at the coupon-size level, proving the feasibility of the process and facilitating the understanding of its behaviour. However, most applications for resistance welding require much larger welding areas. Hence, another issue for the resistance welding process is that a simple scale-up of coupon-size welds leads to substantial power and load requirement [35].

A proposed multiple-step or sequential resistance welding technique has been proposed to solve the problem [31, 54]. This technique consists of dividing the welding area into smaller segments that are welded in sequence. Sequential resistance welding gave rise to higher weld uniformity and better lap shear strength than a single-step welding technique. The problem of non-uniform heating was reduced and a lap shear strength of 28.7 MPa was obtained. For the single step technique, the weld strength was 17.7 MPa [31]. Also, lower load and weld power were required for the sequential welding technique than for the single step welding technique [31]. These findings demonstrated the great potential of the resistance welding process for welding large structures with high quality and performance requirements.

3.4.2 Impulse Resistance Welding

Impulse resistance welding is a new technique aiming at reducing the heating time and the overheating/delamination problems of the resistance welded laminates. This technique consists of applying the power in the form of intense pulses, instead of using a continuous power during the process. Impulse resistance welding requires less energy to melt the matrix due to lower heat losses. Also, the melt front propagation does not penetrate deeply into the laminate, and the edge effects, or overheating of the free laminate surfaces is diminished [41,55]. However, the relatively high power impulses generate significant temperature non-homogeneity at the weld interface and temperature can only be re-distributed if long cooling segments are inserted between impulses. However, this procedure induces longer processing times and raises the potential for heat dissipation to the laminates. Arias *et al.* [41] employed impulsive resistance welding to

successfully join a rib to the skin of an aerodynamic spoiler part, however, mechanical performance was not reported.

3.4.3 Ramped Voltage

The ramped voltage technique consists of applying a power increasing at a constant rate. This technique lowers the total energy input into the weld, decreases the cooling time and improves the strength of the joints [56].

3.4.4 Others

Resistance welding can also be used as a hot-melt adhesive for joining dual-polymer composites [57], thermoplastic composites to thermoset composites [58] and even to metals [59].

3.5 Resistance Welding Process Modelling

Depending on the uniformity of the thermal history of the joint, its quality and performance vary enormously [34, 47, 55, 60]. Thermal analysis can be used to determine thermal insulation, input energy, and heating time for sufficient heating at the interface to ensure a high quality bond [3]. Xiao *et al.* [61] used finite element modelling to show that a good thermal insulation and a correct amount of input energy can reduce the welding time and enhance weld quality. Hence, a better understanding of the thermal history at the weld interface is the key to obtain a good weld quality.

3.5.1 Insulating Material Effect

Maffezzoli *et al.* [62] developed a one-dimensional (1-D) mathematical model for the resistance welding process to predict the heat conduction through the thickness of the welded parts, away from any edge effect, taking into account the kinetics of melting and crystallization of the matrix. The model also compares the effects of different boundary conditions, arising from the use of different insulating materials, such as steel or ceramic: the heating time is longer when using a metallic tool than when using a ceramic tool. Hence, the steel tool acts as a heat sink, causing bulk heating of the weld stack and melt front propagation through the thickness of the weld, increasing the chances of fibre motion. Jakobson *et al.* [53] and Holmes *et al.* [33-34] confirmed Maffezoli's [62] conclusions that the tooling materials influences the heating process. However, Jakobson *et al.* [53] and Holmes *et al.* [33-34] modeled, respectively using finite difference and finite element models, the tooling with an equivalent convection coefficient, h, at the top and bottom boundaries of the welded parts. This is not the proper way to investigate the process, since the process is not in a steady-state regime (See Appendix A).

Colak *et al.* [63] also used a 1-D model to show that the minimum welding time is increased with steel and aluminium, compared to that using ceramic insulation. In addition to that, Colak [63] showed that the heating rate and the cooling down rate are increased when using thicker insulator, up to a certain thickness. They also showed that the minimum welding time decreases with increasing laminate thickness.

Xiao *et al.* [61] developed a 2-D finite element model and obtained similar findings as Holmes *et al.* [33]. Xiao *et al.* [61] showed that a simple variation in the resistance

welding set-up, such as a variation in the tooling-plate thickness or material could greatly influence the thermal history and processing parameters of the weld. Therefore, process modelling of the resistance welding is recommended as a useful tool to reduce the process development cost and improve the weld quality.

3.5.2 Preferential Heating

Jakobson *et al.* [53] simulated the thermal behaviour of the resistance welding process using a transient two-dimensional (2-D) anisotropic finite difference model. The model represented a cross-section of the weld, in the plane of the through-thickness and electrical current directions. The model determined the time-to-melt (i.e., time required for the temperature at the weld interface to reach the polymer melting temperature) and the locations of local heating and preferential heating, along the width of the weld, relying on the heat conduction equation.

Holmes *et al.* [33-34] 2-D model considered the influence of the edge effects on the thermal gradient along the weld interface (i.e., the width of the welds) taking into account the convective and irradiative heat losses from the part of the heating element that are exposed to air. Akin to Jakobson *et al.* [53], they used a constant convection coefficient to represent the ceramic insulation. The 2-D model clearly showed the presence of a large thermal gradient at the edge of the welds, for different heating times and that the temperature gradient decreases radically away from the edges. They conclude that the change in the heat transfer mechanism from convection and radiation to conduction to the adherends causes local overheating of the edges, as observed experimentally.

3.5.3 Latent Heat

One and two-dimensional heat transfer finite element models were developed by Holmes *et al.* [33-34] to simulate large-scale welded assemblies. The 1-D model simulated the thermal gradient through the weld thickness away from edge effects. Their conclusion is that including the latent heat of fusion, energy required to melt the polymer, in the model has not much influence on the modeled thermal history of the weld interface. Moreover, Ageorges et al. [64-65] showed that using temperature-dependant material properties, such as including the latent heat of fusion or the latent heat of crystallisation of the polymer, does not induce significant changes in the time to melt. It should be noted that the latent heat used by Holmes *et al.* [33-34] was 460 kJ/kg, but the correct value is 44 kJ/kg, as used by Ageorges et al. [64-65]. However, although Holmes *et al.* [33-34] did not use the appropriate value, the same conclusions have been drawn.

3.5.4 Surface Roughness and Non-Uniform Heating of Fibre Bundles

Ageorges *et al.* [64] developed a 3-D transient finite element model of the lap-shear specimens. However, their model is only one eighth of the weld, neglecting the heat transfer to the length of the laminates. The model accounts for the surface roughness at the interfaces of polymer films, heating element and adherends, below the melting temperature. The surface roughness was modeled with varying gap thickness and percentage of contact area. They also accounted for non-uniform heating of their carbon fibre heating element by modelling the fibre bundles and assuming that the heat is generated only by the fibre bundles, rather than the entire heating element. These two improvements to the finite element model were not significant.

3.5.5 Effect of Consolidation Pressure

Ageorges *et al.* [66] used their model to determine the local degree of intimate contact and local degree of bonding as a function of process time. They obtained thermal degradation in the heating element for high power levels. They also concluded that the consolidation pressure does not affect the time to reach full intimate contact, but that below a given threshold, the bonding times increase dramatically. Colak *et al.* [63] confirmed that result.

3.5.6 Material Properties

Jakobson *et al.* [53] showed that the variation of density of the APC-2/AS4 laminates with temperature is negligible, but that the resistance of the heating element has a considerable influence on the time to melt. Some modelling studies have shown that fibre orientation also has an influence on the welding time for a given power, since the thermal conductivity of the adherends is a function of fibre orientation [61, 67].

3.5.7 Crystallinity

Ageorges *et al.* [65] modeled the crystallinity of PEEK polymer after welding cool down, using the crystallinity models of Osawa [68], Velisaries *et al.* [69] and Choe *et al.* [70]. They found that for PEEK, an acceptable stable value of about 25% can be achieved, under natural cooling, for power levels ranging from 52-120 kW/m^2. For lower power levels, they showed that the crystallinity level is much lower, due to the existing crystals in the polymer that are not fully melted, restraining the extent of crystallisation of PEEK in the cooling down step.

3.5.8 Impulse Resistance Welding

Ageorges *et al.* [55] created a numerical model of the impulse resistance welding process and concluded that the thermal non-uniformity of very high nominal power levels can be overcome only by increasing the time between the pulses. However, good care must be taken, so that the melt front does not propagate through the thickness of the laminate, causing bulk heating.

3.5.9 Comparison with experimental data

Although all of these models have been realised, only a few of these were compared to some experimental data. In fact, Holmes *et al.* [33-34] compared their 1-D model with limited experimental data, but it did not match well. Ageorges *et al.* [64-66] managed to match the time to melt, with their model, but no thermal history has been shown to match modelling results.

3.6 Summary of the Current Issues with Resistance Welding

These first three sections have shown the current issues with resistance welding. The most important one is the non-consistent mechanical performances reported [34, 47, 55, 60]. This creates doubts on the reliability and repeatability of the process. Then, the current leakage, preferential heating and non-uniform temperature distribution at the weld interface indicate that the process is very delicate and confirm the need for modelling as a tool to have a better understanding of the process. The following table summarizes each item studied with resistance welding modelling and the conclusions drawn.

Table 1: Summary of modelling analysis of the resistance welding process

Parameter	Importance	General Comment
Insulating Material	Yes	Must be selected appropriately and ceramic promotes faster welds. [33-34, 53, 61-63].
Latent Heat	No	Negligible influence on the heat dissipation in the weld stack. [33-34, 64-65]
Surface Roughness	No	Negligible influence on the heat dissipation in the weld stack [64].
Non-Uniform Heating of Fibre Bundles	No	Negligible influence on the heat dissipation in the weld stack [64].
Consolidation Pressure	No	No effect on the time to reach full intimate contact, but below a given threshold, the bonding times increase dramatically [63, 66].
Material Properties	Yes	The adherend fibre orientation does influence the thermal dissipation in the weld stack [61, 67]. Properties do not need to be input as temperature-dependant properties [52].
Crystallinity Level	No, for PEEK	Negligible influence on the heat dissipation in the weld stack [65], for PEEK.
Preferential Heating	Yes	Consequence of the change in the heat transfer mechanism from convection and radiation to conduction to the adherends [33-34, 52].
Impulse Power Input	Yes	Be careful to avoid bulk heating [55].

Also, the power and load limitations for welding large components have been addressed, but sequential welding was shown to be a viable solution. The bulk heating and fibre motion issues have also been raised. These are partly solved, using appropriate tooling materials. Finally, no model has been proven to adequately match any experimental temperature data obtained within the weld.

3.7 Objectives

The main objective of this thesis is to use process modelling of resistance welding to investigate the effects of processing parameters on the thermal history of the weld, in order to address the temperature non-uniformity issue. One-, two-, and three-dimensional transient finite element models are developed to perform a parametric study on the process. The models are used to:

- Determine the effects latent heat and tooling-plates material on the thermal behaviour of the welds during the process using the 1-D model;
- Investigate the effects of local heating and input power level on the welding time using the 2-D model;
- Study the effects of melt front propagation along the length of the laminates on the temperature distribution at the weld interface using the 3-D model.

A series of experiments will then be performed, in order to determine the actual thermal history of different locations within the weld, as well as the temperature distribution at the weld interface.

Finally, the numerical and experimental data are compared and modifications are included to the models in order to have a better representation of the process and experimental setup.

4 Process Model Definition

Finite element analysis (FEA) is used to simulate the resistance welding process, as it involves manufacturing process parameters such as input power, material properties, processing time, and boundary conditions [62]. The coupon size lap shear joint configuration is modeled as shown in Figure 8. The weld stack consists of two adherends, and a heating element sandwiched between two layers of amorphous polymer (see Figure 8). The weld stack is placed between two tooling-plates. ANSYS finite element analysis software was used for pre-processing, solving and post processing.

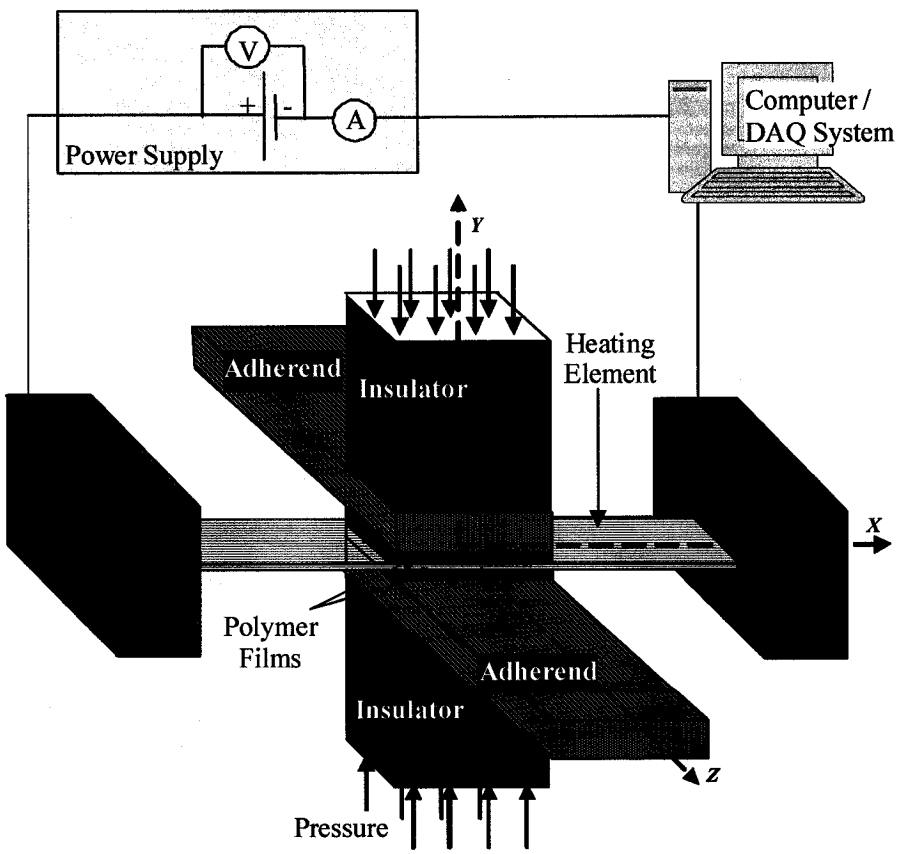

Figure 8: Lap-shear joint weld configuration

4.1 *Assumptions*

In order to simplify the model and to improve computational time, the following assumptions are made.

- The pressure and small displacements of the laminates are neglected.
- The process is modeled as a heat transfer problem only. Therefore, the flow of molten polymer out of the weld, due to the applied pressure, is neglected (i.e. the finite element mesh deformation is neglected).
- The resistance of the heating element is assumed to be independent of temperature. Also, the heat generated by the heating element is assumed to be a constant and uniform volumetric heat generation.
- The heated heating element is assumed to behave as a gray-body radiating object with an emissivity of $\varepsilon = 0.95$ [33-34].
- The surrounding air, providing only natural free convection, has been modeled with a constant convection coefficient h_{air} of 5 $W/m^2 \cdot K$ [33-34].

4.2 *Geometry and Material Properties*

Resistance welding of 16-layer unidirectional APC-2/AS4 laminates is simulated. APC-2/AS4 consists of a PEEK semi-crystalline thermoplastic polymer matrix reinforced with continuous AS4 type carbon fibres. The glass transition and melting temperatures of PEEK are 143°C and 343°C, respectively. The heating element consists of a thin stainless steel mesh, 0.08 mm thick, sandwiched between two layers of amorphous PEEK polymer film, 0.127 mm thick. The weld stack is insulated from the top and bottom with 37.5 mm thick tooling plates. Two sets of tooling plates are considered, i.e. grey Wonderstone alumina silicate ceramic [71] and stainless steel type 304 [72]. The

electrical copper connectors are also included in the model, in order to incorporate their influence on the thermal behaviour of the weld interface. A single lap shear joint configuration with a weld overlap of 12.7 mm is selected. The adherends are 101.6 mm long in the fibre direction, 25.4 mm wide, and 2.16 mm thick [73]. Figure 9 shows the geometry and dimensions of the weld stack.

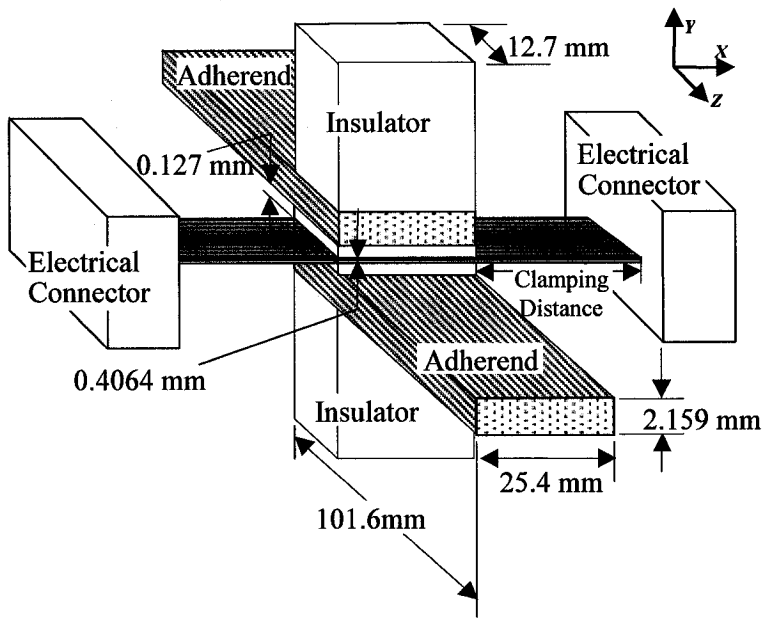

Figure 9: Dimensions of the weld stack (Not to Scale) [6]

Table 2 presents the room temperature material properties for the APC-2/AS4 laminate [34, 74], stainless steel mesh [72-75], PEEK film [34], copper connector [76], ceramic [71] and type 304 stainless steel [72] tooling plates. Note that k_{xx}, k_{yy} and k_{zz} stand for the thermal conductivity, in the x, y and z directions respectively. The heating element is a single plain weave cross-ply layer of stainless steel type 304 [72]. In order to determine its equivalent properties, the metal mesh is assumed to be embedded in PEEK. The

properties used to calculate the metal mesh heating element equivalent thermal conductivities are those of stainless steel type 304 embedded in PEEK. Appendix B shows how the material properties of the metal mesh have been calculated.

Table 2: Room temperature material properties [33-34, 71-76]

Material Properties	APC-2/AS4 Laminate	Metal Mesh	PEEK Film	Copper	Ceramic
k_{xx} (W/m.°C)	0.658	2.18	0.25	345	1.26
k_{yy} (W/m.°C)	0.658	0.21	0.25	345	1.26
k_{zz} (W/m.°C)	6.8	2.18	0.25	345	1.26
Density (kg/m^3)	1598 *	2973	1298 *	8900	2715
Specific Heat (J/kg °C)	930 *	735	944 *	385	1000

* Note that these properties are input as temperature-dependant.

Table 3 introduces the temperature dependent properties for the PEEK film and the APC-2/AS4 laminate [33-34]. Note that these temperature-dependent properties have been used in all the analysis.

Table 3: Temperature dependent properties of PEEK and APC-2/AS4 laminate [33-34]

Temperature (°C)	PEEK Density (kg/m^3)	PEEK Specific Heat (10^6 J/kg °C)	APC-2/AS4 Density (kg/m^3)	APC-2/AS4 Specific Heat (10^6 J/kg °C)
0	1305	610	1601	800
100	1285	1226	1593	1040
200	1239	1893	1575	1300
300	1177	2534	1551	1550
400	1108	2918	1524	1700

4.3 Finite Element Models

One, two, and three-dimensional transient heat transfer finite element models were developed to investigate the resistance welding process. Mesh convergence studies were performed on the obtained results with a convergence criterion of 5%. This means that once the results were obtained, the mesh was coarsened or refined and the model was run again. This process has been repeated, until the results obtained with a given mesh had a maximum of 5% difference with the most refined mesh.

4.3.1 1-D Model

The 1-D transient heat transfer finite element model simulates the thermal history through the weld thickness. This model represents a small section inside the weld, free from any edge effects. Therefore, zero heat flux boundary conditions are imposed on each side of the weld. A symmetry boundary condition, i.e., zero heat flux, is also applied on the XZ plane. Figure 10 shows the schematic of the 1-D model.

The heat exchange between the tooling plate and the ambient air is modeled with a natural convection condition, i.e., a convection coefficient of h_{air} = 5W/m^2·K and a sink temperature of T_∞ = 20°C [6]. A constant volumetric power density (HGEN) of q = 2.0 GW/m^3 is applied to the heating element to account for Joule heating, calculated with $q = R \cdot I^2 / U$, where q is the volumetric power density (W/m^3), R is the electrical resistance (Ω) of the heating element, I is the applied current (A), and U is the volume of the heating element (m^3). The model is meshed with PLANE55 elements [77]. PLANE55 has a 2-D thermal conduction and internal heat generation capabilities. Orthotropic

material properties can be applied to this four-node element with a single degree of freedom, i.e., temperature, at each node. The optimum model has 14 elements on top of each other (10 for the insulator, 2 for the adherent, 1 for the polymer film and 1 for the heating element). The model neglects the heat loss in the adherend.

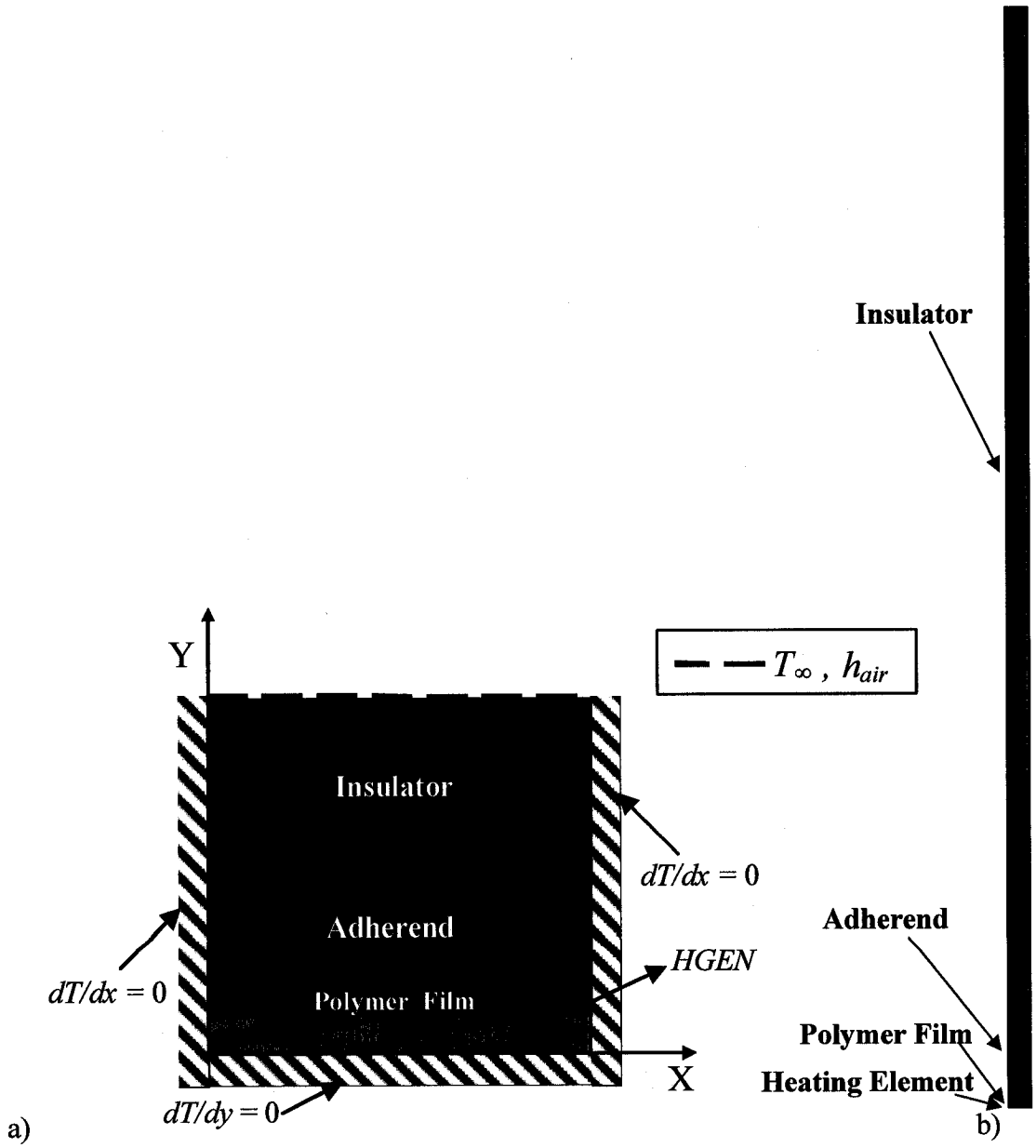

Figure 10: 1-D thermal model a) Schematic with boundary conditions b) Mesh

4.3.2 2-D Model

The 2-D model is used to investigate the temperature gradient along the width of the weld interface (see Figure 11).

The 2-D model accounts for the through-thickness heat transfer, but also the changes of heat transfer condition from convection and radiation to conduction at the edges of the weld due to exposure of the heating element to air. To reduce computational time, symmetry boundary conditions are applied on the X-Z and Y-Z planes. As for the 1-D model, a constant and uniform volumetric power density (HGEN) is applied to the heating element; and a natural convection boundary condition is applied to any surfaces that are exposed to air. In addition, a radiation boundary condition, with emissivity ε = 0.95 [7] and Stefan-Boltzman constant $\sigma = 5.67 \cdot 10^{-8}$ W/m^2·K^4, is applied to the areas of the heating element that are exposed to air. Finally, the 2-D model is meshed with PLANE 55 elements [77]. The optimum model has 320 elements, with the nominal clamping distance of 12.7 mm. The heat transfer in the adherend is neglected.

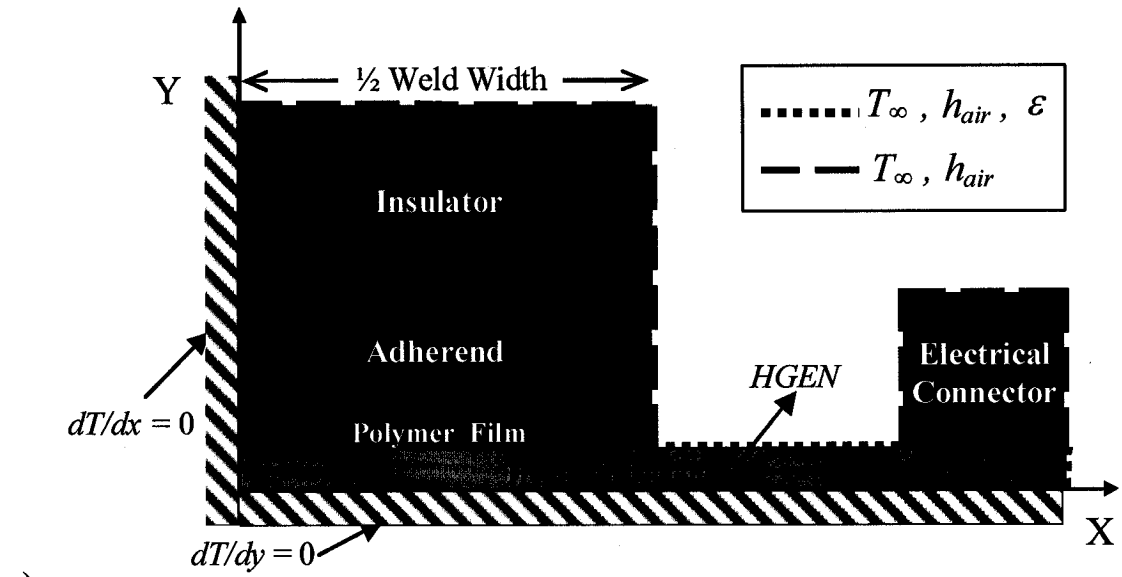

a)

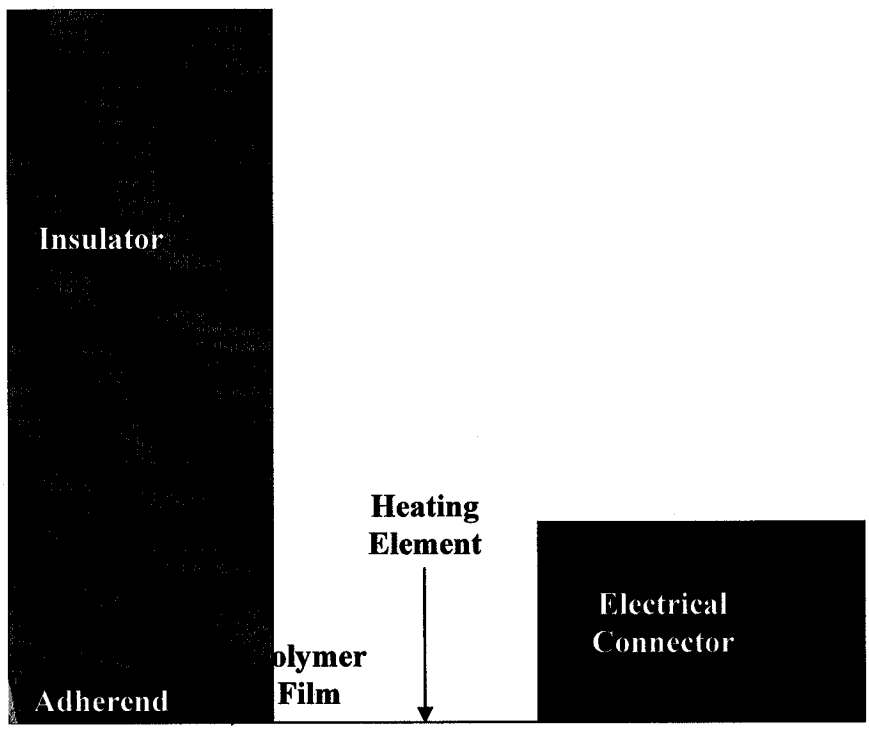

b)

Figure 11: 2-D thermal model a) Schematic with boundary conditions b) Mesh

4.3.3 3-D Model

The 3-D model, shown in Figure 12, is used to investigate the effects of heat conduction to the laminates (along their length) on the thermal history of the weld interface. A zero heat flux boundary condition is applied to the Y-Z plane. The boundary conditions and applied volumetric power density are similar to the 2-D model, i.e. a constant and uniform volumetric power density (HGEN) is applied to the heating element, a natural convection boundary condition is applied to any surfaces that are exposed to air and a radiation boundary condition, with emissivity $\varepsilon = 0.95$ [7], is also imposed on the areas of the heating element that are exposed to air. SOLID70 [77] elements are used to mesh the model. This element has 3-D thermal conduction and heat generation capabilities. Orthotropic material properties can be applied to this eight-node element with a single degree of freedom, temperature, at each node. The optimum model has 10336 elements, again using the nominal clamping distance.

Finally, Table 4 gives the values for the boundary condition parameters [33-34].

Table 4: Boundary condition parameters [33-34]

Parameter	Value	Units
h_{air}	5	$W/m^2 \cdot K$
T	293	K
ε	0.95	-
$\sigma_{blackbody}$	5.67 x 10-8	$W/m^2 \cdot K^4$

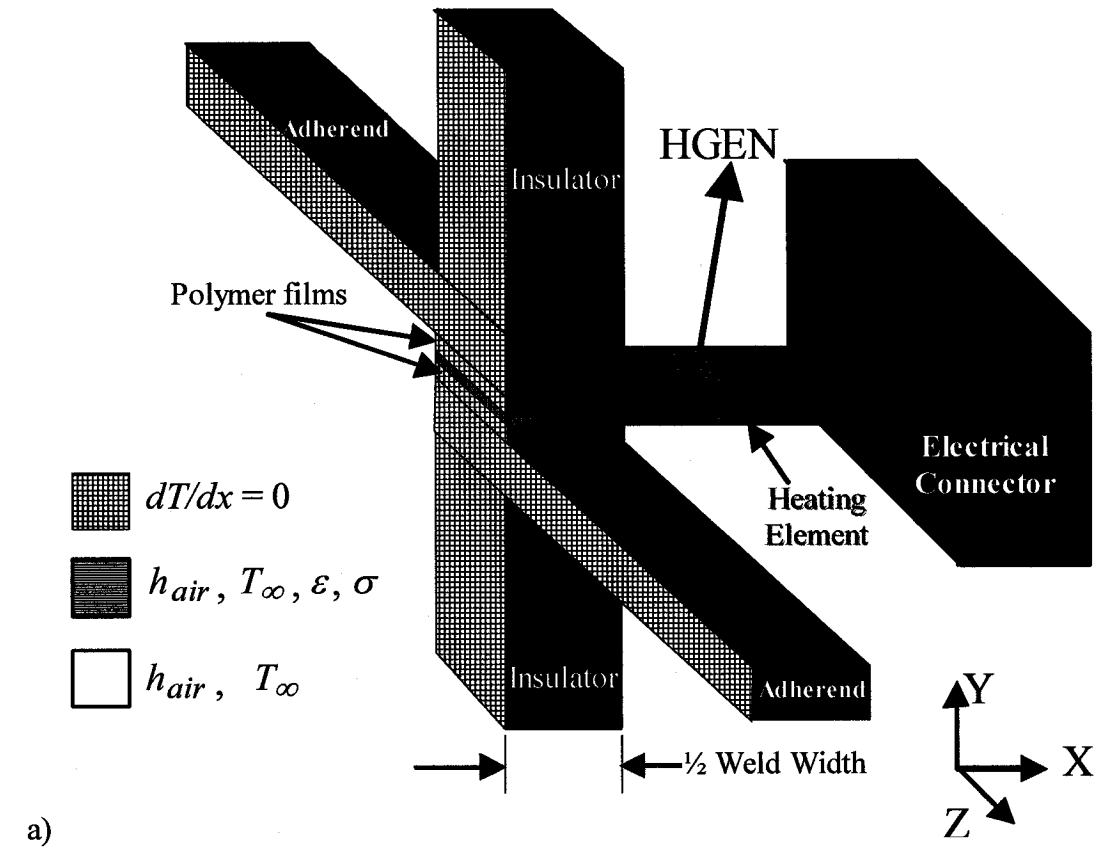

a)

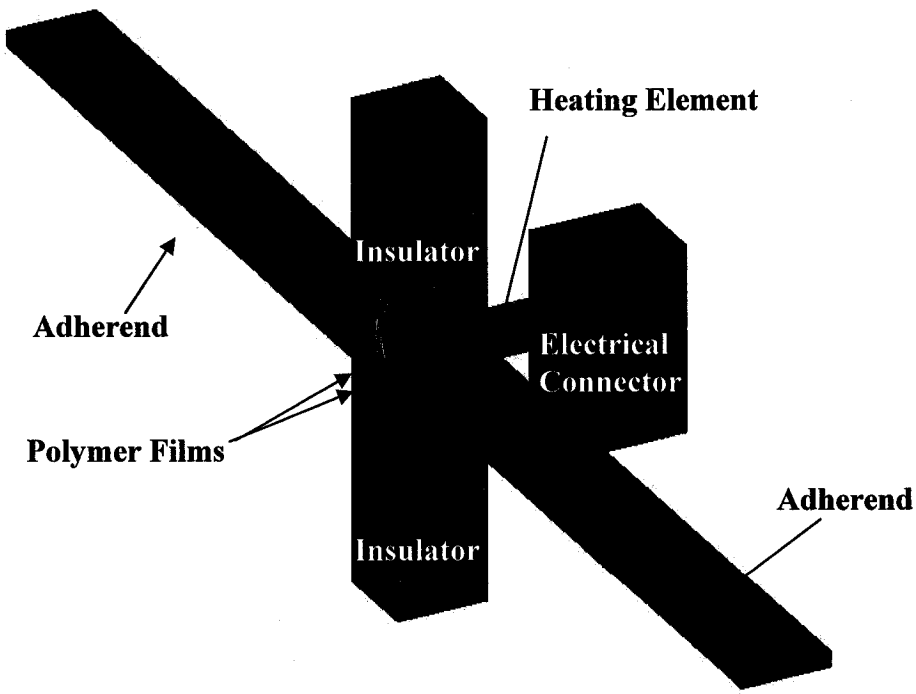

b)

Figure 12: 3-D thermal model a) Schematic with boundary conditions b) Mesh

A parameterized macro has been created for each model, using ANSYS Parametric Design Language (APDL), in order to facilitate the run of many numerical analyses, and change only the parameter of interest. These macros are presented in Appendix C. The numerical analyses have been conducted on ANSYS 8.0, using a Dell workstation (P-1V, 2 GHz, 1024 MB RAM) with a Windows 2000 platform.

5 Numerical Results

In this section, the influences of the latent heat, tooling-plates material, welding time and input power on the thermal history of the weld are addressed. However, in order to facilitate the description of the observed phenomena, the following definitions must be clarified.

- The Processing Temperature of PEEK is 390°C [74].
- The Minimum Welding Time is the time required to reach 343°C, PEEK melting temperature, *everywhere* at the weld interface, so that the entire weld interface is melted.
- The Maximum Welding Time is the time required to reach 450°C, PEEK degradation temperature, *anywhere* at the weld interface, in order to completely avoid degradation.
- The Processing Window is the difference between the *maximum welding time* and the *minimum welding time*.
- A Complete Weld is obtained when all temperatures at the weld interface are between the maximum and minimum welding temperatures, i.e., 343°C and 450°C, respectively.
- The Weld Interface is the surface between the laminate and the PEEK film.
- The Clamping Distance is defined as being the distance between the edge of the weld, and the electrical copper connector, as shown in Figure 9.

5.1 Latent Heat Effects

The 1-D model is first used to investigate the effect of latent heat of fusion of the polymer on the heating rate at the weld interface. Ceramic tooling plates are used. The latent heat of fusion is the energy required to change the polymer from solid to liquid state. For PEEK, the latent heat of fusion, L_f, is 44 kJ/kg [64]. The latent heat effect is incorporated in the enthalpy property of the polymer within the melting zone, i.e. between the solidus and liquidus temperatures of 330°C and 343°C, respectively. The enthalpy variation is computed as follows.

$$dH = \rho \cdot c_p \cdot dT + \rho \cdot L_f \tag{1}$$

where dH is the enthalpy variation (J/m^3), ρ is the density (kg/m^3), c_p is the specific heat (J/kg·°C), dT is the temperature variation (°C) and L_f is the latent heat of fusion (J/kg). L_f is zero for all temperatures, except in the melting zone, i.e., between 330°C-343°C. This results in a slope discontinuity in the enthalpy versus temperature curve.

Figure 13 shows the enthalpy variation of PEEK and APC-2/AS4 laminates with and without the latent heat, as a function of temperature. Note that the temperature-dependant enthalpy of APC-2/AS4 laminates have been calculated from the properties of PEEK, and AS4 carbon fibres ($v_f = 61\%$) [53], using the rule of mixtures.

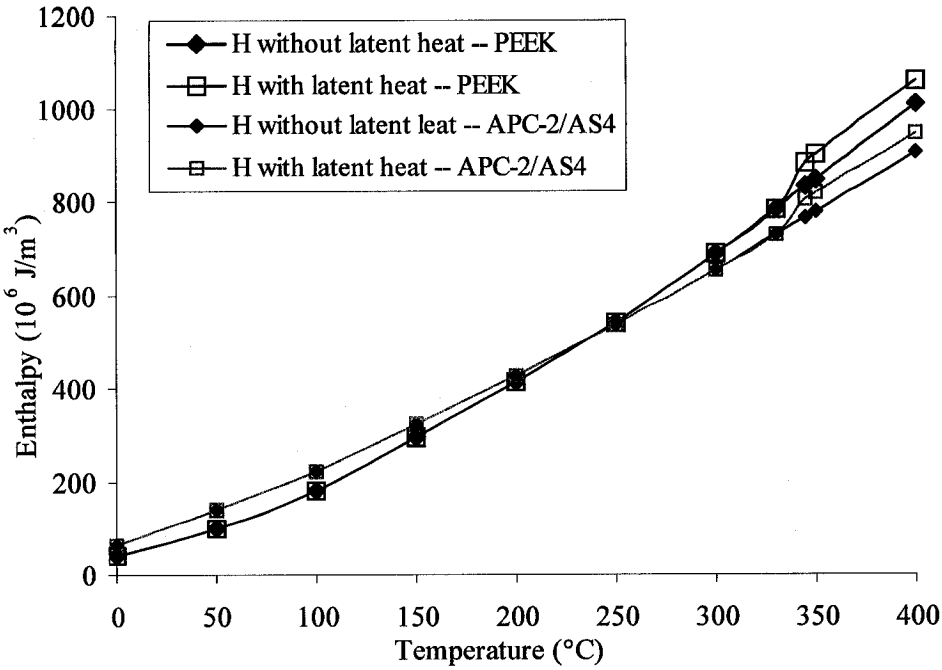

Figure 13: Temperature dependent enthalpy for PEEK and APC-2/AS4 laminates

Figure 14 shows the temperature-time curves at the weld interface between the laminate and the heating element without and with the effect of latent heat, for an input power of 2.0 GW/m^3. Figure 14 shows that including the latent heat in the model slightly decreases the heating rate. The polymer melting temperature (T_m = 343°C) is reached in 21 s and 21.5 s for the models without and with latent heat, respectively. Thus, the minimum welding time without the latent heat is 2.3% faster. This insignificant influence of the latent heat on the heating rate is explained by the phase transformation of only a very small quantity of PEEK polymer at the weld interface. Previously reported results also support this affirmation [33-34, 64]. Note that, in the following analyses, the latent heat of fusion of PEEK is neglected.

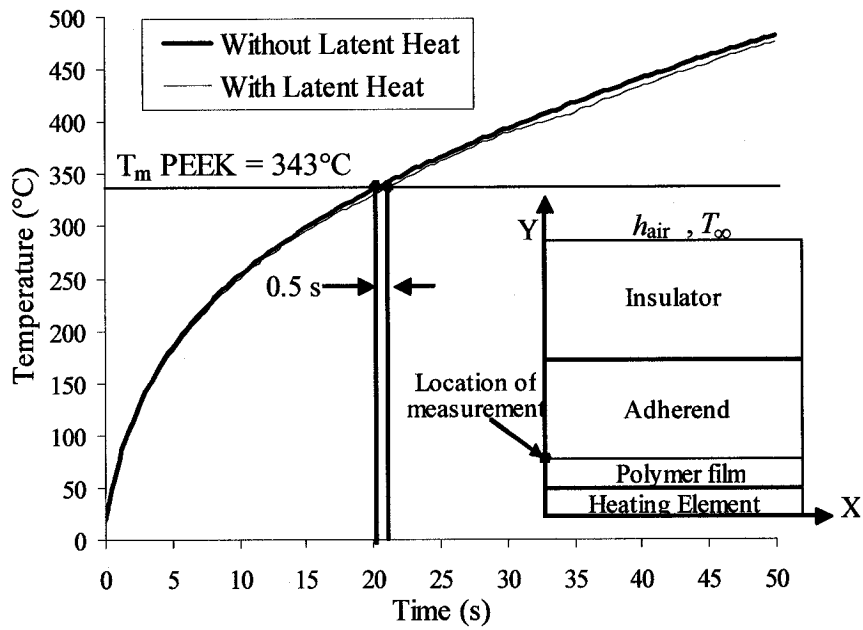

Figure 14: Effect of the latent heat on the heating rate, at a power of 2.0 GW/m^3, using the 1-D model

5.2 Effects of Tooling-Plates Material

The 1-D model is also used to determine the influence of the tooling plates on the through-thickness temperature gradient of the weld stack, and on the weld interface thermal history. Three cases are studied: i) no tooling-plate, i.e. free convection is applied directly to the top of the laminate; ii) ceramic tooling-plates and iii) stainless steel tooling-plates, with their corresponding thermal properties (see Table 2).

Figure 15 depicts the through-thickness thermal gradient at a power of 2.0 GW/m^3 after 60 seconds for the different tooling-plates materials. The stainless steel tooling-plate leads to the largest through the weld thickness temperature gradient (-136 °C/mm),

because of the considerable heat conduction capability of steel. The second largest temperature gradient belongs to the ceramic tooling-plates with -124 °C/mm. For the no-tooling plate case, a temperature gradient of only -80 °C/mm is observed. These results confirm that the most insulated condition, i.e., air, provides the lowest through-thickness temperature gradient, which can promote melt front propagation through the laminate thickness. On the other hand, the lowest insulation condition, i.e., stainless steel tooling plates, insures a larger through-thickness temperature gradient, thereby preventing bulk heating through the thickness of the part.

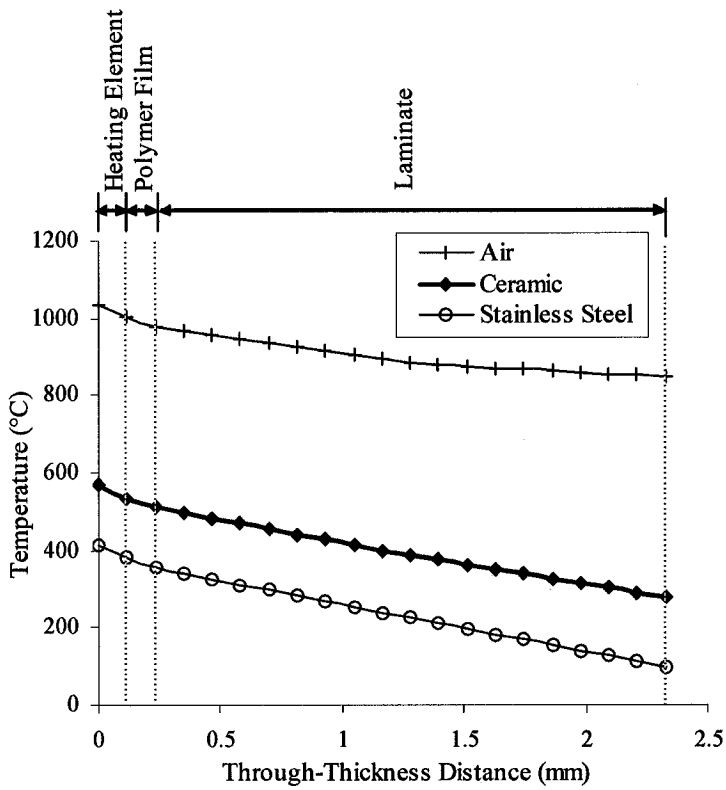

Figure 15: Through the weld thickness thermal gradient for different tooling-plates materials, for a power of 2.0 GW/m^3, after 60 seconds, using the 1-D model

Figure 16 shows the influence of the different insulation conditions on the welding time, under a power of 2.0 GW/m^3.

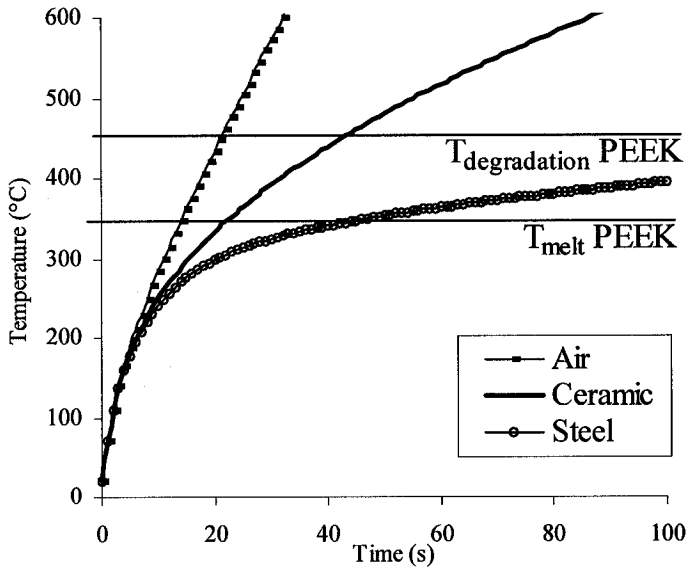

Figure 16: Weld interface thermal history for different tooling-plates materials, for a 2.0 GW/m^3 weld, 1-D model

Figure 16 shows that using stainless steel tooling-plates leads to a minimum welding time of 41 seconds, whereas using ceramic tooling-plates lowers this time to 21 seconds. The no-tooling-plate case, i.e. free convection to air, lowers the minimum welding time even more, to only 14 seconds. Figure 16 also shows that the maximum welding times are 21 seconds, 43 seconds and more than 100 seconds, for the no-tooling-plate, ceramic and stainless steel cases, respectively. This shows that there are considerable heat losses in the stainless steel tooling plates. Therefore, the thermal properties of the tooling-plates have significant effects on the welding time and temperature gradient through the weld thickness. Appropriate selection of the tooling plate material can control these

parameters. One can conclude that the optimum insulation material is air, but it obviously cannot be used, since practically, the tooling plates must be used to apply pressure on the weld stack, insuring the consolidation of the joint. Therefore, ceramic is a suitable compromise for the tooling plate material.

5.3 Edge Effects Issues

The 2-D model is used to investigate the edge effects, i.e., overheating of the edges of the weld, due to the areas of the heating element exposed to air. Figure 17 shows the temperature distribution along the weld interface after 10, 20, 30 and 40 seconds.

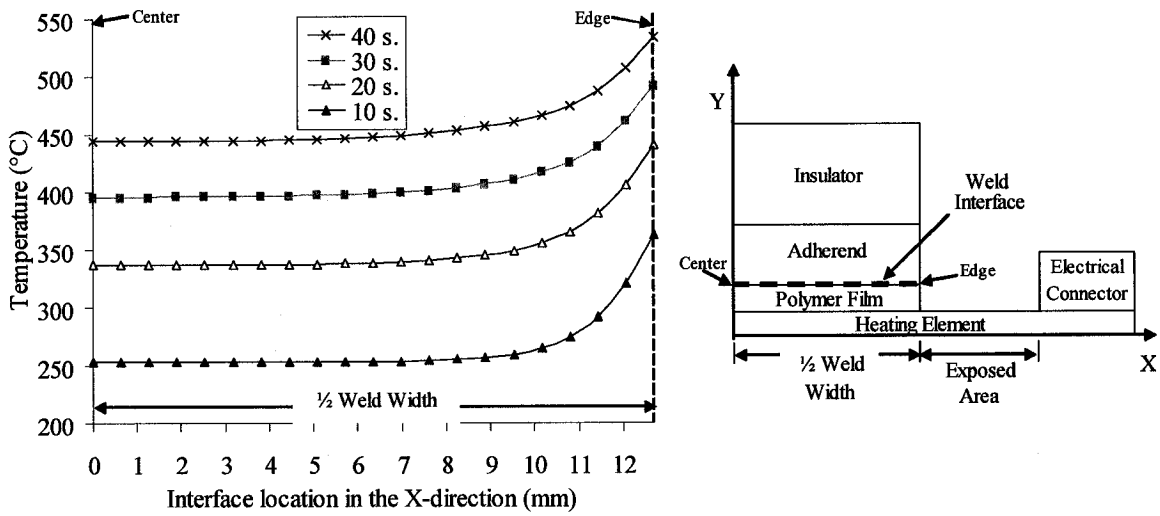

Figure 17: Temperature profile along the weld interface for the 2.0 GW/m^3 power, using the 2-D model

The results of Figure 17 clearly show that the temperature at the edges of the weld is substantially higher than the temperature inside the weld, e.g., at the weld center. This temperature difference introduces a large temperature gradient in the weld, particularly 3 mm away from the edge, after 10, 20, 30 and 40 seconds. The source of the large temperature gradient is the change of heat transfer mechanisms at the edge of the weld from convection and radiation to conduction condition. Non-uniform temperature distribution across the weld and edge effects are two major limiting factors for welding large-scale structures and obtaining consistent mechanical performance [47].

Figure 18 a), b), c) and d) show the temperature distribution and location of the localized overheating after 10, 20, 30, and 40 seconds, respectively. It is clear that the localized overheating is attributed to sudden changes of heat transfer mechanism from convection and radiation to conduction at the edges of the weld. It is shown that the temperature at the edge of the weld rapidly reaches 340°C after 10s, whereas the temperature at the center of the weld is only at 200°C. After 20s, the edge of the weld reaches the polymer degradation temperature of 450°C whereas the center of the weld has not yet reach to even the melting temperature of the polymer, i.e., 343°C. After 30 seconds, the entire weld interface is above 343°C, but a small region of degraded polymer is appearing at the edge. After 40s, the polymer at the weld interface is entirely degraded since the temperature at the weld interface is everywhere above 450°C.

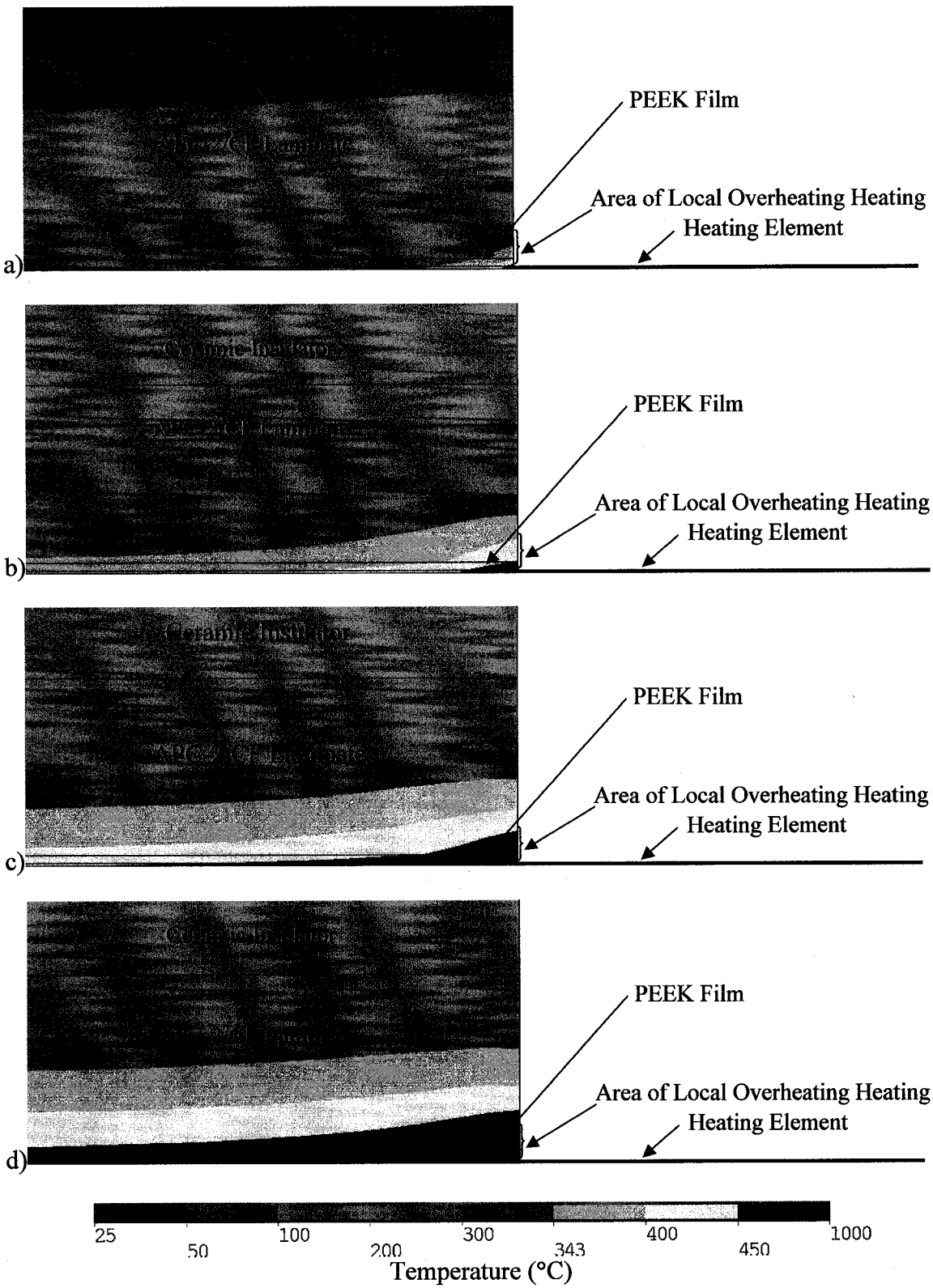

Figure 18: Temperature distribution for the power of 2.0 GW/m^3, after a) 10s, b) 20s, c) 30 s and d) 40s , using the 2-D model

5.4 Local Overheating Issue

The problem of local overheating arises from sudden changes of heat transfer mechanisms from convection and radiation to conduction at the edges of the weld. The areas of the heating element exposed to air have poor heat transfer properties due to free convection. As a result, the exposed areas reach a higher temperature faster than the areas of the heating element in contact with the weld interface. Clearly, the sudden temperature rise of the exposed areas generates a sharp temperature gradient at the edges of the weld that leads to local overheating, possible polymer degradation and melt front propagation through the weld thickness [14].

Cooling the edges, insulating the exposed areas, or reducing the clamping distance, i.e., the length of the areas of the heating element exposed to air [15] are possible solutions to reduce the sharp temperature gradient at the edges of the weld. At first, it seems that having a zero clamping distance can solve the local overheating at the edges of the weld. However, a zero clamping distance is not a possible solution because of the heat dissipation into the electrical copper connectors [15]. A zero clamping distance leads to cold edges and promotes un-welded zones at the edges of the weld. Thus, it is believed that there is an optimum clamping distance offering a uniform temperature distribution in the welds [6]. It is important to recall that a *complete weld* can only be produced once the temperatures at the weld interface are between the polymer melting and degradation temperatures, i.e., 343°C and 450°C, respectively. However, to obtain a *good* weld quality, it is *necessary* to have a uniform temperature distribution at the weld interface. Optimization of the clamping distance using finite element analysis has not been reported and this is one of the objectives of this work.

In order to determine an optimum clamping distance, an optimization algorithm is incorporated in the 2-D heat transfer finite element model. The objective is to reach the uniform processing temperature of 390°C *everywhere* along the width of the weld by varying the clamping distance. This objective function can be schematised as follows:

$$Min(f(T)) = Min(|T_{centre} - T_{edge}|) \quad (1)$$

$$\text{with } T_{centre} = 390°C$$

where T_{centre} is the temperature at the centre of the weld, T_{edge} is the temperature at the edge of the weld. Figure 19 shows the algorithm applying the objective function.

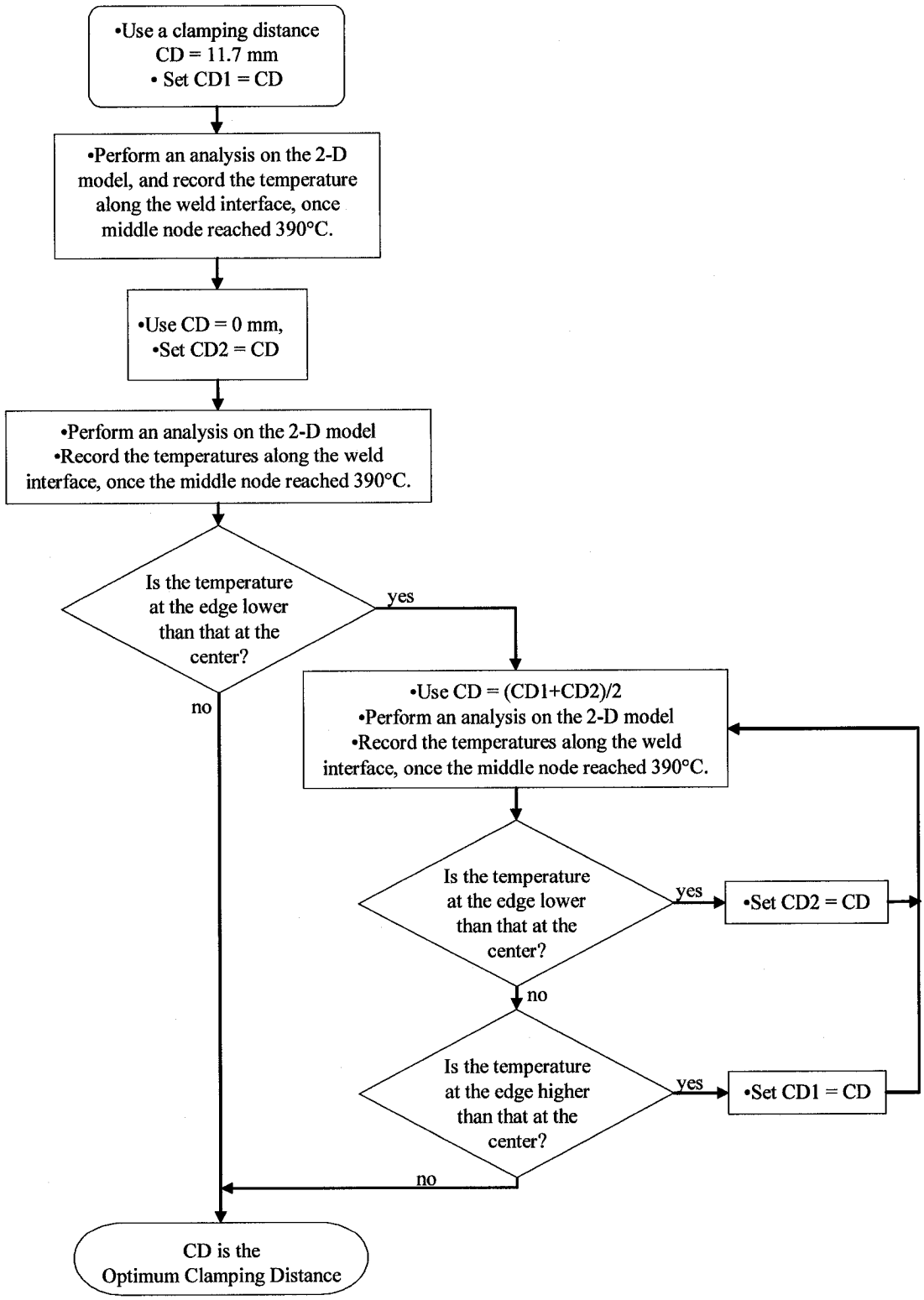

Figure 19: Clamping distance optimisation chart

Figure 20 shows the temperature distribution along the width of the weld interface for different clamping distances and a constant power of 2.0 GW/m^3.

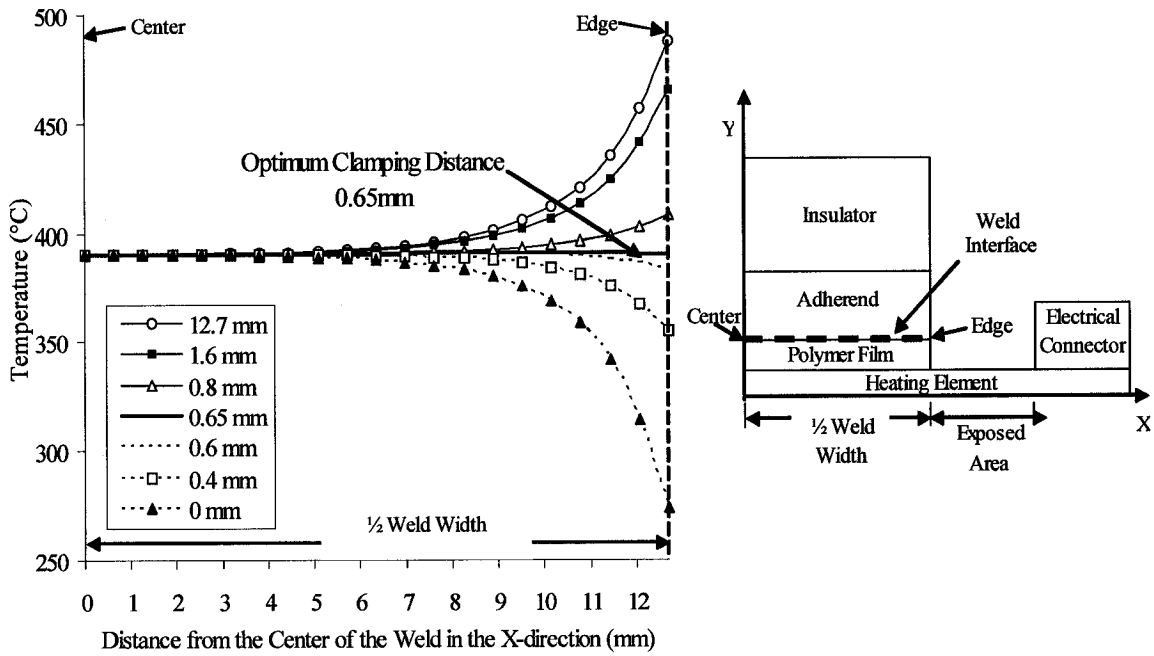

Figure 20: Effect of the clamping distance on local overheating

Figure 20 shows that for the power of 2.0 GW/m^3, the optimum clamping distance of 0.65 mm is found, after a 29 seconds welding time. The implications of this optimization are shown in Figure 21 and Figure 22, where the thermal history at the weld interface of a typical and the optimum clamping distance, i.e., 12.7 mm and 0.65 mm, are respectively examined. For both cases, a power of 2.0 GW/m^3 is applied for 50 seconds. The transient temperature profiles at different locations across the width of the weld, i.e., at 0 mm (center), 9.5 mm, 11.1 mm and 12.7 mm (edge), are presented.

For the clamping distance of 12.7 mm, the obtained processing window for a complete weld is only 0.5 second, ranging from 21 to 21.5 seconds. Decreasing the welding time below 21 seconds leads to an un-welded zone at the center of the weld, while increasing the welding time above 21.5 seconds causes polymer degradation and local overheating at the edges of the weld.

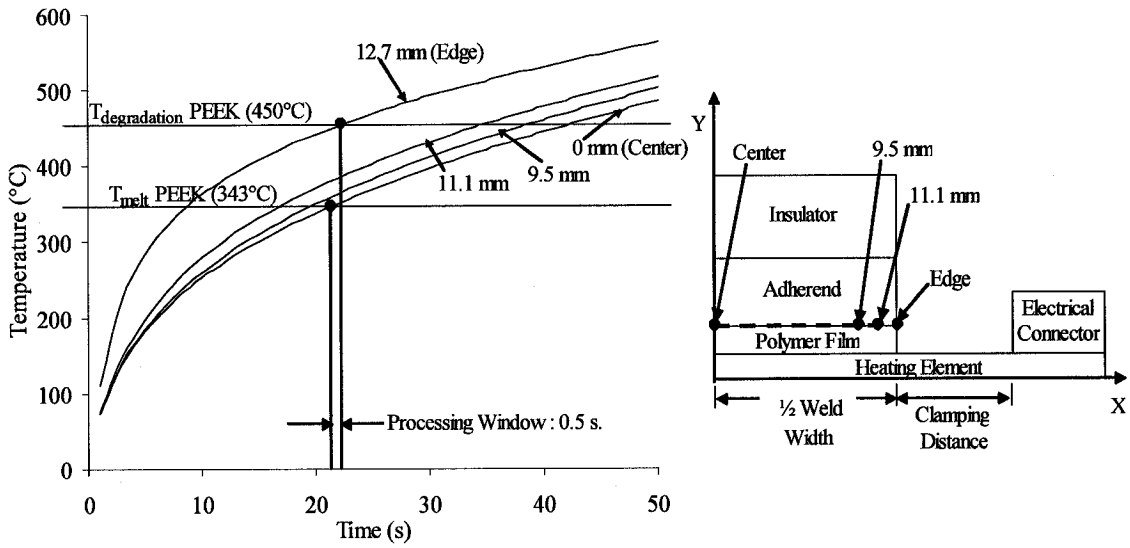

Figure 21: Temperature profiles at various locations in the weld, for the clamping distance of 12.7 mm, at a power level of 2.0 GW/m^3, using the 2-D model

For the clamping distance of 0.65 mm, the processing window for a complete weld is 18.5 seconds, ranging from 21 to 41.5 seconds, as shown in Figure 22. This clearly shows that using an appropriate clamping distance can provide a more uniform temperature distribution across the weld and significantly enlarge the size of the processing window.

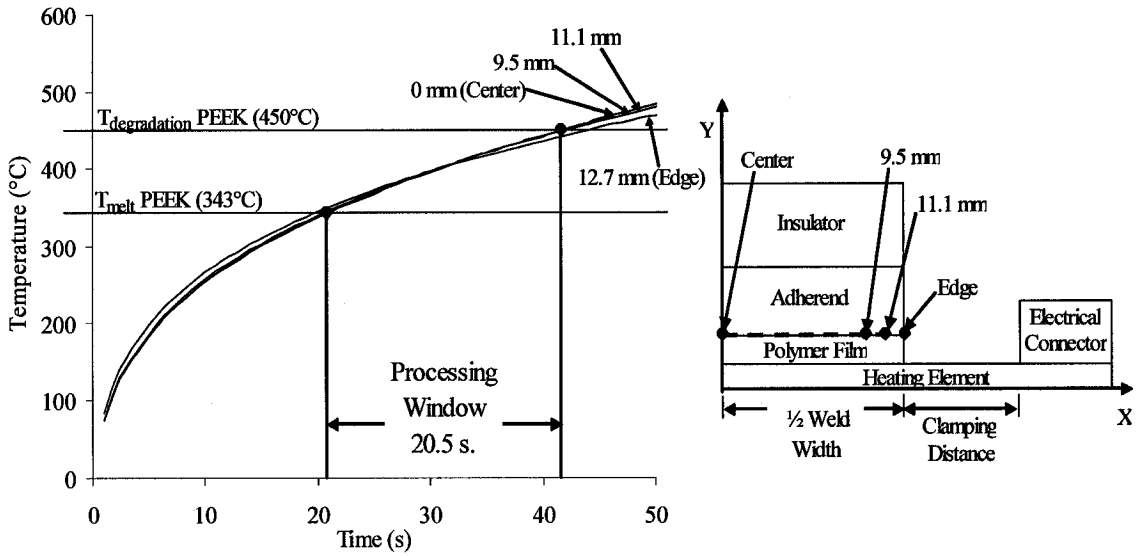

Figure 22: Temperature profiles at various locations in the weld, for the clamping distance of 0.65 mm, at a power level of 2.0 GW/m^3, using the 2-D model

5.5 Effects of Power Level

The 2-D model is also used to investigate the influence of various power levels on the welding times. Table 5 shows the minimum and maximum welding times, as well as the size of the processing window, for the 1.0, 1.5, 2.0 and 2.5 GW/m^3 applied powers and the clamping distances of 12.7 mm, 0.65 mm and 0 mm.

For a clamping distance of 12.7 mm and power of 2.5 GW/m^3, a negative processing window size is obtained, meaning that under these conditions polymer degradation at the edges of weld occurs before the polymer at the center of the weld reaches the melting temperature. Therefore, no complete weld is possible at any welding time under a clamping distance of 12.7 mm and power of 2.5 GW/m^3. For the same clamping distance, the lowest power of 1.0 GW/m^3 provides the largest processing window of 10 seconds.

The drawback of this low power is a long welding time of 43 seconds, causing melt front propagation through the weld thickness, which in turn promotes fibre movement at the weld interface. For the 0.65 mm clamping distance, the size of the processing window can be expanded for all power levels, even for the highest power of 2.5 GW/m^3, where the processing window size expanded from -0.8 seconds to 10.8 seconds. However, when the clamping distance is reduced to 0 mm, the processing windows are negative for all power levels, meaning that no weld is possible, at any welding time. Therefore, adjusting the clamping distance can significantly improve the size of the processing window especially for the higher power levels.

Table 5: Processing windows for different clamping distances and power levels

Clamping Distance = 12.7 mm			
Power (GW/m^3)	**Minimum Welding Time (s)**	**Maximum Welding Time (s)**	**Processing Window (s)**
1.0	43	53	10
1.5	28.5	31.5	3
2.0	21	21.5	0.5
2.5	14.8	14	-0.8
Clamping Distance = 0.65 mm			
Power (GW/m^3)	**Minimum Welding Time (s)**	**Maximum Welding Time (s)**	**Processing Window (s)**
1.0	46.5	87.5	41
1.5	28.5	57	28.5
2.0	21	41.5	20.5
2.5	15.2	30	14.8
Clamping Distance = 0 mm			
Power (GW/m^3)	**Minimum Welding Time (s)**	**Maximum Welding Time (s)**	**Processing Window (s)**
1.0	112	88	-24
1.5	72	57	-15
2.0	52	41.5	-10.5
2.5	18.8	14.7	-4.1

5.6 *Heat Transfer along the Length of the Laminates*

The 3-D model is used to provide additional insight during the resistance welding process, taking into account the heat transferred along the laminates. Figure 23 shows the weld interface temperature distributions along the Z-direction at the edge and center of the weld for the power level of 2.0 GW/m^3, the clamping distance of 0.65 mm and the processing temperature of 390°C.

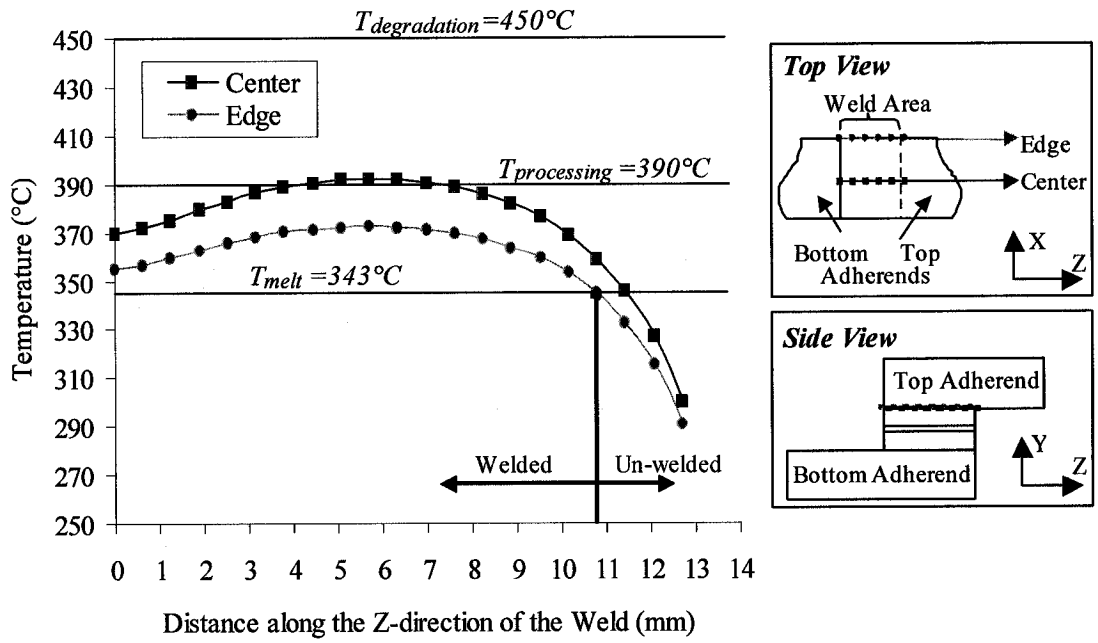

Figure 23: Thermal history along the length of the weld for the input power level of 2.0 GW/m^3 , and a clamping distance of 0.65 mm, using the 3-D model

The welding simulation is terminated after 43 seconds, which is the time at which the processing temperature is attained at the center of the weld interface. This welding time of 43 seconds is different from the 29 seconds obtained with the 2-D model and the

temperature curves at the edge and at the center of the weld do not lie on top of each other, due to the heat conduction along the length of the laminates, which influences the temperature distribution of the whole weld. Hence, these two arguments indicate that a 3-D model is necessary to determine the thermal behaviour of the weld and to optimize the clamping distance. Consequently, the 3-D model has been coupled with the optimization algorithm and lead to a new optimum clamping distance of 0.8 mm. Figure 24 shows the weld interface temperature distributions along the Z-direction at the edge and center of the weld for the power level of 2.0 GW/m^3, the clamping distance of 0.65 mm and the processing temperature of 390°C.

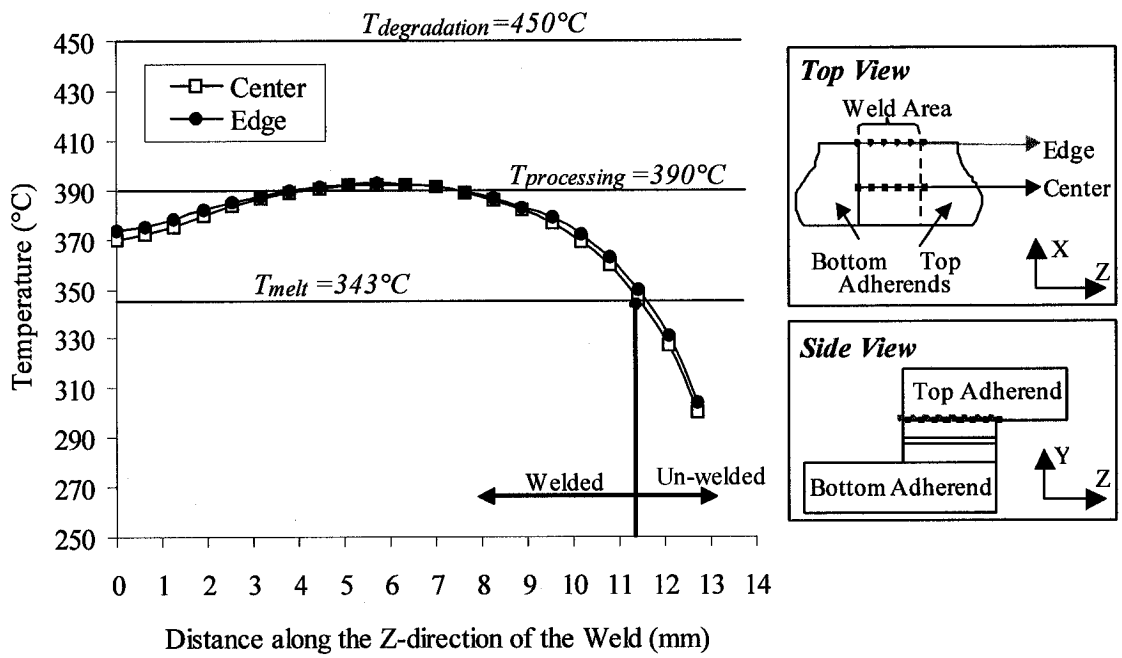

Figure 24: Thermal history along the length of the weld for the input power level of 2.0 GW/m^3 for 43s, and a clamping distance of 0.8 mm, using the 3-D model

A combination of welded and un-welded zones, i.e., an incomplete weld can be identified. The non-uniform temperature distributions are attributed to the heat transfer into the laminates along the Z-direction. To obtain a complete weld, one possible solution is to increase the processing temperature from 390°C to 440°C. Figure 25 depicts the temperature distributions along the Z-direction at the edge and center of the weld for the processing temperature of 440°C.

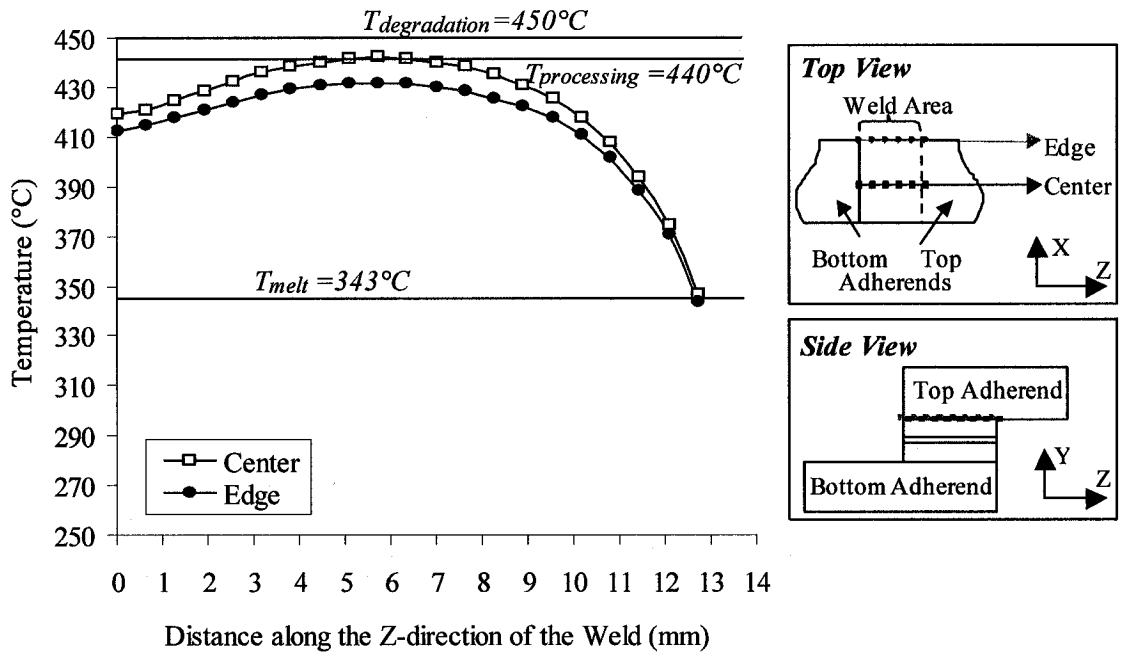

Figure 25: Thermal history along the length of the weld for the input power level of 2.0 GW/m^3 for 61s, and a clamping distance of 0.8 mm, using the 3-D model

In this case where the processing temperature set to 440°C and the optimum clamping distance used has been calculated with the 3-D model, a complete weld is finally achieved. However, it is possible to observe that a non-optimal clamping distance would

bring the curves further apart, causing non-welded zones or degraded zones. Also, it shows that the processing window for this power level is very small, since a small variation in the welding time could cause unwelded or degraded/overheated zones.

Finally, Figure 25 shows that it is impossible to obtain a uniform temperature distribution at the weld interface for the current resistance welded lap-shear joint configuration.

5.7 Conclusions of the Modelling Section

In this section, 1-D, 2-D and 3-D transient heat transfer finite element models were developed to simulate the resistance welding of APC-2/CF laminates. The main conclusions drawn from the analysis of the models are listed below.

- The latent heat of fusion of the polymer can be neglected in the models. This model confirms the findings of Ageorges *et al.* [64-65] and Holmes et al. [33-34].

- High power levels lead to very narrow processing window. In fact, they are possible *only* using the optimum clamping distance.

- The clamping distance has a direct impact on the local overheating at the edges of the welds.

- The optimum clamping distance can enlarge the processing window. Optimization of the clamping distance reduces polymer degradation at the edges of the weld.

- Under no circumstances, a uniform temperature distribution can be obtained along the Z-direction of the weld. However, a complete weld can only be obtained by using an appropriate processing temperature and clamping distance.

- The heat transfer in the laminates has a significant influence on the welding time. Therefore, the 3-D model simulation is recommended.

- Using the 2-D model is not sufficient to obtain the optimum clamping distance.

6 Experimental Validation

In order to verify the validity and precision of the model, experiments must be performed. In that sense, a setup has been realised, allowing for enough data acquisition. This setup has been provided by the Aerospace Manufacturing Technology Center.

6.1 Setup Description

Figure 26 is a photo of the experimental setup, showing, the computer/data-acquisition system, the pressure system and the resistance welding jig.

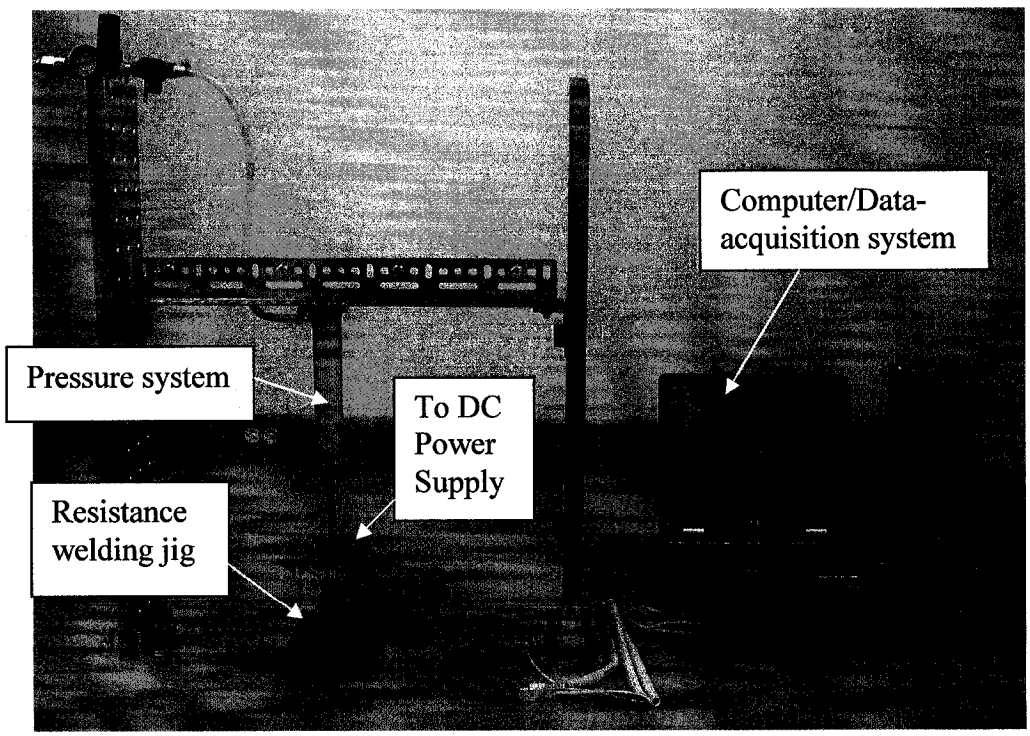

Figure 26: Experimental setup with data-acquisition system

Figure 27 shows a the resistance welding jig, consisting of copper connectors, ceramic sample holders and insulators, guiding rods for the ceramic insulator, the glass fibre/epoxy insulating base and a spacer underneath the second ceramic holder.

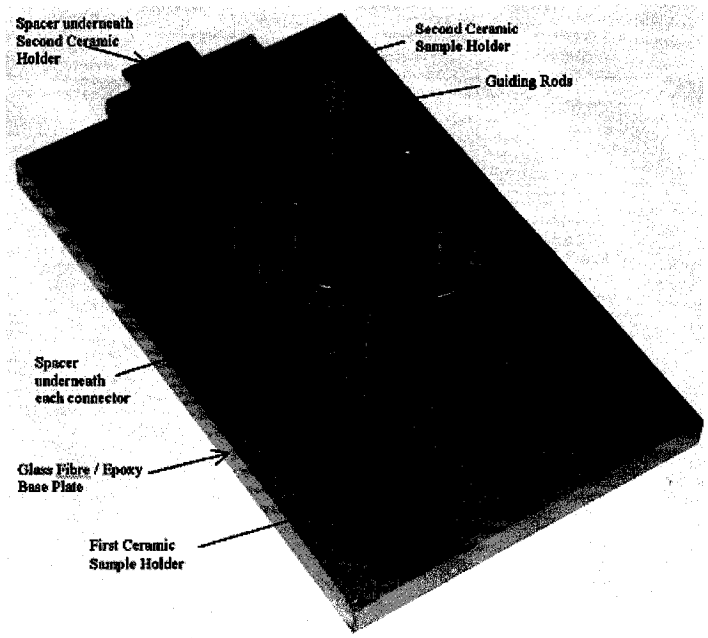

Figure 27: Resistance welding jig

Figure 28 shows how to assemble the resistance welding jig. It first shows the resistance welding jig, as shown in Figure 27. In step 1, a first laminate is positioned, on top of the first ceramic sample holder. In step 2, the heating element is inserted between the copper connectors and placed on top of the weld surface. Step 3 shows the addition of the polymer films on top and beneath the heating element, to have a resin rich interface, avoid current leakage and provide a better bond quality. Step 4 consists of adding the second laminate, as well as a ceramic insulator on top of the first laminate. Finally, in

step 5, a ceramic insulator is added on top of the second laminate. Note that the materials used in this setup have been presented in Section 2.

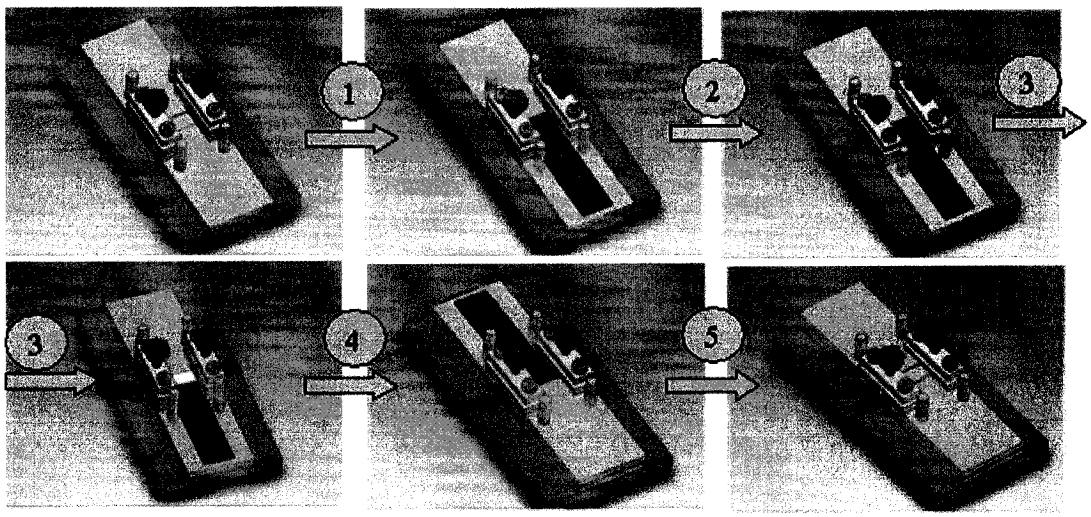

Figure 28: Step-by-step resistance welding jig assembly

6.2 Control and Data Acquisition

The welds are performed under a pressure control criterion. Thus, a pneumatic cylinder insures a constant pressure on the weld. The power is controlled via a home-made software developed using *LabVIEW*. The user imposes a given voltage on the DC power supply, for a given duration of time. The power supply has a feedback loop, allowing for a better precision and control on the voltage output. Simultaneously, thermocouples acquire temperature measurements at 3 different locations in the weld stack. Figure 29, shows the locations of the thermocouples, on a 2-D cross-section of the model. However,

one must remember that the numerical results compared with experimental data come from the 3-D model (see Section 4.3.3). Finally, the system is designed to stop when the temperature of T_1 reaches a user-defined processing temperature. In our case, as it has been shown in the modelling section, the processing temperature is set to 440°C. A timeout of 200 seconds is also imposed, in order to avoid infinite time welds.

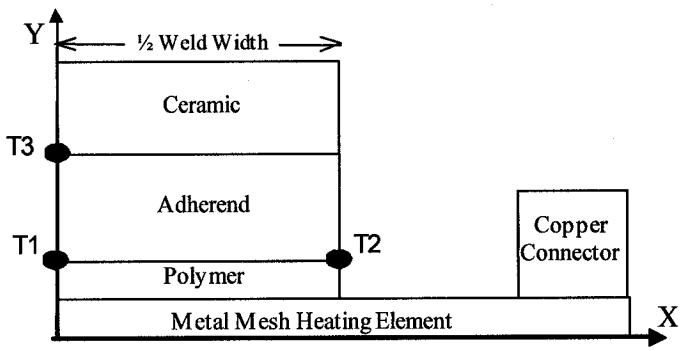

Figure 29: Thermocouple locations

6.3 Data Reduction

Four power levels have been studied, corresponding to the imposed voltages of 5, 6, 7 and 8 Volts. These power levels are calculated using the average voltage and current measured with the data-acquisition system. For each power level, the power density is the power divided by the total volume of the heating element, between the two copper connectors. Table 6 shows the average power and power density corresponding to the imposed voltages.

Table 6: Average power and power density corresponding to the imposed voltages

Voltage (V)	Power (W)	Power Density (GW/m^3)
5	72	2.7
6	112	4.3
7	156	5.9
8	202	7.7

For each power level studied, five welds were performed. Note that all welds have been performed at a clamping distance of 1.0 mm ± 0.5 mm, due to the experimental setup precision. Therefore, the numerical models have all been run at a clamping distance of 1.0 mm.

6.4 Experimental Results for Different Power Levels

Table 7 shows the welding times obtained when welding the samples under the studied imposed voltages, for each weld. Note that the grey areas show rejected data.

Table 7: Experimental welding times

Case	Welding Time (s)				
	#1	#2	#3	#4	#5
5V	**135**	200	36	140	200
6V	**26**	30	24.2	26	46
7V	8.2	8	10.8	**8.8**	9.6
8V	7.6	**7.2**	8.6	6.4	5.6

For each voltage case, the weld trial having the median welding time is shown in bold. This representative weld's temperature history is used in the following figures to compare the model and experimental results. Note that below 5 Volts, the welding time increases substantially and the temperature at the interface never reaches the processing temperature. This causes bulk heating of the laminates, inducing severe fibre motion, while some areas of the weld are still unwelded. Above 8 Volts, welds are performed within a very short time, where the processing window is reduced significantly, leading to unwelded and overheated/degraded zones in the same weld.

Figures 30 to 33 respectively show the comparison between the modelling and experimental data, for the 5, 6, 7 and 8V cases. The experimental results are plotted with markers, and the modelling results are the bold lines. The location of the thermocouples in the measurements is shown besides each figure, in order to facilitate the understanding of the graphs.

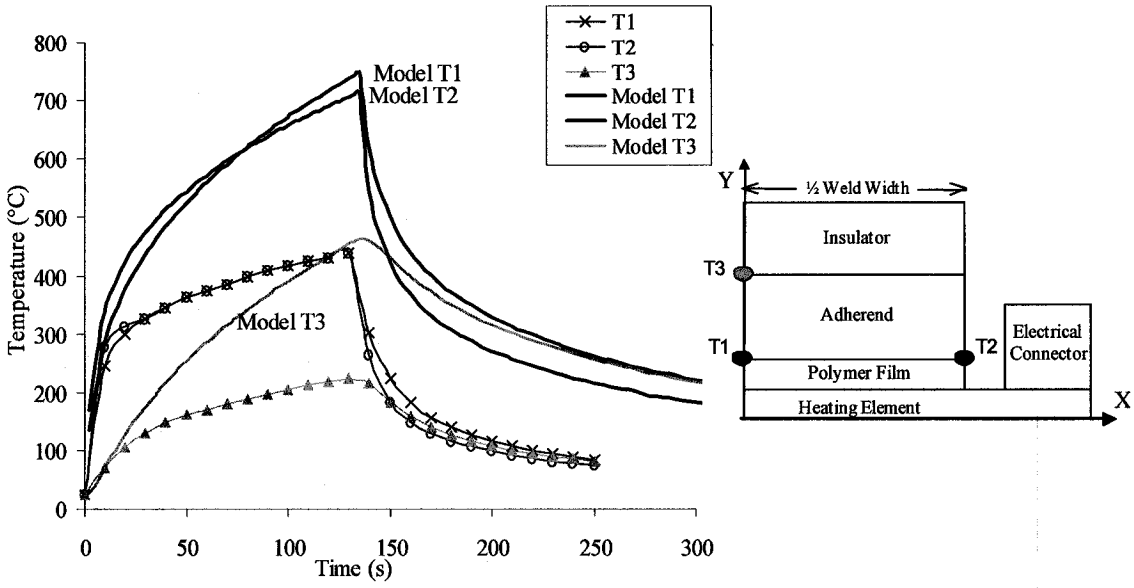

Figure 30: Comparison of the 3-D model and experimental thermal history at different locations in the weld, for the 5V case

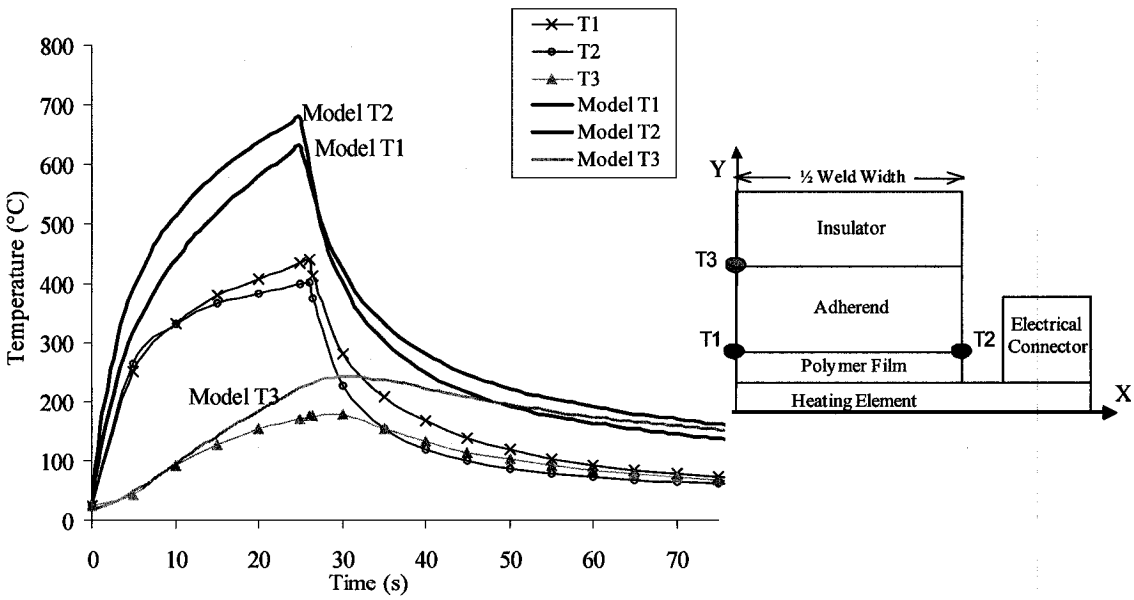

Figure 31: Comparison of the 3-D model and experimental thermal history at different locations in the weld, for the 6V case

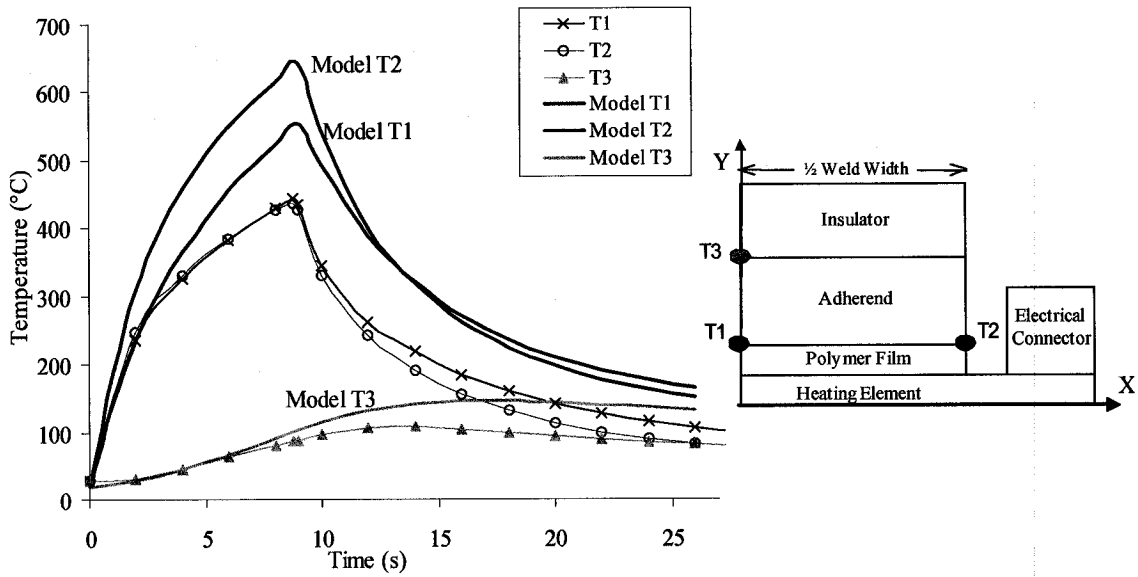

Figure 32: Comparison of the 3-D model and experimental thermal history at different locations in the weld, for the 7V case

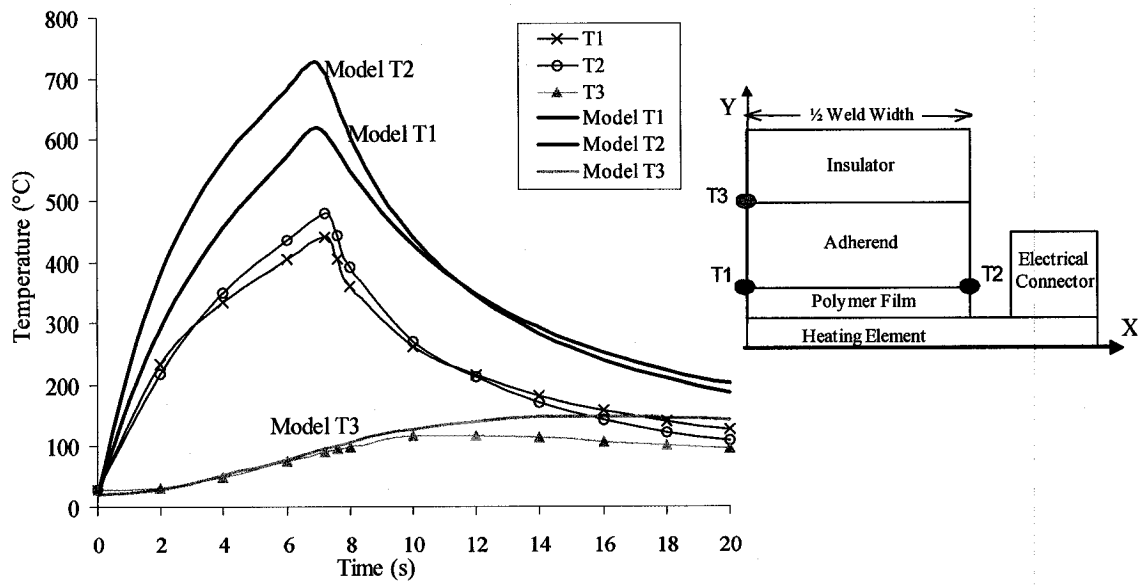

Figure 33: Comparison of the 3-D model and experimental thermal history at different locations in the weld, for the 8V case

These results clearly show that the actual model cannot predict the process. Table 8 shows a comparison of the maximum temperature reached for each experiment with that of the model. (Note that, as specified previously, the experimental welding temperature has been set to 440°C.)

Table 8: Comparison between the first 3-D model and experimental temperature at the welding time, at T1

Case	Temperature (°C) at welding time		% Error
	Experiment	Model	
5V	440	747	70%
6V	440	630	43%
7V	440	553	26%
8V	440	619	41%

According to Table 8, the predictions for the low power input are further (70% error) from the experimental data, than those of the higher power levels (down to about 40%). Moreover, the large discrepancies observed in Table 8, illustrate that some heat losses might have been neglected, since heat losses induce longer welding times, as observed in the experimental data. The larger amount of ceramic present in the resistance welding jig, compared to the model can have a larger influence on the numerical results than first expected.

6.5 New 3-D Model

In order to remedy to the fact that the model does not suit the experimental data very well, the model has been improved. First, all of the ceramic included in the setup was modeled, as shown in the second 3-D model of Figure 34. As it has been seen in Figure 16, the ceramic extracts more heat out of the weld than air does, so it is expected that this will influence the temperature history at the weld interface. The experimental data compared with the new model results are shown in Figures 35-38.

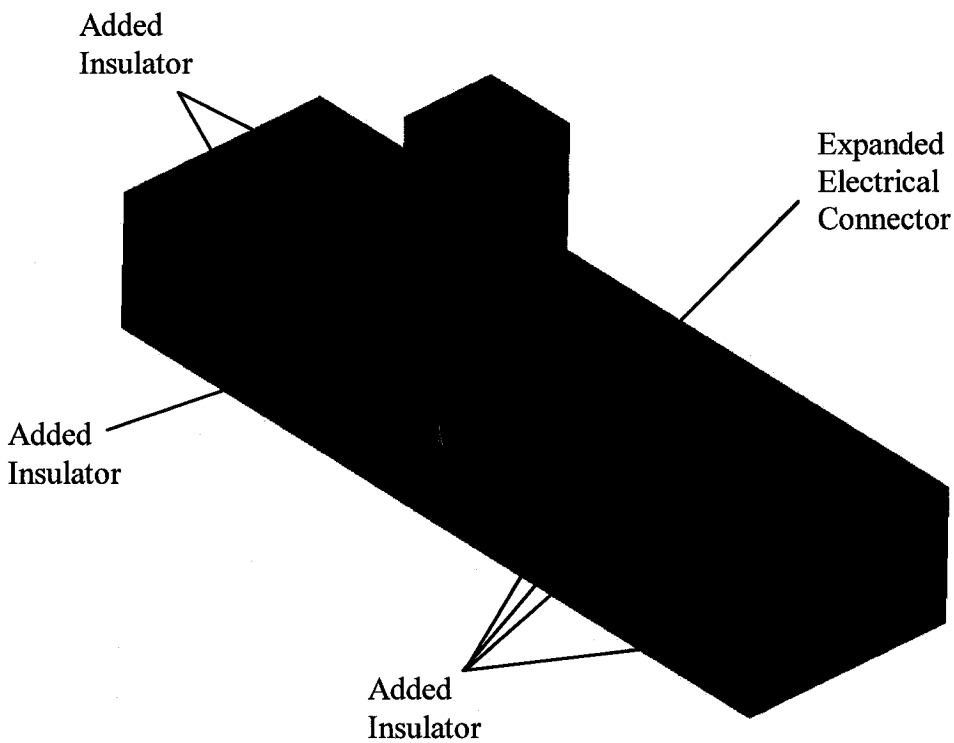

Figure 34: Second 3-D model (Half model, for symmetry)

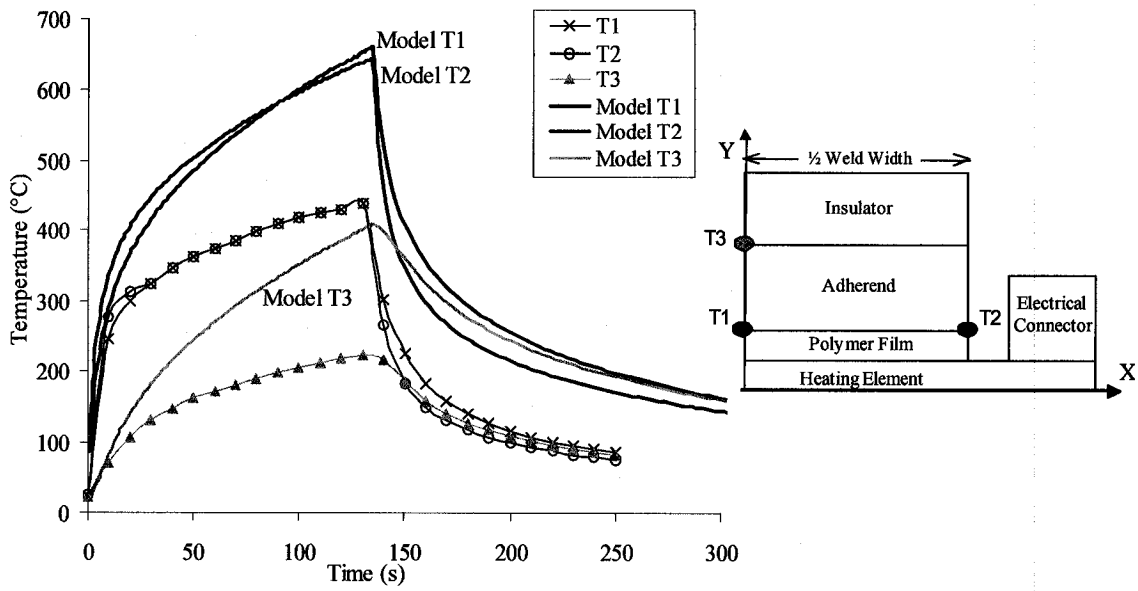

Figure 35: Comparison of the improved 3-D model and experimental thermal history at different locations in the weld, for the 5V case

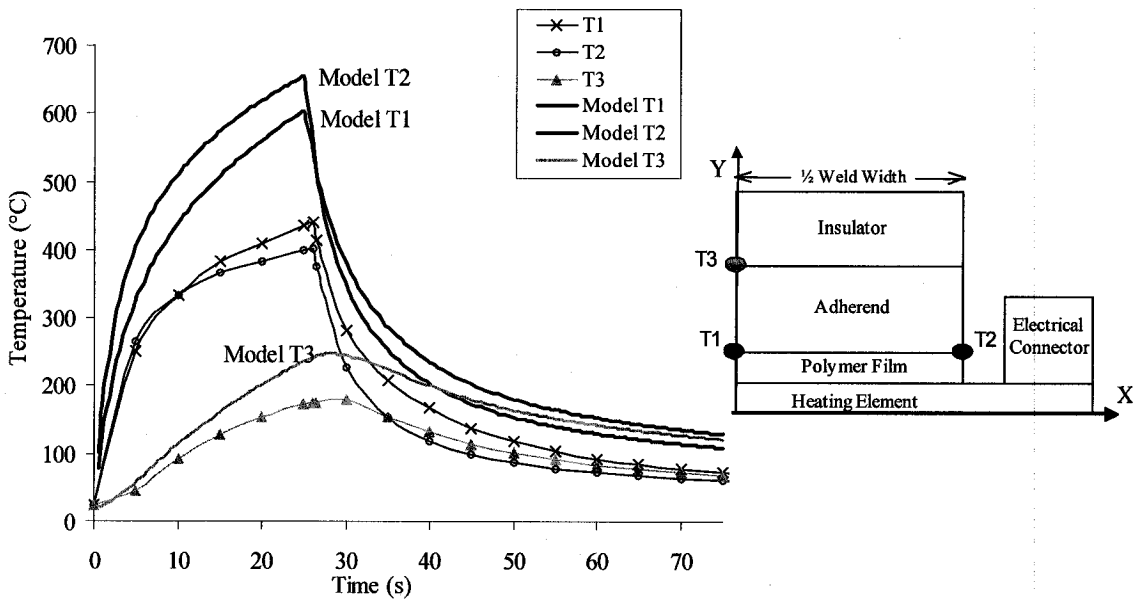

Figure 36: Comparison of the improved 3-D model and experimental thermal history at different locations in the weld, for the 6V case

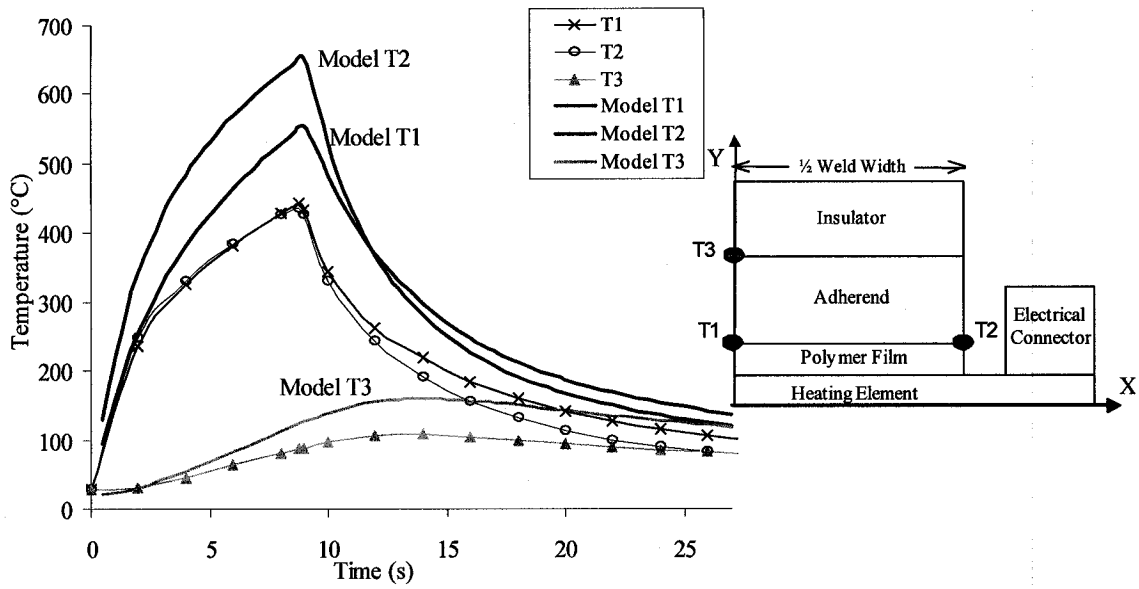

Figure 37: Comparison of the improved 3-D model and experimental thermal history at different locations in the weld, for the 7V case

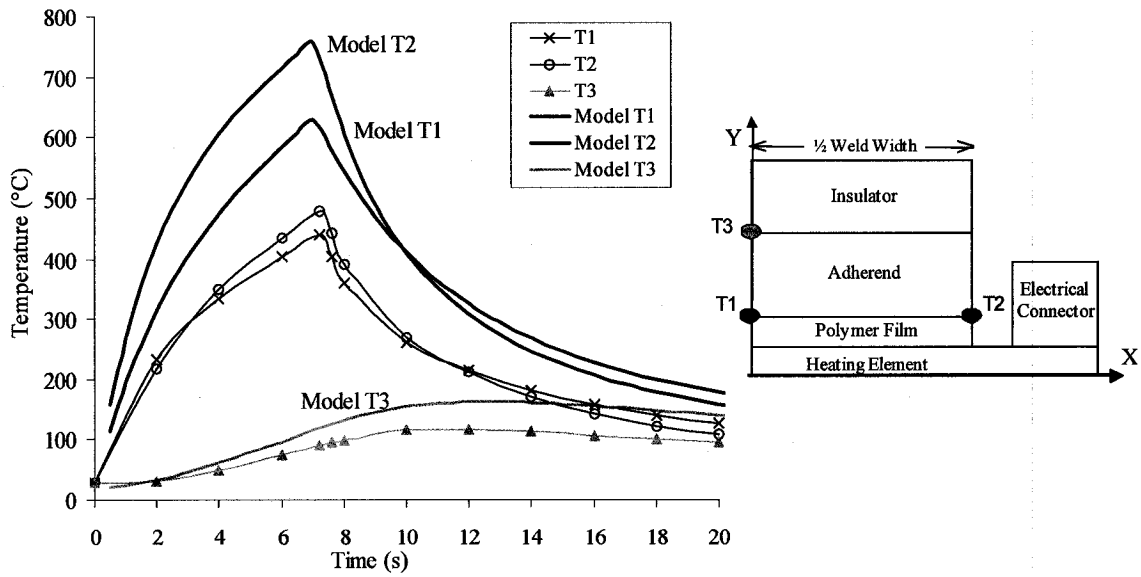

Figure 38: Comparison of the improved 3-D model and experimental thermal history at different locations in the weld, for the 8V case

In order to have a better understanding of the results of figures 35 to 38, the maximum temperatures obtained with the model are compared to the experimental data in Table 9.

Table 9: Comparison between the second 3-D model and experimental temperature at the welding time, at T1

Case	Temperature (°C)		% Error
	Experiment	Model	
5V	440	662	50%
6V	440	603	37%
7V	440	554	26%
8V	440	628	43%

Table 8 and Table 9 reveal that including the exact amount of ceramic and copper influences the temperature profile at the center of the weld, especially for the lower power levels. Hence, the error between the experimental data and the model is significantly reduced from 70% to 50% for the 5V case, and is practically unchanged, for the 7V and 8V cases, respectively at 26% and 43%. Table 10 compares the temperature at T2, for both models.

Table 10: Comparison between the second 3-D model and experimental temperature at the welding time, at T2

Case	Temperature T2 (°C) at welding time		% difference
	3D Model 1	3D Model 2	
5V	725	757	4%
6V	643	653	2%
7V	677	655	3%
8V	713	646	9%

Table 10 shows that including the exact amount of ceramic and copper slightly influences the temperature at the edge of the welds. Hence, the model including this additional amount of copper and ceramic should be taken into account in the simulation when determining the precise optimum clamping distance.

However, since the actual experiments are controlled by an imposed voltage, the energy generated in the model should be applied in the same manner. Therefore, the input power density must be replaced by imposed voltage boundary conditions at the top of the copper connectors and in the center of the weld. This can be done by replacing the SOLID70 elements by SOLID69 elements. This element also requires the input of resistivity properties for each material. That of the metal mesh heating element is calculated in Appendix B, and the values for the other materials have been taken from the literature. In that sense, the proper Joule heating will be calculated by ANSYS, improving the results.

Figure 39 shows the third version of the 3-D model, with the voltage boundary conditions. Note that the 3V shown on the figure is for symmetry purposes. Then, Figures 40 to 43 show the numerical results obtained with this third 3-D model, with voltage boundary conditions, compared to their respective experimental data.

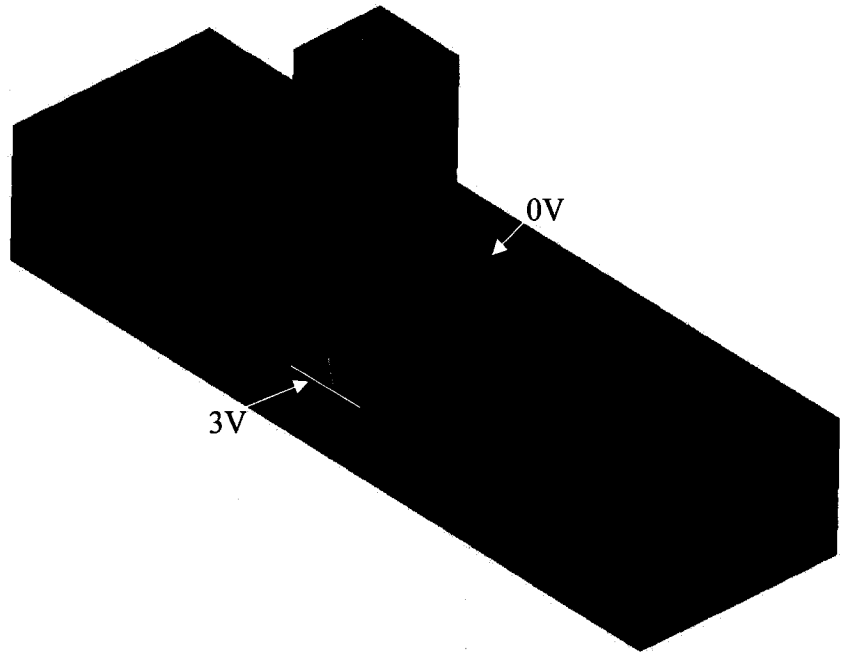

Figure 39: Third 3-D model, 6V case, voltage boundary conditions (3V for symmetry)

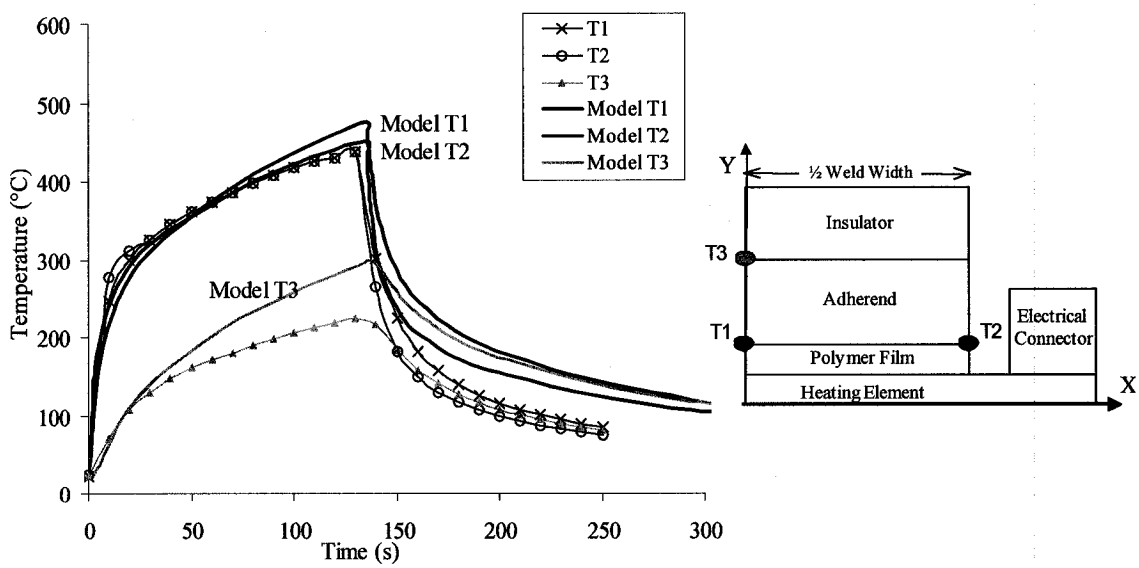

Figure 40: Comparison of the improved 3-D model, voltage boundary conditions, and experimental thermal history at different locations in the weld, for the 5V case

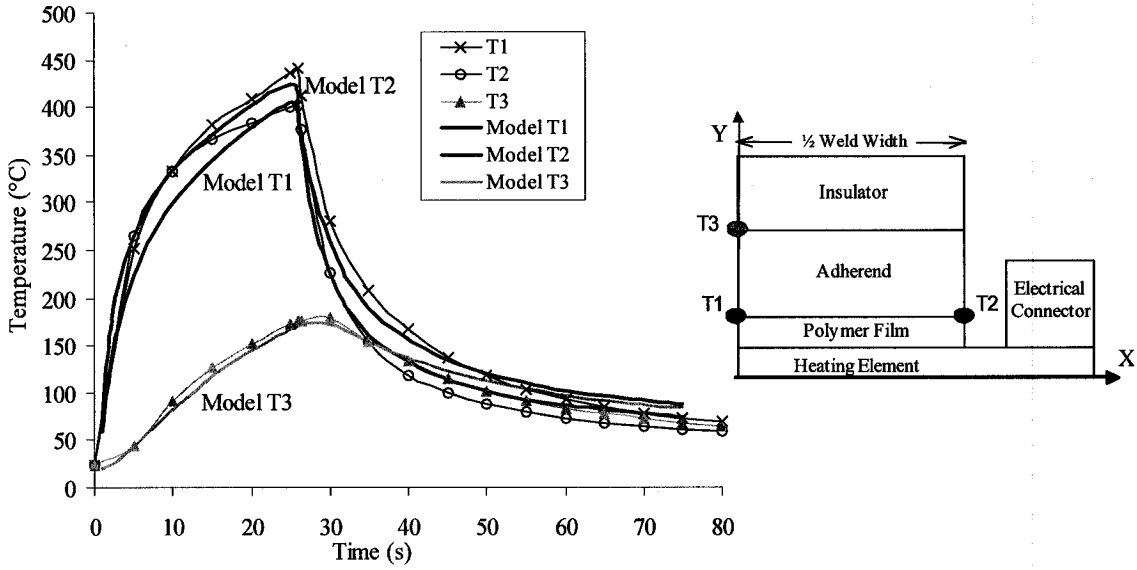

Figure 41: Comparison of the improved 3-D model, voltage boundary conditions, and experimental thermal history at different locations in the weld, for the 6V case

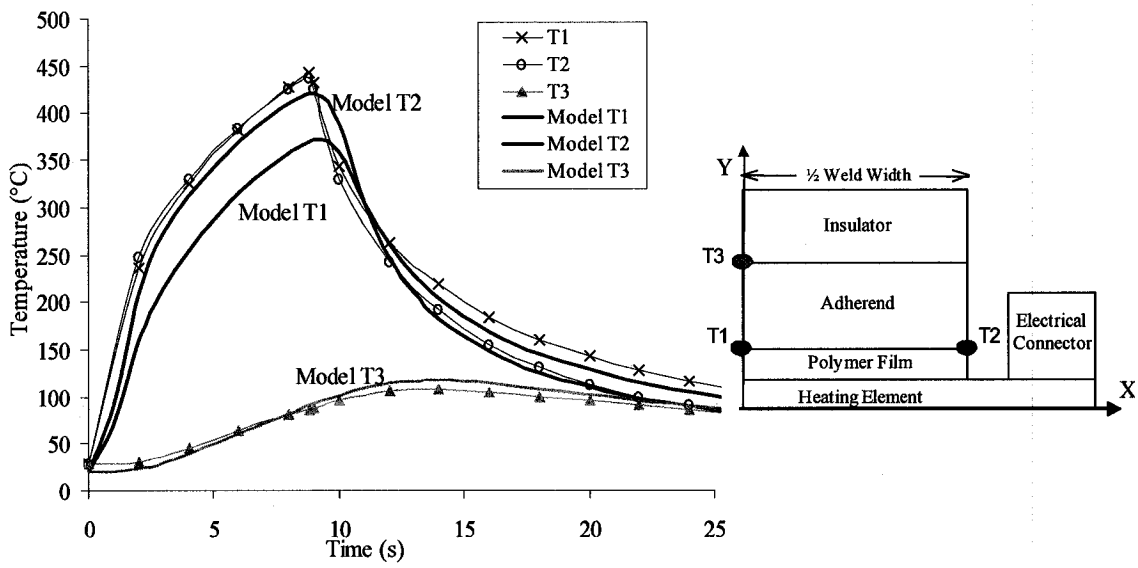

Figure 42: Comparison of the improved 3-D model, voltage boundary conditions, and experimental thermal history at different locations in the weld, for the 7V case

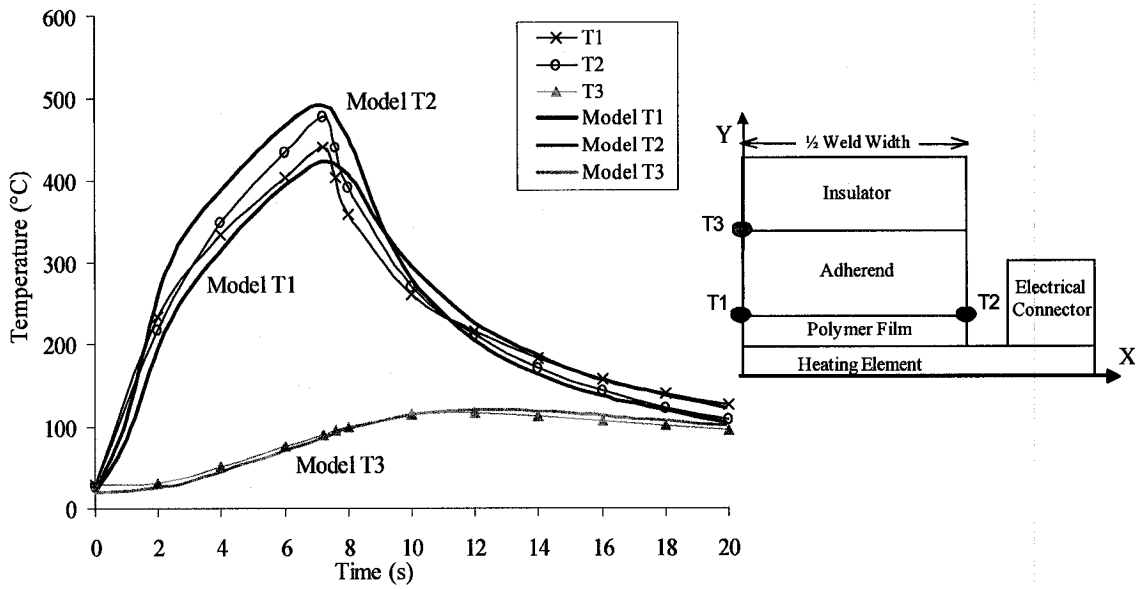

Figure 43: Comparison of the improved 3-D model, voltage boundary conditions, and experimental thermal history at different locations in the weld, for the 8V case

As depicted in Figures 40-43, the model effectively predicts the experimental data. Table 11 shows the welding temperature T1 obtained with the model, compare to that obtained experimentally.

Table 11: Comparison between the third 3-D model and experimental temperature at the welding time, at T1

Case	Temperature (°C)		% Error
	Experiment	Model	
5V	440	476	8%
6V	440	405	8%
7V	440	372	15%
8V	440	422	4%

The 15% or less error shows that the model is well suited to the experiment. The voltage boundary condition provides more appropriate results than the heat generation boundary condition. This might be due to the fact that the same power is obtained with unidirectional heating elements, as with fabric heating elements, as mentioned by Ageorges *et al.* [46]. Hence, only the wires in the direction of the current participate in the heat generation, the others act as conductors to homogenise the heat distribution in the weld. For the 5V case, the temperature at the laminate-ceramic interface (T3) is overestimated by the model, as reported by Ageorges *et al.* [46]. This can be explained by some neglected heat losses, such as the latent heat of fusion of the polymer film and matrix of the adherends, which is in fact more influent at low power levels, since the longer welding times cause bulk heating of the laminates.

Moreover, as Ageorges *et al.* [46] reported, the contact resistance, the power dissipated at the contact between the electrical connectors and the heating element, accounts for up to 8 % of the power density. However, in this case, the heat losses correspond to less than that, since the temperature at the center of the weld does match the experimental data.

Finally, the fact that the thermocouples may move in the joint, when the polymer softens and melts also induces some uncertainties in the measurements.

Table 12 shows the power density for the imposed heat generation and that obtained when using the imposed voltage boundary condition.

Table 12: Power Density of the Imposed Heat Generation and Imposed Voltage Conditions

Voltage (V)	Power Density, Heat Generation (GW/m^3)	Power Density Imposed Voltage (GW/m^3)
5	2.7	1.5
6	4.3	2.1
7	5.9	2.5
8	7.7	3.9

The difference (factor of 2) in the power densities of these two models is hard to explain. The power measured experimentally does not match this second power density. However, the results do match this third 3-D model, with the imposed voltage. This can be due to the fact that not all power input into the weld is converted to heat generation at the weld interface. In fact, since the metal mesh has as a wire density equal in its two in-plane directions, the heat generated in the heating element is not uniform and generated by only half of the wires of the mesh. Moreover, uncertainties in the measurements of the current and voltage imposed are another source of error. The investigation of this peculiarity is suggested as future work.

6.6 Heat Transfer along the Length of the Laminates

In order to confirm the results of section 5.6, the third and validated 3-D model has been coupled with the optimisation algorithm of Figure 19 and lead to a new optimum clamping distance of 0.8 mm. Figure 44 shows the weld interface temperature distributions along the Z-direction at the edge and center of the weld for the 6V case, the optimum clamping distance of 0.8 mm and the processing temperature of 450°C.

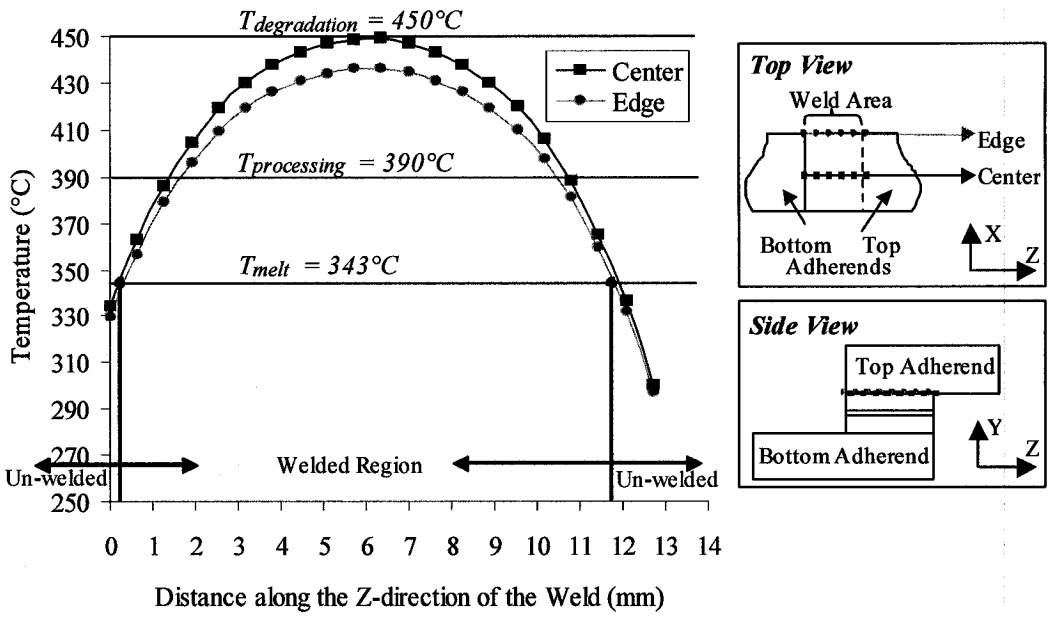

Figure 44: Thermal history along the length of the weld for the 6V case, a welding time of 23 s, and a clamping distance of 0.8 mm, using the 3-D model

Figure 44 shows again that it is impossible to obtain a uniform temperature distribution at the weld interface for the current resistance welded lap-shear joint configuration. According to this model, even a complete weld can not be obtained, since the maximum temperature of the joint would reach the *maximum welding temperature* of 450°C before the *minimum welding temperature* of 343°C is reached *everywhere*. However, a complete weld can be assumed for this particular temperature distribution, since the small regions (less than 1 mm wide), where the melting temperature is not reached, is considered welded. This is due to the squeeze flow of the polymer towards the edges of the weld in the plane. Therefore, the size of the processing window is nil in all voltage cases. The appropriate welding time must absolutely be determined with the model.

6.7 *Temperature Contours*

In order to further validate the third model, some welds have been performed. In fact, the 6V case is extensively studied. Three processing temperatures of 390°C, 450°C and 500°C, corresponding to the numerically determined welding times of 14.5 seconds, 23 seconds and 33 seconds, have been compared, using a constant optimum distance of 0.8 mm. Then, the effect of the clamping distance has been confirmed, using three clamping distances of 3.2 mm, 0.8 mm and 0 mm, at the optimum processing temperature of 450°C, corresponding to the welding time of 23 seconds. This implies five different welding conditions. Three samples were welded for each condition. Afterwards, the samples were lap-shear tested, using the ASTM standard D-5868 [73], in order to verify their lap shear strength.

The following three figures show the weld interface of the average lap shear strength sample welded under these conditions next to the numerically obtained temperature contours, for each condition, using the clamping distance of 0.8 mm.

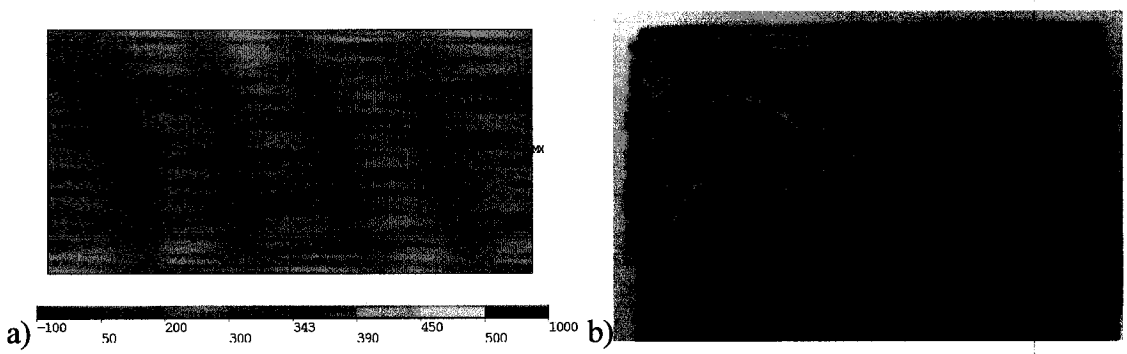

Figure 45: Weld Interface of the samples welded for 14.5s, using the optimum clamping distance of 0.8 mm a) Temperature Contours, b) Fracture surface

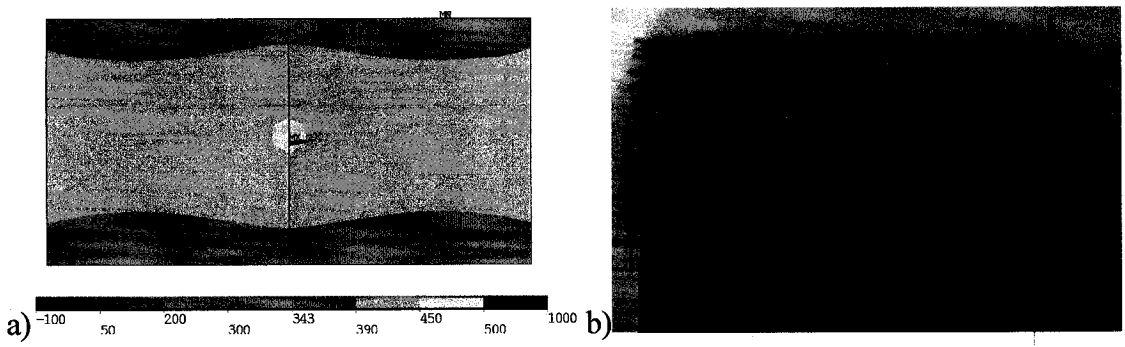

Figure 46: Weld Interface of the samples welded for 23s, using the optimum clamping distance of 0.8 mm a) Temperature Contours, b) Fracture surface

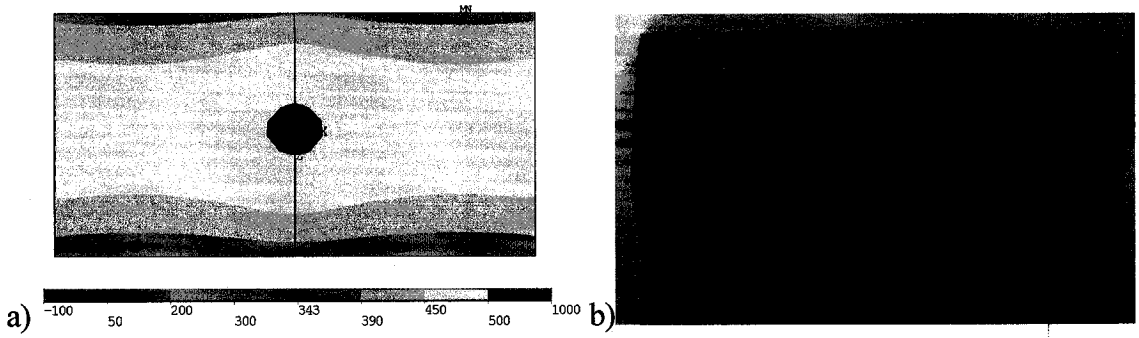

Figure 47: Weld Interface of the samples welded for 33s, using the optimum clamping distance of 0.8 mm a) Temperature Contours, b) Fracture surface

Figure 45, 26 and 27 show that the model predicts adequately the evolution of the temperature distribution at the weld interface. The black areas on each side of the weld show that the heating element is oxidized, due to the contact with air, during heating, causing polymer degradation. The numerical and experimental temperature distributions at the weld interface matches for all welds, showing a brighter color at the weld interface of the welded samples. The following table shows the strength of the joint welded under these first three conditions.

Table 13: Strength of joints welded for different times, using a clamping distance of 0.8 mm

Processing Temperature (°C)	Welding Time (s)	Tensile Strength (MPa)
390	14.5	28.6
450	23	47.4
500	33	41.6

Comparing Figure 45, 26, 27 and Table 13, we can confirm that increasing the processing temperature, hence the welding time, increases the welded area, up to the optimum processing time of 23 seconds. Then, the welded area stays constant even when the processing temperature of 500°C. However, the optimum weld strength obtained is also at 450°C, showing weaker polymer when it is heated up to 500°C. Hence, it is shown that the optimum welding conditions match that of numerical results, showing that the optimum processing temperature is 450°C, leading to a 23 seconds weld.

Figures 28 and 29 show the temperature contours and weld interface of the clamping distance of 0 mm and 3.2 mm respectively, for a 6V weld, for 23 seconds (processing temperature of 450°C). Table 9 lists the average strength of the welded specimens.

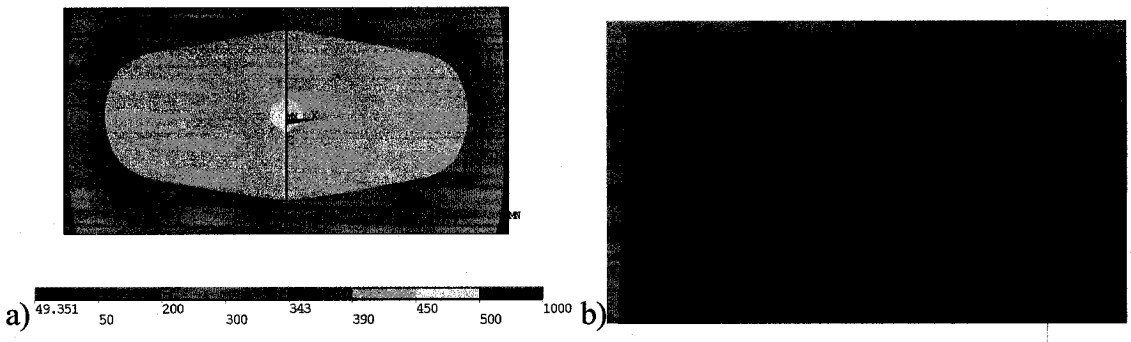

Figure 48: Weld Interface of the samples welded for 23s, using the clamping distance of 0 mm a) Temperature Contours, b) Fracture surface

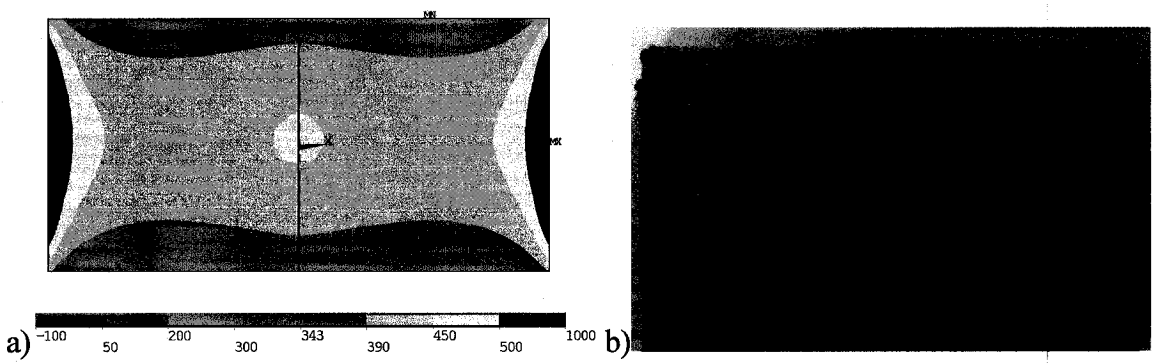

Figure 49: Weld Interface of the samples welded for 23s, using the clamping distance of 3.2 mm a) Temperature Contours, b) Fracture surface

Table 14: Strength of joints welded for 23 s., using different clamping distances

Clamping Distance (mm)	Processing Temperature (°C)	Welding Time (s)	Tensile Strength (MPa)
0	450	23	36.9
0.8	450	23	47.4
3.2	450	23	38.5

Comparing Figures 26, 28, 29, and Table 9, we can confirm that the clamping distance of 0 mm leads to unwelded edges, the clamping distance of 3.2 mm leads to overwelded edges and the optimum clamping distance of 0.8 mm leads to a complete weld, for the 6V case, 23 seconds welding time. Moreover, the optimum weld strength is obtained at the optimum clamping distance of 0.8 mm. Hence, it is shown that the optimum experimental welding conditions match that of the numerical optimum clamping distance of 0.8 mm.

7 Conclusions

1-D, 2-D, and 3-D transient heat transfer finite element models were developed to simulate the resistance welding of APC-2/CF laminates. APC-2/CF sandwiched between the PEEK polymer films was used as a heating element. The models were used to investigate the influences of latent heat, tooling-plates, and input power on the welding time, thermal history along and through the weld thickness. Here are the main outcomes of this work:

- The effects of latent heat on the heating rate and thermal history of the weld was insignificant due to the small amount of polymer at the weld interface.
- Tooling-plates with high thermal conductivity such as steel promote longer welding time than ceramic tooling-plate with low thermal conductivity.
- It was shown that the clamping distance influences the local overheating at the edges of the welds. An optimum clamping distance can considerably enlarge the processing window. Optimization of the clamping distance is recommended to reduce polymer degradation at the edges of the weld.
- High power levels promote very narrow processing windows, and result in polymer degradation at the edges of the welds.
- The 3-D model showed a large temperature gradient along the Z–direction, resulting in a combination of degradation, weld, and no weld zones at the weld interface due thermal conductivity along the length of the laminates.

- The model must include at least all objects that are within 50 mm of the weld interface, such as ceramic, copper connectors, etc., in order to appropriately determine the optimum clamping distance for a given power level.

- The imposed heat generation does not predict the process appropriately. Better results are obtained with the voltage input.

- The temperature contours obtained showed the pertinence of the model and its usefulness in determining the welding parameters required to obtain an optimal joint.

7.1 Future Work

Future work to be done on resistance welding includes:

- Investigate the different results obtained with the imposed voltage condition over the imposed uniform heat generation.

- Development of better quality large-scale welds, using modelling as a tool to improve the process.

- Durability performance evaluation of the optimal joint.

- Welding of large-scale carbon fibre laminates

- Non-destructive evaluation of the performance of resistance welded parts.

- Use resistance welding of carbon fibre laminates to join aerospace components.

8 References

1. K.K. Chawla, Composite Materials, Science and Engineering, Springer-Verlag, New York, (1998).
2. Yousefpour, A., Hojjati, M. and Immarigeon, J.-P., Welding of Thermoplastic Composites, An Overview. *Journal of Thermoplastic Composite Materials*, **17**, 303-341 (2004).
3. Xiao, X. R., Hoa, S. V., and Street, K. N. (1992). Processing Modelling of Resistance Welding of APC-2 Composite. *Journal of Composite Materials.* **26**(7):1031-1049.
4. Taylor, N.S. and Davenport, R. The Resistive Implant Welding of Thermoplastic Composite Materials. *ANTEC'91*, 2038-2041 (1991).
5. Stavrov, D. and Bersee, H. E. N., Thermal Aspects in Resistance Welding of Thermoplastic Composites. *ASME Summer Heat Transfer Conference 2003,* Las Vegas, NV, USA (2003).
6. Talbot, E., Yousefpour, A., Hubert, P. and Hojjati, M., Thermal Behavior During Thermoplastic Composites Resistance Welding. *Annual Technical Conference (ANTEC) of the Society of Plastics Engineers*, Boston, MA, USA (2005).
7. Mallick, P.K., Fiber-Reinforced Composites: Materials, Manufacturing and Design, 2nd Ed. Marcel Dekker inc. (1993) 566 p.
8. Davies, P., Cantwell, W. J., Jar, P-Y., Bourban, P. -E., Zysman, V. and Kausch, H. H. (1989). Joining and Repair of a Carbon Fiber-Reinforced Thermoplastic. *Composites*. **22**(6): 425-431.
9. Messler, R. W. Jr. (1995). The Challenges for Joining to Keep Pace with Advancing Materials and Designs. *Materials & Design.* **16**(5): 261-269.
10. Maguire, D. (1989). Joining Thermoplastic Composites. *SAMPE Journal.* **25** (1): 11-14.
11. Gehde, M., Giese, M., and Ehrenstein, G. W. (1997). Welding of Thermoplastics Reinforced with Random Glass Mat. *Polymer Engineering and Science.* **37**(4): 702-714.
12. Grimm, R. A. (1995). Welding Processes for Plastics. *Advance Materials and Processes*. **3**: 27-30.
13. Silverman, E.M. and Griese, R.A. (1989). Joining Methods for Graphite/PEEK Thermoplastic Composites, *SAMPE Journal*, **25**(5): 34-38.
14. Grimm, R. A. (1990). Fusion Welding Techniques for Plastics. *Welding Journal.* pp. 23-28.

15. Vetter, J., Benende, V., and Erlangen, G. W. (2000). Failure Behavior of Extrusion Welding Seams Made of Thermoplastic Plastics. *Welding and Cutting*. **52**(2): E34-E40.

16. Hilton, P. A., Jones, I. A., and Sallavanti, R. A. (2000). Laser Welding of Fabrics Using Infrared Absorbing Dyes. *ASM International/Proceedings from Joining of Advanced and Specialty Materials*. pp. 136-141.

17. Bates, P., Couzens, D., and Kendall, J. (2001). Vibration Welding of Continuously Reinforced Thermoplastic Composites. *Journal of Thermoplastic Composite Materials*. **14**: 344-354.

18. Grimm, R. A. (1995). Welding Processes for Plastics. *Advance Materials and Processes*. **3**: 27-30.

19. Potente, H. and Uebbing, M. (1997). Friction Welding of Polyamides. *Polymer Engineering and Science*. **37**(4): 726-737.

20. Eveno, E. C. and Gillespie, Jr., J. W. (1989). Experimental Investigation of Ultrasonic Welding of Graphite Reinforced Polyetheretherketone Composites. *21st International SAMPE Technical Conference*. **21**:923-934.

21. Shinoda, T. (2001). Recent Development of Friction Stir Welding-New Solid State Joining Technology. *International Journal of Materials and Product Technology*. **2**:453-460.

22. Ageorges, C., Ye, L., and Hou, M. (2001). Advances in Fusion Bonding Techniques for Joining Thermoplastic Matrix Composites: A Review. *Composites Part A: Applied Science and Manufacturing*. **32**: 839-857.

23. Sanders, P. (1987). Electromagnetic Welding: An Advance in Thermoplastics Assembly. *Materials and Design*. **8**(1): 41-45.

24. Lawless, G. W. and Reinhart, T. J. (1992). A Study of the Induction Heating of Organic Composites. *24th International SAMPE Technical Conference*. pp. T375-T384.

25. Varadan, V. K. and Varadan, V. V. (1991). Microwave Joining and Repair of Composite Materials. *Polymer Engineering and Science*. **31**(7): 470-486.

26. Staicovici, S., Wu, C-Y., and Benatar, A. (1999). Welding and Disassembly of Microwave Welded HDPE Bars. *Journal of Reinforced Plastics and Composites*. **18**(1): 35-43.

27. Volpe, V. (1980). Estimation of Electrical Conductivity and Electromagnetic Shielding Characteristics of Graphite/Epoxy Laminates. *Journal of Composite Materials*. **14**: 189-198.

28. Ageorges, C. and Ye, L. (2001). Simulation of Impulse Resistance Welding for Thermoplastic Matrix Composites. *Applied Composite Materials*. **8**: 133-147.

29. Yang, F. and Pitchumani, R. (2002). Interlaminar Contact Development During Thermoplastic Fusion Bonding. *Polymer Engineering and Science*. **42**(2) pp. 424-438.

30. Don, R. C., Bastien, L., Jakobsen, T. B., and Gillespie, Jr., J. W. (1990). Fusion Bonding of Thermoplastic Composites by Resistance Heating. *SAMPE Journal.* pp. 59-66.

31. Mcknight, S. H., Holmes, S. T., Gillespie, Jr., J. W., Lambing, C. L. T., and Marinelli, J. M. (1997). Scaling Issues in Resistance-Welded Thermoplastic Composite Joints. *Advances in Polymer Technology.* **6**(4):279-295.

32. Ageorges, C., Ye, L., and Hou, M. (2001). Experimental Investigation of the Resistance Welding for Thermoplastic-Matrix Composites. Part I: Heating Element and Heat Transfer. *Composites Science and Technology.* **60**: 1027-1039.

33. Holmes, S. T. and Gillespie, Jr., J. W. (1992). Thermal Analysis for Resistance Welding of Large-Scale Thermoplastic Composite Joints. *Proceedings of the American Society for Composites.* pp. 135-146.

34. Holmes, S. T. and Gillespie, Jr., J. W. (1993). Thermal Analysis for Resistance Welding of Large-Scale Thermoplastic Composite Joints. *Journal of Reinforced Plastics and Composites.* **12**(6): 723-736.

35. Ageorges, C., Ye, L., and Hou, M. (2000). Experimental Investigation of the Resistance Welding for Thermoplastic-Matrix Composites. Part II: Optimum Processing Window and Mechanical Performance. *Composites Science and Technology.* **60**: 1191-1202.

36. Eveno, C. and Gillespie, Jr. J. W. (1988). Resistance Welding of Graphite Polyetheretherketone Composites: An Experimental Investigation. *Journal of Thermoplastic Composite Materials.* **1**: 322-338.

37. Ageorges, C. and Ye, L. (2002) Fusion Bonding of Polymer Composites. Berlin, Springer. 273p.

38. Eveno, E. C., Gillespie, Jr., J. W., and Vinson, J. R. (1989). Resistance Welding of Graphite Polyetheretherketone Composites. *47th Annual Technical Conference/American Society of Mechanical Engineers* : 493-495.

39. Stavrov, D., Bersee, H. E. N., and Beukers, A. (2003) The Influence of the Heating Element on Resistance Welding of Thermoplastic Composite Materials. *Proceedings of ICCM – 14 Conference 2003,* San Diego, CA, USA. ID-1581.

40. Hou, M., andYang, M. (1999). Resistance Welding of Carbon Fibre Reinforced Thermoplastic Composite using Alternative Heating Element, *Composite Structures*, **47**: 667-672.

41. Arias, M. and Ziegmann, G. (1996). The Impulse Resistance Welding: A new Technique for Joining Advanced Thermoplastic Composite Parts. *41st International SAMPE Symposium and Exhibition.* **41**(2): 1361-1371.

42. Hou, M. and Friedrich, K. (1992) Resistance Welding of Continuous Glass-fiber Reinforced Polypropylene composites. *Composite Manufacturing.* **3**(2): 153-163.

43. Hou, M. and Friedrich, K. (1992) Resistance Welding of Continuous Carbon-Fiber/Polypropylene composites. *Plastic, Rubber and Composite Processing Applications*. **18**(4): 205-213.

44. Bastien, L.J., Gillespie, Jr. J. W. (1991). A Non-Isothermal Healing Model for Strength and Toughness of Fusion Bonded Joints of Amorphous Thermoplastics. *Polymer Engineering and Science*. **31**(24): 721-744.

45. Eveno, C. and Gillespie, Jr. J. W. (1988). Resistance Welding of Graphite Polyetheretherketone Composites: An Experimental Investigation. *Journal of Thermoplastic Composite Materials.* **1**: 322-338.

46. Ageorges, C., Ye, L., and Hou, M. (2000). Experimental Investigation of the Resistance Welding for Thermoplastic-Matrix Composites. Part I: Heating Element and Heat Transfer. *Composites Science and Technology*. **60**: 1027-1039.

47. Yousefpour, A., Simard, M., Octeau, M-A., Laramée, M., and Hojjati, M. , Effect of Mesh size on Resistance Welding of Thermoplastic Composites using Metal Mesh Heating Element, *SAMPE Europe 2004*, Paris, France (2004).

48. Yousefpour, A., Simard, M., Octeau, M-A., Laramée, M., and Hojjati, M., "Resistance Welding of Thermoplastic Composites," *COM 2004: The Conference of Metallurgists*, Hamilton, ON August 22-25, 2004.

49. Hou, M., Yang, M., Beehag, A., Mai, Y-W., and Ye, L. (1999). Resistance Welding of Carbon Fiber Reinforced Thermoplastic Composite using Alternative Heating Element. *Composite Structures*. **47**:667-672.

50. Taylor, N. S. and Davenport, R. (1991). The Resistive Implant Welding of Thermoplastic Composite Materials. *49th Annual Technical Conference/American Society of Mechanical Engineers.* pp. 2039-2041.

51. Stavrov, D. and Bersee, H.E.N. (2005). Resistance Welding of Thermoplastic Composites – An Overview. *Composites: Part A*. **36**: 39-54

52. Ageorges, C., Ye, L., and Hou, M. (2000). Experimental Investigation of the Resistance Welding for Thermoplastic-Matrix Composites. Part II: Optimum Processing Window and Mechanical Performance. *Composites Science and Technology.* **60**: 1191-1202.

53. Jakobson, T. B., Don, R. C., and Gillespie, Jr., J. W. (1989). Two Dimensional Thermal Analysis of Resistance Welded Thermoplastic Composites. *Polymer Engineering and Science*. **29**(23): 1722-1729.

54. Lambing, C.L.T., Andersen, S.M., Holmes, S.T., Leach, B.S., Don, R.C. and Gillespie, J.W.Jr. (1990) Design and Manufacture of an Automated Resistance Welder for Thermoplastic Composites. *Proceedings of the 49th SPE ANTEC Conference*, May 1990.

55. Ageorges, C. and Ye, L. (2001). Simulation of Impulse Resistance Welding for Thermoplastic Matrix Composites. *Applied Composite Materials*. **8**: 133-147.

56. Yousefpour, A., Simard, M., Octeau, M.-A. and Hojjati, M. (2005) Process Optimization of Resistance Welded Thermoplastic Composites using Metal Mesh Heating Elements. *SAMPE Long Beach*, California, May 2005.

57. Howie, I., Gillespie, Jr. J.W. and Smiley, J. (1993) Resistance Welding of Graphite Polyarylsulfone/polysulfone dual-polymer composites. *Journal of Composite Materials*. **6**: 205-225.

58. Ageorges, C. and Ye, L. (2001) Resistance Welding of Thermosetting composite/thermoplastic composite joints. *Composites: Part A*. **32**: 1603-1612.

59. McKnight, S.H., Holmes, S.T., Gillespie, Jr. J.W., Lambing, C.L.T. and Marinelli. J.M. (1991) Resistance Heated Fusion Bonding of Carbon Fiber/PEEK composites and 7075-T6 Aluminium. ANTEC 1991: 1474-1479.

60. Taylor, N.S. and Davenport, R. The Resistive Implant Welding of Thermoplastic Composite Materials. *ANTEC'91*, 2038-2041 (1991).

61. Xiao, X. R., Hoa, S. V., and Street, K. N. (1992). Processing Modelling of Resistance Welding of APC-2 Composite. *Journal of Composite Materials*. **26**(7): 1031-1049.

62. Maffezzoli, A. M., Kenny, J. M. and Nicolais, L. (1989). Welding of PEEK/Carbon Fibre Composite Laminates. *SAMPE Journal*. **25**(1): 35-39.

63. Colak, Z.S., Sonmez, F.O. and Kalenderoglu, V. (2002) Process Modelling and Optimisation of Resistance Welding for Thermoplastic Composites.

64. Ageorges, C., Ye, L., Mai, T. -W., and Hou, M., Characteristics of Resistance Welding of Lap Shear Coupons. Part I: Heat Transfer. *Composites Part A*, **29A**, 899-909 (1998).

65. Ageorges, C., Ye, L., Mai, T. -W., and Hou, M., Characteristics of Resistance Welding of Lap Shear Coupons. Part III: Crystallinity. *Composites Part A*, **29A**, 921-932 (1998).

66. Ageorges, C., Ye, L., Mai, T. -W., and Hou, M., Characteristics of Resistance Welding of Lap Shear Coupons. Part II: Consolidation. *Composites Part A*, **29A**, 911-919 (1998).

67. Don, R. C., Gillespie, Jr., J. W., and Lambing, C. L. T. (1992). Experimental Characterization of Processing Performances Relationships of Resistance Welded Graphite/Polyetheretherketone Composite Joints. *Polymer Engineering and Science*. **32**(9): pp. 620-631.

68. Ozawa, T. (1971). Kinetics of Non-Isothermal Crystallisation. *Polymer*. **12**: 150-158.

69. Velisaris, C.N. and Seferis, J.C. (1986) Crystallization Kinetics of Polyetheretherketone (PEEK) Matrices. *Polymer Engineering and Sciences*. **26**(22): 1574-1581.

70. Choe, C.R. and Lee, K.H. (1989) Non-Isothermal Crystallisation Kinetics of Polyetheretherketone. *Polymer Engineering and Sciences*. **29**: 801-805.

71. Graphtek LLC, *Grade GCGW-5110 Product Data Sheet*, Buffalo Grove, IL (2004).

72. *Engineering Properties of Steels*. Philip D. Harvey Editor, ASM, Metals Park, OH (1982).

73. American Society for Testing and Materials, D5868-01 Standard Test Method for Lap Shear Adhesion for Fiber Reinforced Plastic (FRP) Bonding (2001).

74. *Thermoplastic Composite Materials Handbook*. CYTEC Fiberite Inc, Anaheim, CA (1999).

75. Xu, J. and Wirtz, R. A., In-Plane Effective Thermal Conductivity of Plain-Weave Screen Laminates. *IEEE Transactions on Components and Packaging Technologies*, **25**(4), 615-620 (2002).

76. *ASM Specialty Handbook - Copper and Copper Alloys,* Davis & Associates ed., ASM, Metals Park, OH (2001).

77. *ANSYS User's Manual*. ANSYS, Inc., Canonsburg, PA (1999).

Appendix A

Remarks on Replacing Ceramic with a Convection Coefficient

In their model of the resistance welding process, Holmes *et al.* [33-34] assumed that the ceramic insulator on top of the weld could be represented by a simple convection coefficient ($h_{convection}$). The following picture shows a representation of this assumption.

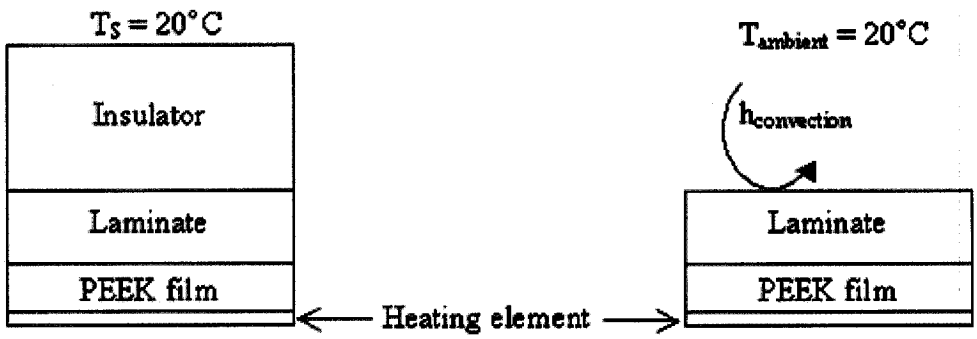

Figure 50: Two different representations for ceramic, 1-D models

Maffezzoli [62] found that heat loss in the tooling influences greatly the thermal history of the weld, for an asbestos insulator thickness of 20 mm. Holmes *et al.* [33-34] used this information and came up with an equivalent convection coefficient for ceramic of h = 75 $W/m^2 \cdot °C$. This equivalent convection coefficient approach used by Holmes *et al.* [33-34] comes from a steady-state conduction analysis, where the energy balance equation is reduced to equation A-1.

$$q = \frac{k \cdot A}{L}(T_2 - T_1), \tag{A-1}$$

where q (W) is the rate of heat transfer through the insulator, T_2 (°C) is the temperature at the interface laminate – insulator, T_1 (°C) is the temperature at the exterior surface of the insulator, L (m) is the thickness of the insulator, A (m^2) is the area of laminate in contact with the insulator and k ($W/m^2 \cdot °C$) is the thermal conductivity of the material.

Holmes *et al.* [33-34] coupled the conduction equation to the relation for a simple surface convection analysis, shown in equation A-2.

$$q = h \cdot A(T_2 - T_0), \tag{A-2}$$

where q (W) is the rate of heat transfer to "air", T_2 (°C) is the temperature at the exterior surface of the laminate, T_0 (°C) is the ambient temperature, A (m^2) is the area of laminate exposed to "air" (in contact with the insulator) and h ($W/m^2 \cdot °C$)is the convection coefficient.

Merging equations A-1 and A-2, in order to equate the heat losses by both conduction and convection models, and setting $T_1 = T_0$, leads to equation 3.

$$h = \frac{k}{L} \tag{A-3}$$

With a typical value for ceramics of k = 1.5 $W/m \cdot °C$ and L = 0.020 m, h = 75 $W/m^2 \cdot °C$. This proves that Holmes *et al.* [33-34] used this steady-state rule to determine their so-called equivalent heat convection coefficient. The same happened for steel, with a typical

k = 20 W/m·K and L = 0.020 m, where a so-called equivalent convection coefficient h = 1000 W/m^2·K is obtained.

However, since resistance welding is a transient thermal process, the temperatures vary with time, equations 1 and 2 are not valid. The energy balance equation must include the time dependence, in order to take into account the thermal inertia (density and heat capacity) of all the materials.

$$k\frac{\partial^2 T}{\partial x^2} + q_G''' = \rho \cdot c_P \frac{\partial T}{\partial t}. \tag{A-4}$$

where k is the thermal conductivity of the material, d^2T/dx^2 is the variation in the temperature gradient through the ceramic, q_G''' is the volumetric heat generated, ρ is the density of the material and c_p is the heat capacity or specific heat of the material.

Solving equation 4 for the temperature at the surface of the insulator, defined as x = 0, leads to the following heat flux [62].

$$q''(t) = \frac{k(T_2 - T_0)}{\sqrt{\pi \cdot \frac{k}{\rho \cdot c_P} \cdot t}}. \tag{A-5}$$

Rearranging the terms, we get:

$$q''(t) = \sqrt{\frac{k \cdot \rho \cdot c_P}{\pi}}(T_2 - T_0) \cdot t^{(-1/2)}. \tag{A-6}$$

Merging equations (6) and (2), which is valid at all times, it is possible to get the convection coefficient as a function of time.

$$h = \sqrt{\frac{k \cdot \rho \cdot c_P}{\pi}} \cdot t^{(-1/2)} \tag{A-7}$$

From equations 3 and 7, it can be seen that the total energy dissipated by the two phenomena shown in Figure A-1, have a different behaviour in time. Therefore, the equivalent convection coefficient varies with time, so it is not recommended to use an equivalent convection coefficient, calculated with the steady-state energy balance equation.

Appendix B

Heating Element Modelling

The heating element is a single plain weave cross-ply layer of stainless steel type 304. Table 15 shows the principal dimensions of the mesh and Figure 51 shows the 3-D representation of the mesh, as well as a zoom on a small repeated pattern, called unit cell.

Table 15: Geometry of the stainless steel metal mesh

Variable(s)	Dimension	Value
dx, dy	Wire Diameter (mm)	0.04064
Mx My	Number of Wires/in *X*-direction *Y*-direction	 200 200
c_f	Compression factor	1
n	Number of Screens	1

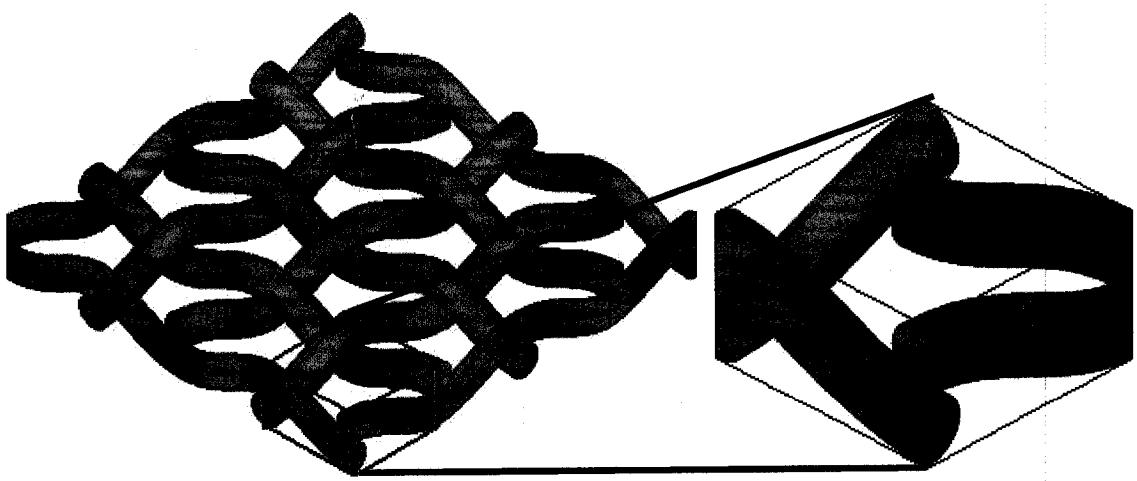

Figure 51. Plain weave, 3-D representation (On the right, one Unit Cell)

This square woven metal mesh heating element is made of Stainless Steel Type 304 [73]. Using Table 1, the volume fraction of stainless steel is calculated to be v_{steel} = 25%. Table 16 presents the thermal and electrical properties of stainless steel type 304.

Table 16: Properties of stainless steel type 304 [73]

Property (Units)	Value
Density (kg/m3)	8000
Specific Heat (J/kg·°C)	500
Thermal Conductivity (W/m·°C)	16.2
Resistivity (Ω·m)	1.4 *10-6

The equivalent properties of the metal mesh have been calculated using those of stainless steel type 304 [72], embedded in poly-ether-ether-ketone polymer (PEEK) [33-34]. These properties could also have been calculated with a stainless steel mesh in air, but the properties of the heating element do not influence the heat dissipation in the weld during heating, due to the heat generated in that material. Therefore, it only has influence when cooling the joint, and during cooling, the mesh is assumed to be filled with PEEK polymer.

The effective specific heat and density of the heating element are calculated using the rule of mixture, as shown in equation B-1.

$$\rho_{heating\ element} = \rho_{steel} \cdot v_{steel} + \rho_{PEEK} \cdot v_{PEEK} \quad \text{(B-1)}$$

$$c_{p\,heating\,element} = \frac{\rho_{steel} \cdot v_{steel} \cdot c_{p\,steel} + \rho_{PEEK} \cdot v_{PEEK} \cdot c_{p\,PEEK}}{\rho_{mesh}\left(v_{steel} + v_{PEEK}\right)} \qquad \text{(B-2)}$$

In order to determine the effective thermal conductivity and electrical resistivity of the metal mesh, in all directions, a small repeated pattern is studied. Figure 52 shows 2-D representations of this pattern, called unit cell, as well as an equivalent model of the cell, as proposed by Xu *et al.* [75]. In Figure 52, *Mx* and *My* are the mesh numbers, *dx* and *dy* are the wire diameters of the wires, in the ***x*** and ***y*** directions, *g* is a measure of the contact between the wire filaments at the intersections: $g = \pi/(4 \cdot c_f)$, and c_f is the compression factor of a mesh stack. In this case, since there is only one layer of mesh, $c_f = 1$.

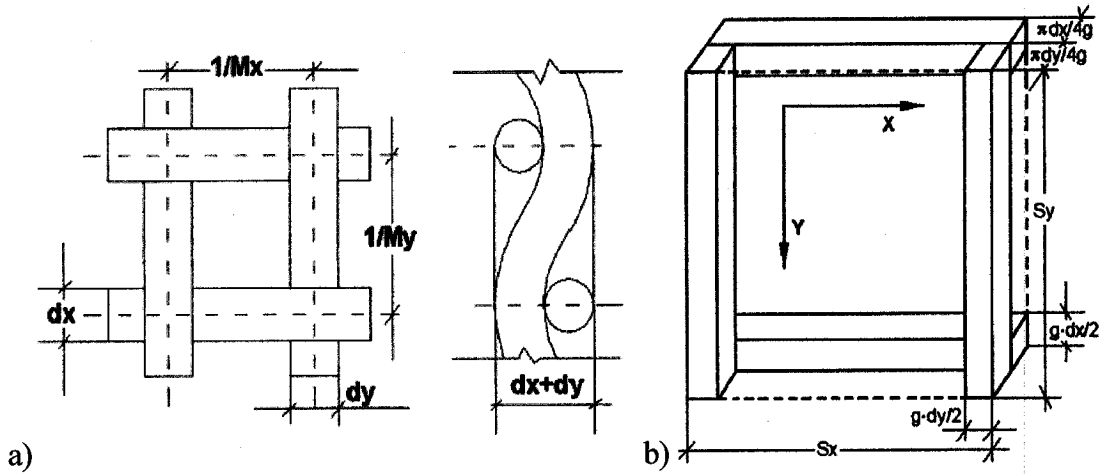

Figure 52: Unit Cell, a) 2-D sketch b) Transformed [75]

Equations B-3 and B-4 shows the calculations of *Sx* and *Sy*, the equivalent filament lengths of the unit cell in the ***x*** and ***y*** directions, as shown in Figure 52.

$$Sx = \frac{1}{Mx}\left[1 + 9.6\left(\frac{dy \cdot Mx}{4}\right)^2 - 49.2\left(\frac{dy \cdot Mx}{4}\right)^4\right] \quad \text{(B-3)}$$

$$Sy = \frac{1}{My}\left[1 + 9.6\left(\frac{dx \cdot My}{4}\right)^2 - 49.2\left(\frac{dx \cdot My}{4}\right)^4\right] \quad \text{(B-4)}$$

Xu *et al.* [75] calculated the equivalent thermal conductivity and electrical resistivity of a porous material (metal mesh) in another medium, using the equivalent composite plane wall thermal resistance analogy, for the mesh and its surrounding medium. Figure 53 and Figure 54 show the application of the equivalent composite plane wall thermal resistance analogy, on Xu *et al.* [75] unit cell, for the calculation of the in-plane and through-thickness thermal conductivity.

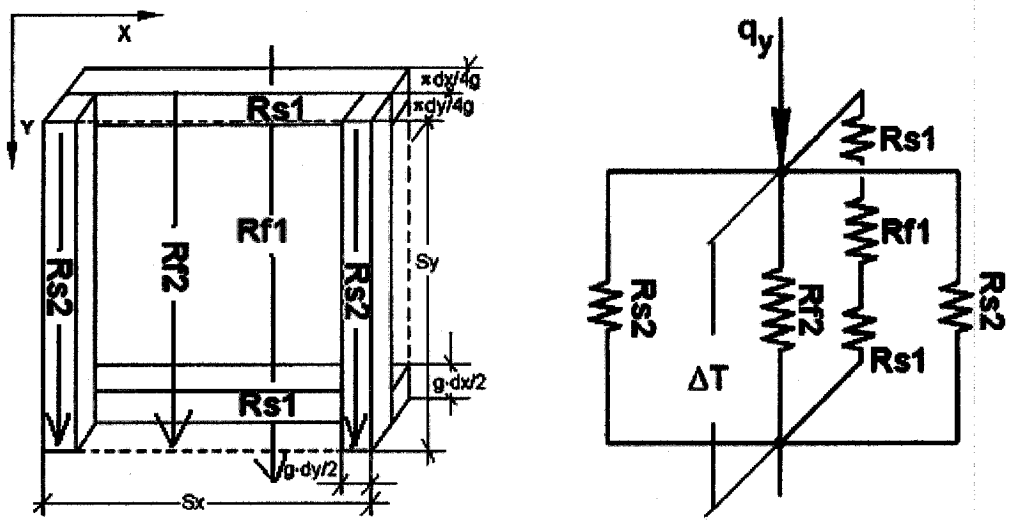

Figure 53: Thermal circuit for the in-plane properties [75]

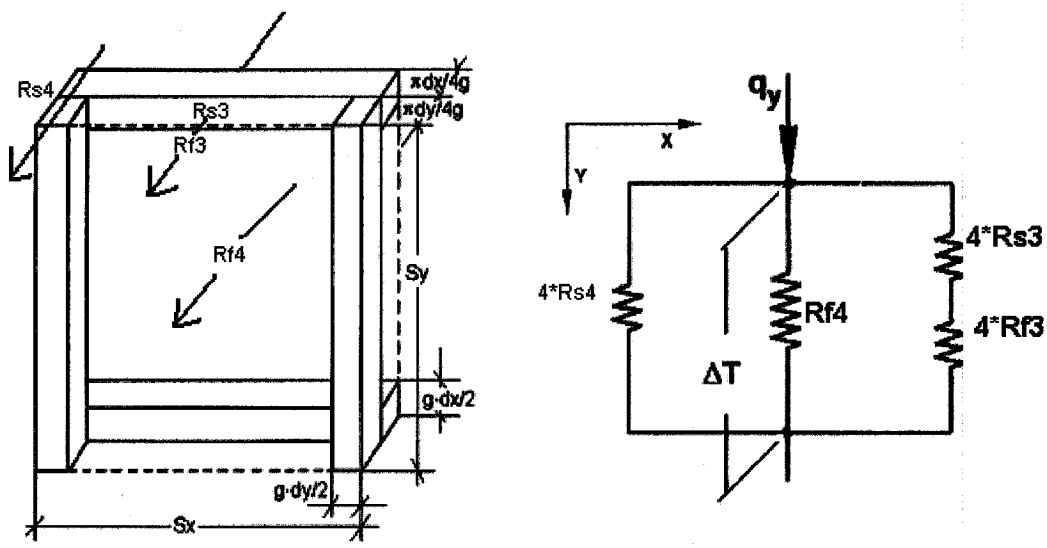

Figure 54: Thermal circuit for the through-thickness properties

In Figure 53 and Figure 54, R is the resistance, whether thermal or electrical, the subscripts *"s"* means steal, *"f"* means fluid (representing the surrounding medium), and 1,2,3,4 are the numbering of the different sections of the composite plane wall. Next to the unit cells of Xu *et al.* [75] are the equivalent thermal circuits. First, the thermal resistance is calculated for each section, using equation B-5.

$$R = \frac{L}{k \cdot A} \tag{B-5}$$

where L is the length in the axis of interest, A is the cross-sectional area, k is the thermal conductivity of the material. Then, the equivalent in-plane thermal resistance is calculated, from the circuit of Figure 53 and equation B-6.

$$R_{Y-TOTAL} = \left(\frac{1}{2 \cdot R_{S2}} + \frac{1}{R_{f2}} + \frac{1}{2 \cdot R_{S1} + R_{f1}} \right) \tag{B-6}$$

Since $Mx = My$ and $dy = dx$, the mesh is symmetric, $R_{Y-TOTAL} = R_{X-TOTAL}$. The equivalent through-thickness thermal resistance is calculated from Figure 54 and equation B-7.

$$R_{Z-TOTAL} = \left(\frac{1}{4 \cdot R_{S4}} + \frac{1}{R_{f4}} + \frac{1}{4 \cdot R_{S3} + 4 \cdot R_{f3}} \right). \quad \text{(B-7)}$$

The equivalent total thermal conductivities $k_{Y\text{-}TOTAL}$ and $k_{Z\text{-}TOTAL}$ are finally determined, solving equation 1, replacing R by $R_{Y\text{-}TOTAL}$ and $R_{Z\text{-}TOTAL}$, respectively. The circuit of Figure 53 and equation B-6 also apply to determine the equivalent through-thickness electrical resistivity, using R calculated as in equation B-8.

$$R = \frac{\rho \cdot L}{A} \quad \text{(B-8)}$$

where R is the electrical resistance, ρ is the electrical resistivity (Ω·m), A is the cross-sectional area, L is the length in the axis of interest. Again, the results of equations 2 and 3 are put back into equation B-8, in order to obtain the equivalent electrical resistivity of the mesh. Table 4 finally shows the calculated properties of the metal mesh heating element, as discussed in this section.

Table 17: Calculated effective properties of the heating element

Parameter (Units)	Variable	Value
Equivalent In-Plane Thermal Conductivity (W/m·K)	$k_{xx\ EQ}$	2.181
Equivalent Through-Thickness Thermal Conductivity (W/m·K)	$k_{yy\ EQ}$	0.248
Equivalent Resistivity (Ω·m)	ρ_{EQ}	$1.82945 \cdot 10^{-5}$

Appendix C

ANSYS APDL Macros

1-D Model

```
/units,si
/PREP7
```

Element Definition

```
ET,1,PLANE55
KEYOPT,1,1,0
KEYOPT,1,3,0
KEYOPT,1,4,0
KEYOPT,1,8,0
KEYOPT,1,9,0
```

Constant Material Properties

```
Toffst,273

!---------------------------------- 1 - Metal Mesh Heating Element
MP,KXX,1,2.181
MP,KYY,1,0.2148
MP,KZZ,1,2.181
DENS,1,2973
C,1,735

!---------------------------------- 2 - PEEK Polymer
MP,KXX,2,0.251

!---------------------------------- 3 - Laminate
MP,KXX,3,0.658
MP,KYY,3,0.658
MP,KZZ,3,6.8

!---------------------------------- 4 - Ceramic Insulator
MP,KXX,4,1.26
MP,C,4,1000
MP,DENS,4,2715
```

*ASK,VALUE, "1" to NOT consider latent heat or "2" to consider Latent Heat

Temperature-Dependant Material Properties, without Latent Heat

*IF,VALUE,EQ,1,THEN
MPTEMP,1,0,50,100,150,200,250
MPTEMP,7,300,350,400,1000

!---------- 2 - PEEK Polymer
MPDATA,DENS,2,1,1305,1298,1285,1267,1239,1208
MPDATA,DENS,2,7,1177,1141,1108, 1108
MPDATA,C,2,1,610,944,1226,1790,1893,2149
MPDATA,C,2,7,2534,2790,2918, 1108

!---------- 3 - Laminate
MPDATA,DENS,3,1,1601,1598,1593,1586,1575,1563
MPDATA,DENS,3,7,1551,1537,1524,1524
MPDATA,C,3,1,800,930,1040,1260,1300,1400
MPDATA,C,3,7,1550,1650,1700, 1700

Temperature-Dependant Material Properties, with Latent Heat

*ELSEIF,VALUE,EQ,2
MPTEMP,,,,,,,,
MPTEMP,1,0,50,100,150,200,250
MPTEMP,7,300,350,400,1000

!---------- 2 - PEEK Polymer
MPDATA,DENS,2,1,1305,1298,1285,1267,1239,1208
MPDATA,DENS,2,7,1177,1141,1108,1108

!---------- 3 - Laminate
MPDATA,DENS,3,1,1601,1598,1593,1586,1575,1563
MPDATA,DENS,3,7,1551,1537,1524,1524

MPTEMP,,,,,,,,
MPTEMP,1,0,50,100,150,200,250
MPTEMP,7,300,330,345,350,400
!---------- 2 - PEEK Polymer
MPDATA,enth,2,1,39802500,101068100,179838600,293235100,410506450,540306050
MPDATA,enth,2,7,689431950,784659150,880835100,896752050,1058409250

!---------- 3 - Laminate
MPDATA,enth,3,1,64040000,138347000,221183000,321101000,423476000,532886000
MPDATA,enth,3,7,653088500,727712000,790867400,803547650,933087650
*ENDIF

Input Variables

```
FilmThickness=0.000127
LaminateThickness=0.002159
CeramicThickness=5/4*0.0254
WeldLength=0.0254
Width1D=0.002159
T_ambient=20
H_air=5
WeldWidth=0.0254/2

TT=100      !Duration of the heating step
ElementThickness=2*(0.0016*0.0254)/2
Power=2.0E9
```

1-D Geometry

```
K,1
K,2,Width1D
K,3,Width1D,ElementThickness
K,4,0,ElementThickness
K,5,0,ElementThickness+FilmThickness
K,6,Width1D,ElementThickness+FilmThickness
K,7,Width1D,ElementThickness+FilmThickness+LaminateThickness
K,8,0,ElementThickness+FilmThickness+LaminateThickness
K,9,Width1D,ElementThickness+FilmThickness+LaminateThickness+CeramicThickness
K,10,0,ElementThickness+FilmThickness+LaminateThickness+CeramicThickness

A,1,2,3,4
A,4,3,6,5
A,5,6,7,8
A,8,7,9,10
```

1-D Mesh

```
MSHAPE,0,2-D
MSHKEY,1
!------------------------------- 1 - Metal Mesh Heating Element
MAT,1
AESIZE,1,ElementThickness*10
AMESH,1

!------------------------------- 2 – PEEK Polymer
MAT,2
AESIZE,2,ElementThickness*10
AMESH,2
```

```
!------------------------------ 3 - Laminate
MAT,3
AESIZE,3,ElementThickness*40
AMESH,3

!------------------------------ 4 - Ceramic Insulator
MAT,4
AESIZE,4,ElementThickness*80
AMESH,4
```

1-D Boundary Conditions

```
SFL,12,CONV,H_air, ,T_ambient
BFA,1,HGEN,Power
FINISH
```

Transient Analysis

```
/SOL
ANTYPE,4
neqit,35
TUNIF,T_ambient
TIME,TT          ! Duration of the analysis
AUTOTS,ON
DELTIM,1, , ,    ! Time interval between each solution
KBC,1

ALLSEL,ALL
OUTPR,ALL,ALL,
OUTRES,ALL,ALL
SOLVE
FINISH
```

Post-Processing

```
/POST1
PLNSOL,TEMP, ,0,
/CVAL,1,50,100,200,300,343,400,450,1000
/REPLOT
FINISH
```

2-D Model with Clamping Distance Optimisation

```
/units,si
CD1=0.0127
CD2=0.000001
GO=1 !Stop index for the *dowhile loop. (stops when Go=0)
*ASK,Toler, the tolerance (%) on the temperature variation at the weld interface (>0)
Tolerance=Toler/100*343!
i=1
TT=100
deltat=1
*DIM,Center,ARRAY,100,TT/deltat
*DIM,Edge,ARRAY,100,TT/deltat
```

*** Beginning of the Optimisation Loop ***

```
*dowhile,Go
/Filname,STRCAT('Clamp2D-CstPower-',chrval(i)),1

/PREP7
*IF,i,EQ,1,THEN
ClampingDistance=CD1 !12.7mm
*ELSEIF,i,EQ,2
ClampingDistance=CD2
*ELSE
ClampingDistance=(CD1+CD2)/2
*endif
```

Element Definition

```
ET,1,PLANE55
KEYOPT,1,1,0
KEYOPT,1,3,0
KEYOPT,1,4,0
KEYOPT,1,8,0
KEYOPT,1,9,0
```

Constant Material Properties

```
Toffst,273

!------------------------------- 1 - Metal Mesh Heating Element
MP,KXX,1,2.181
MP,KYY,1,0.2148
MP,KZZ,1,2.181
DENS,1,2973
C,1,735
```

```
!------------------------------ 2 - PEEK Polymer
MP,KXX,2,0.251
!MP,RSVX,2,0.1
!------------------------------ 3 - Laminate
MP,KXX,3,0.658
MP,KYY,3,0.658
MP,KZZ,3,6.8
!------------------------------ 4 - Ceramic Insulator
MP,KXX,4,1.26
MP,C,4,1000
MP,DENS,4,2715
!------------------------------ 5 - Copper Connector
MP,DENS,5,8900
MP,KXX,5,345
MP,C,5,0.385
```

Temperature-Dependant Material Properties, without Latent Heat

```
MPTEMP,1,0,50,100,150,200,250
MPTEMP,7,300,350,400,1000
!------------------------------ 2 - PEEK Polymer
MPDATA,DENS,2,1,1305,1298,1285,1267,1239,1208
MPDATA,DENS,2,7,1177,1141,1108
MPDATA,C,2,1,610,944,1226,1790,1893,2149
MPDATA,C,2,7,2534,2790,2918

!------------------------------ 3 - Laminate
MPDATA,DENS,3,1,1601,1598,1593,1586,1575,1563
MPDATA,DENS,3,7,1551,1537,1524
MPDATA,C,3,1,800,930,1040,1260,1300,1400
MPDATA,C,3,7,1550,1650,1700
```

Input Variables

```
WeldWidth=0.0254
ElementLength=WeldWidth/2+ClampingDistance
FilmThickness=0.000127
LaminateThickness=0.002159
LaminateLength=0.0254*1/2
CeramicThickness=5/4*0.0254
T_ambient=25
H_air=5
CopperWidth=0.01571
CopperThickness=0.375*0.0254
ElementThickness=2*(0.0016*0.0254)/2
Power=2.0E9
```

2-D Geometry

K,1
K,2,LaminateLength
K,3,LaminateLength,ElementThickness
K,4,0,ElementThickness
K,5,ElementLength
K,6,ElementLength,ElementThickness
K,7,0,ElementThickness+FilmThickness
K,8,LaminateLength,ElementThickness+FilmThickness
K,9,LaminateLength,ElementThickness+FilmThickness+LaminateThickness
K,10,0,ElementThickness+FilmThickness+LaminateThickness
K,11,LaminateLength,ElementThickness+FilmThickness+LaminateThickness+CeramicThickness
K,12,0,ElementThickness+FilmThickness+LaminateThickness+CeramicThickness
K,13,ElementLength+CopperWidth
K,14,ElementLength+CopperWidth,ElementThickness
K,15,ElementLength+CopperWidth,ElementThickness+CopperThickness
K,16,ElementLength,ElementThickness+CopperThickness

A,1,2,3,4
A,2,5,6,3
A,4,3,8,7
A,7,8,9,10
A,10,9,11,12
A,5,13,14,6
A,6,14,15,16

2-D Mesh

MSHAPE,0,2-D
MSHKEY,1

!---------- 1 - Metal Mesh Heating Element, in the weld
MAT,1
AESIZE,1,0.0008
AMESH,1

!---------- 2 – PEEK Polymer
MAT,2
AESIZE,3,0.0008
AMESH,3

```
!------------------------------ 1 - Metal Mesh Heating Element, out of the weld
MAT,1
AESIZE,2,0.0008
AESIZE,6,0.0008
AMESH,2
AMESH,6

!------------------------------ 3 - Laminate
MAT,3
AESIZE,4,0.0016
AMESH,4

!------------------------------ 4 - Ceramic Insulator
MAT,4
AESIZE,5,0.0032
AMESH,5

!------------------------------ 5 - Copper Connector
MAT,5
AESIZE,7,0.0032
AMESH,7
```

2-D Boundary Conditions

```
spctemp,1,20
stef,5.65E-8

SFL,7,RDSF,0.95, ,1
SFL,7,CONV,H_air, ,T_ambient
SFL,18,RDSF,0.95, ,1
SFL,18,CONV,H_air, ,T_ambient
allsel,all
LSEL,S,LOC,X,LaminateLength
LSEL,A,LOC,X,ElementLength
LSEL,A,LOC,X,ElementLength+CopperWidth
LSEL,U,LOC,Y,0,ElementThickness
LSEL,A,LOC,Y,ElementThickness+FilmThickness+LaminateThickness+CeramicThickn
ess
LSEL,A,LOC,Y,ElementThickness+CopperThickness
SFL,ALL,CONV,H_air,,T_ambient

BFA,1,HGEN,Power
BFA,2,HGEN,Power

FINISH
```

Transient Analysis

```
/SOL
ANTYPE,4
TUNIF,T_ambient
TIME,TT
AUTOTS,OFF
DELTIM,deltat, , ,
KBC,1

ALLSEL,ALL
OUTPR,ALL,ALL,
OUTRES,ALL,ALL
SOLVE
FINISH
```

Post-Processing

```
/POST1
PLNSOL,TEMP, ,0,
/CVAL,1,50,200,300,343,400,450,500,10000
/REPLOT
FINISH

/POST26
numvar,200
NSOL,2,36,TEMP,, Center
STORE,MERGE
NSOL,3,35,TEMP,, Edge
STORE,MERGE
```

Create a table to look for the time where Tcenter is equal to 390℃

```
VGET,Center(1,i,1),2
VGET,Edge(1,i,1),3

k=1
Test=1
*dowhile,Test
Test=390-Center(k,i)
k=k+1
*enddo

CenterTemp=Center(k-1,i)
EdgeTemp=Edge(k-1,i)

*IF,i,GT,2,THEN
*IF,CenterTemp-EdgeTemp,LT,Tolerance,THEN
```

```
CD1=ClampingDistance
*ELSEIF,CenterTemp-EdgeTemp,GT,Tolerance
CD2=ClampingDistance
*endif
*IF,EdgeTemp-CenterTemp,ABLT,Tolerance,THEN
GO=0
*endif
*endif

FINISH

/POST1
SET,,, ,,, ,k-1
PATH,Path,2,30,20,
PPATH,1,0,0,ElementThickness+FilmThickness,,0,
PPATH,2,0,LaminateLength,ElementThickness+FilmThickness,,0,
PDEF,,TEMP, ,AVG
/PBC,PATH, ,0
PLPATH,TEMP
FINISH

OptimumC=ClampingDistance
Title=STRCAT('Clamp2D-CstPower-',chrval(i))
save,Title,db,,all
i=i+1

PARSAV,all,,,
/CLEAR,NOSTART
PARRES,NEW,,,

*enddo                    ** End of the Optimisation Loop **
```

3-D Model at the Optimum Clamping Distance

```
/units,si

TT=100
deltat=1
i=1
/Filname,STRCAT('Clamp3D- opt',chrval(i)),1
/PREP7
ClampingDistance=0.0008
Toffst,273
```

Element Definition

```
ET,1,SOLID69
KEYOPT,1,2,0
DOF,VOLT,CURR,TEMP
```

Constant Material Properties

```
!------------------------------- 1 - Metal Mesh Heating Element
MP,KXX,1,2.181
MP,KYY,1,0.2148      !9.17E-5
MP,KZZ,1,2.181
DENS,1,2973
C,1,735
!MP,RSVX,1,1.82945E-05
!------------------------------- 2 - PEEK Polymer
MP,KXX,2,0.251
!MP,RSVX,2,1E13
!------------------------------- 3 - Laminate
MP,KXX,3,0.658
MP,KYY,3,0.658
MP,KZZ,3,6.8
!MP,RSVX,3,1E12
!------------------------------- 4 - Ceramic Insulator
MP,KXX,4,1.26
MP,C,4,1000
MP,DENS,4,2715
!MP,RSVX,4,1E12
!------------------------------- 5 - Copper Connector
MP,DENS,5,8900
MP,KXX,5,345
MP,C,5,0.385
!MP,RSVX,5,1.92E-08
```

Temperature-Dependant Material Properties, without Latent Heat

```
MPTEMP,1,0,50,100,150,200,250
MPTEMP,7,300,350,400,1000

!------------------------------ 2 - PEEK Polymer
MPDATA,DENS,2,1,1305,1298,1285,1267,1239,1208
MPDATA,DENS,2,7,1177,1141,1108
MPDATA,C,2,1,610,944,1226,1790,1893,2149
MPDATA,C,2,7,2534,2790,2918

!------------------------------ 3 - Laminate
MPDATA,DENS,3,1,1601,1598,1593,1586,1575,1563
MPDATA,DENS,3,7,1551,1537,1524
MPDATA,C,3,1,800,930,1040,1260,1300,1400
MPDATA,C,3,7,1550,1650,1700
```

Input Variables

```
ElementLength=0.0254/2+ClampingDistance
FilmThickness=0.000127
LaminateThickness=0.002159
LaminateWidth=0.0254/2          ** Half the width of the laminate (1/2 Weld length) **
LaminateLength=0.0254*4                          ** Length of a laminate sample**
CeramicThicknessTOP=0.0254*1.25
CeramicThicknessPlates=0.0254*.25
Width=0.0254/2/2          ** Half the width of the heating element  (1/2 weld width) **
CopperWidth=0.01571
CopperThicknessTOP=0.375*0.0254
CopperThicknessBottom=0.0254*(0.286+0.375)
CopperLength=1.5*0.0254
ElementThickness=2*(0.0016*0.0254)/2  ** Half the thickness of the heating element **
T_ambient=25
H_air=5                                          ** Free convection coefficient for air **
SPCTEMP,1,T_ambient                    ** Defining an enclosure for radiation (3-D) **
STEF,5.65E-8
emissivity=0.95
```

3-D Geometry

```
K,1,0,-ElementThickness,-Width
K,2,LaminateWidth,-ElementThickness,-Width
K,3,ElementLength,-ElementThickness,-Width
K,4,LaminateWidth,ElementThickness,-Width
K,5,0,ElementThickness,-Width
K,6,LaminateWidth,ElementThickness+FilmThickness,-Width
```

```
K,7,LaminateWidth,ElementThickness+FilmThickness+LaminateThickness,-Width
K,8,LaminateWidth,ElementThickness+FilmThickness+LaminateThickness+CeramicThi
cknessTOP,-Width
K,9,LaminateWidth,ElementThickness+FilmThickness+LaminateThickness+CeramicThi
cknessPlates,-Width
K,10,0,-
(ElementThickness+FilmThickness+LaminateThickness+CeramicThicknessTOP),-Width

KGEN,2,all, , , , ,2*Width,10,0
KGEN,2,16,,, , ,LaminateLength-Width,2,0

L,2,4
L,4,6
L,6,7
L,7,8
L,7,9
L,16,18

A,1,2,12,11
A,2,3,13,12
```

3-D Mesh

```
!------------------------------- 1 - Metal Mesh Heating Element, in the weld
MAT,1
ESIZE,ElementThickness*20
VDRAG,1,2,,,,,1
MSHAPE,0,3-D
MSHKEY,1
ESIZE,ElementThickness*20
VSWEEP,1

!------------------------------- 2 – PEEK Polymer
MAT,2
vdrag,7,,,,,,2

!------------------------------- 1 - Metal Mesh Heating Element, out of the weld
MAT,1
VSWEEP,2

!------------------------------ 3 - Laminate
MAT,3
ESIZE,ElementThickness*40
vdrag,16,,,,,,3
ESIZE,ElementThickness*20
vdrag,19,,,,,,6
```

*** Copy laminate and polymer elements with a 180 deg rotation about the X-axis***

```
LOCAL,11,0,0,0,0,0,180,0
CSYS,0
VTRAN,11,3,5,1,,0,0,
!VTRAN,11,all,,0,0,
CSYS,0

!------------------------------- 4 - Ceramic Insulator on top of the weld
MAT,4
ESIZE,ElementThickness*80
vdrag,21,,,,,,4

!------------------------------- 4 - Ceramic Insulator below the weld
L,50,10
ESIZE,ElementThickness*80
vdrag,37,,,,,,87

!------------------------------- 1 - Metal Mesh Heating Element, in the copper connector
K,63,ElementLength+CopperWidth,-ElementThickness,-Width
L,3,63
MAT,1
ESIZE,ElementThickness*20
vdrag,9,,,,,,96

!------------------------------- 5 - Copper Connector
K,68,ElementLength+CopperWidth,-ElementThickness-CopperThicknessBottom,-Width
L,63,68
MAT,5
ESIZE,ElementThickness*80
vdrag,53,,,,,,105
K,73,ElementLength+CopperWidth,ElementThickness+CopperThicknessTop,-Width
L,67,73
vdrag,55,,,,,,114
```

*** Merge Nodes ***

```
EPLOT
/VIEW,1,1,1,1
/ANG,1
nummrg,node,4e-8
nummrg,kp,4e-8
numcmp,all
FINISH
```

3-D Boundary Conditions

```
/SOL
Power=2.0E9
BFV,1,HGEN,Power
BFV,2,HGEN,Power

ASEL,S,LOC,X,LaminateWidth
ASEL,A,LOC,Z,LaminateLength
ASEL,A,LOC,Z,-LaminateLength
ASEL,A,LOC,Y,-
(ElementThickness+FilmThickness+LaminateThickness+CeramicThicknessPlates)
ASEL,A,LOC,Y,+(ElementThickness+FilmThickness+LaminateThickness+CeramicThic
knessTOP)
ASEL,A,LOC,Y,+(ElementThickness+FilmThickness+LaminateThickness)
ASEL,A,LOC,Z,+Width
ASEL,A,LOC,Z,-Width
ASEL,U,AREA,,4
ASEL,U,AREA,,21
ASEL,A,LOC,X,ElementLength
ASEL,U,AREA,,9
ASEL,A,LOC,X,ElementLength+CopperWidth
ASEL,A,LOC,Y,ElementThickness+CopperThicknessTop
ASEL,A,LOC,Y,-ElementThickness-CopperThicknessBottom
ASEL,A,AREA,,22
ASEL,A,AREA,,37
SFA,all,,CONV,H_air,T_ambient
ALLSEL,all
ASEL,S,AREA,,10,11,1
ASEL,A,AREA,,2,8,6
SFA,all,,CONV,H_air,T_ambient
SFA,all,,RDSF,emissivity,1
ALLSEL,all
```

Transient Analysis

```
ANTYPE,4
neqit,50
TUNIF,20
TIME,TT
AUTOTS,OFF
DELTIM,deltat, , ,
KBC,1
ALLSEL,ALL
OUTRES,ALL,ALL
SOLVE
FINISH
```

Post-Processing

```
/POST1
PLNSOL,TEMP, ,0,
WPLANE,,0,ElementThickness,0,1,0,0,0,0,1
/cplane,1

SUCR,heating element_TOP,CPLANE, ,
SUSEL,S,heating element_TOP
SUMAP,TEMP,TEMP
/VIEW,1,,1
/ANG,1,-90,ZS,1
/CVAL,1,50,200,300,343,400,450,500,10000
/REPLOT
FINISH

/post26
numvar,200
NSOL,2,635,TEMP,, Center
STORE,MERGE
NSOL,3,604,TEMP,, Edge
STORE,MERGE
NSOL,4,992,TEMP,, LamCer
STORE,MERGE
```